TÜRKİYE CUMHURİYETİ
ADANA ALPARSLAN TÜRKEŞ SCIENCE AND TECHNOLOGY UNIVERSITY

GRADUATE SCHOOL
ELECTRICAL AND ELECTRONIC ENGINEERING DEPARTMENT

ROOFTOP MOUNTED VEHICULAR ANTENNA FOR V2X COMMUNICATION

EMRAH YAYLI

Ph.D.

ADANA 2025

TÜRKİYE CUMHURİYETİ
ADANA ALPARSLAN TÜRKEŞ SCIENCE AND TECHNOLOGY UNIVERSITY

GRADUATE SCHOOL
ELECTRICAL AND ELECTRONIC ENGINEERING DEPARTMENT

ROOFTOP MOUNTED VEHICULAR ANTENNA FOR V2X COMMUNICATION

EMRAH YAYLI

Ph.D.

THESIS ADVISOR

Assoc. Prof. Dr. ŞULE ÇOLAK

ADANA, 2025

DECLARATION OF CONFORMITY

In this thesis study, which was prepared following the thesis writing rules of Adana Alparslan Türkeş Science and Technology University Institute of Graduate School, I declare that I provide all the information, documents, evaluations and results in accordance with scientific ethics and moral codes without resorting to any means or assistance that would be contrary to scientific ethics and traditions. I also declare that I refer to all of the articles I used in this study with appropriate references and accept all moral and legal consequences if a situation is found contrary to my statement regarding my work.

..../..../20..

[Signature]

Emrah YAYLI

ÖZET

V2X İLETİŞİMİ İÇİN TAVANA MONTE EDİLMİŞ ARAÇ ANTENİ TASARIMI

Emrah YAYLI

Doktora, Elektrik-Elektronik Mühendisliği Anabilim Dalı

Danışman: Doç. Dr. Şule ÇOLAK

Ocak 2025, 77 sayfa

Bu çalışmada, V2X iletişim antenlerinin tasarımında iyi bir bant genişliği, üretimde basitlik ve düşük maliyet sağlanmasına odaklanılarak yenilikçi bir yaklaşım geliştirildi. Önerilen iki tür yeni anten, bir dipol-yama anten elemanı ve bir düzenli altıgen mikroşerit antendir. Her ikisi de IEEE 802.11p tanımlı araç iletişim bandında, rezonans frekansı 5.9 GHz'de çalışacak şekilde tasarlanmıştır. Önerilen antenlerin en önemli avantajlarından biri, daha az karmaşık bir geometrik yapıya sahip olmalarıdır. Bu özellik, üretim süreçlerini basitleştirerek maliyet ve zaman açısından verimlilik sağlamaktadır. Bunun yanı sıra, üretim maliyetlerinin son derece düşük olabileceği belirtilmiş olup, bu durum özellikle otomotiv endüstrisinde yaygın olarak benimsenmeleri açısından önemli bir faktör olarak değerlendirilmektedir. Prototip antenlerin kazıma işlemi, LPKF Lazer Kaynak teknolojisi gibi ileri düzey üretim yöntemleri kullanılarak gerçekleştirilmiştir. Bu durum, üretim sürecinde yüksek hassasiyet sağlanmasına katkıda bulunmakta olup, antenlerin performans özelliklerinin korunmasında önemli bir rol oynamaktadır. Antenler, FR4 epoksi bir substrat üzerine (dielektrik sabit ε_r = 4.3, kayıp tanjant δ = 0.025) basılmıştır ve 1 mm kalınlığındadır. Antenlerin düşük profilli olması (1 mm yükseklik), araçlara entegrasyon açısından uygunluk sağlamakta olup, V2X iletişimi için çatıya veya köpekbalığı yüzgeci içine gizli şekilde monte edilebilmelerine olanak tanımaktadır. Her iki anten de yatay düzlemde tüm yönlere ışıma deseni sergilemekte olup, bu özellik, ilgili araçların göreceli yöneliminden bağımsız olarak etkili iletişimi mümkün kıldığı için V2X iletişim uygulamaları açısından avantajlıdır. Bu tez, performans, maliyet, üretim kolaylığı ve araçlara entegrasyon için uygunluk gibi ana hususları ele alan V2X iletişim antenlerinin tasarımına kapsamlı bir yaklaşım sunmaktadır. Bu çalışma, V2X iletişim teknolojisinin ilerlemesine önemli ölçüde katkı sağlama potansiyeline sahiptir.

Anahtar Kelimeler: V2X haberleşme, mikroşerit anten, CST.

ABSTRACT

ROOFTOP MOUNTED VEHICULAR ANTENNA FOR V2X COMMUNICATION
Emrah YAYLI
Ph.D., Department of Electrical and Electronic Engineering

Supervisor: Assoc. Prof. Dr. Şule ÇOLAK
January 2025, 77 pages

In this study, an innovative approach has been developed for designing V2X communication antennas, focusing on achieving good bandwidth, simplicity in fabrication, and low cost. Two novel antenna types are proposed: a dipole patch antenna element and a regular hexagon microstrip antenna. Both are designed to operate within the IEEE 802.11p defined vehicular communication band at a resonant frequency of 5.9 GHz. One of the significant advantages of proposed antennas is their simplified geometry, which facilitates easier fabrication. Moreover, we've mentioned that they can be fabricated at a very low cost, which is crucial for widespread adoption, especially in the automotive industry. We utilized advanced technology, specifically LPKF Laser Welding technology, for engraving the prototype antennas. This suggests a high level of precision in the fabrication process, which is essential for maintaining the antennas' performance characteristics. The antennas are printed on an FR4 epoxy substrate with specific dielectric properties (dielectric constant ε_r = 4.3, loss tangent δ = 0.025) and a thickness of 1 mm. The low-profile design(1 mm height) of the antennas makes them suitable for integration into vehicles, where they can be discreetly mounted on the roof or inside the shark fin for V2V communication. Both antennas exhibit an omni-directional radiation pattern in the horizontal plane, which is desirable for V2X communication applications as it ensures effective communication regardless of the relative orientation of the vehicles involved. Overall, this thesis presents a comprehensive approach to design V2X communication antennas that address key considerations such as performance, cost, ease of fabrication, and suitability for integration into vehicles. This study has the potential to contribute significantly to the advancement of V2X communication technology.

Keywords: V2X communication, microstrip antenna, CST.

ACKNOWLEDGEMENTS

I would like to express my deepest gratitude to the following people, without whom this thesis work would not have been possible.

My advisor, Assoc. Prof. Dr. Şule ÇOLAK, provided invaluable guidance and support throughout my PhD research. Her extensive wisdom, endless patience, and commitment to achieving excellence inspired and motivated me daily. I could not have completed this demanding journey without her dedicated mentorship. I sincerely thank my thesis committee members. Asst. Prof. Dr. Amira T. GÜRSEL and Assoc. Prof. Dr. Özkan ATAN.

I would like to express my special thanks to my father Enver YAYLI, my mother Gülüzar YAYLI and my sister Ezel YAYLI for their encouragement, patience, and love. It would have been impossible for me to complete this work without their support, inspiration and understanding. I am profoundly grateful to my daughter and love, Arya Güliz YAYLI. Many thanks go to my brothers, Utku PARLAK and Serkan SEVEN. Finally, I thank my friend, Salih ŞAHİN who gave key inputs on antenna design and CST.

TABLE OF CONTENTS

CERTIFICATION OF APPROVAL Hata! Yer işareti tanımlanmamış.

DECLARATION OF CONFORMITY **i**

ÖZET **ii**

ABSTRACT **iii**

ACKNOWLEDGEMENTS **iv**

TABLE OF CONTENTS **v**

LIST OF FIGURES **vii**

LIST OF TABLES **x**

LIST OF ABBREVIATIONS **xi**

LIST OF SYMBOLS **xiii**

1. INTRODUCTION **1**

1.1. The Evolution of V2X 1

2. LITERATURE REVIEW **5**

3. ANTENNA TYPES **10**

3.1. Monopoles 10

3.2. On-glass antenna 10

3.3. Glued foil antenna 10

3.4. Fractal antenna 11

3.5. Patch antenna 11

4. ANTENNA PARAMETERS **12**

4.1. Antenna Efficiency 12

4.2. Gain 12

4.3. Directivity 12

4.4. Antenna Polarization 13

4.5. Bandwidth 13

4.6. Input Impedance 13

4.7. Reflection Coefficient, Return Loss and Voltage Standing Wave Ratio (VSWR) 14

4.8. Radiation Pattern 14

4.9. Beamwidth 15

5. FEEDING TECHNIQUES **16**

5.1. Microstrip line feed 16
5.2. Coaxial line feed 16
5.3. Proximity coupling 17
5.4. Aperture coupling 17
6. DESIGN OF PATCH ANTENNA 18
7. ANTENNA PLACEMENTS 21
7.1. Roof 21
7.2. Screens and windows 21
7.3. Fender and bumper 21
7.4. Trunk cover 22
7.5. Side-Mirrors 22
8. MATERIAL AND METHOD 23
8.1. Simulation Design and Results with FR-4 23
8.2. Simulation Design and Results with ROGERS RT5880 38
8.3. Fabrication Stage 50
9. CONCLUSION 73
REFERENCES 74

LIST OF FIGURES

Figure 1.1. The scenarios of V2X 2
Figure 2.1. Shark fin antenna 6
Figure 2.2. Roof automobile antenna 7
Figure 3.1. Structure of patch antenna[29] 11
Figure 5.1. Structure of coaxial line feed [48] 16
Figure 5.2. Structure of proximity coupling [51] 17
Figure 5.3. Structure of aperture coupling [51] 17
Figure 7.1. Alternative positions for antenna placements 21
Figure 8.1. Dimensions of designed patch antenna, a) Front view b) Perspective view 24
Figure 8.2. S_{11} parameter graph of patch antenna 25
Figure 8.3. VSWR simulated result of patch antenna 25
Figure 8.4. 3D Radiation Pattern of patch antenna 26
Figure 8.5. Far-field Radiation Pattern at Phi=0° and Phi=90° 26
Figure 8.6. Dimensions of the designed two-element array antenna 27
Figure 8.7. S_{11} parameter graph of two-element array antenna 28
Figure 8.8. VSWR simulated result of two-element array antenna 29
Figure 8.9. 3D Radiation Pattern of two-element array antenna 29
Figure 8.10. Far-field Radiation Pattern at Phi=0° and Phi=90° 30
Figure 8.11. Dimensions of the designed antenna 30
Figure 8.12. S_{11} graph of dipole antenna 31
Figure 8.13. VSWR simulated result of dipole antenna 31
Figure 8.14. 3D Radiation Pattern of dipole antenna 32
Figure 8.15. Far-field Radiation Pattern at Phi=0° and Phi=90° 32
Figure 8.16. Dimensions of designed hexagon microstrip antenna 33
Figure 8.17. S_{11} graph of hexagon microstrip antenna 33
Figure 8.18. VSWR simulated result of hexagon microstrip antenna 34
Figure 8.19. 3D Radiation Pattern of hexagon microstrip antenna 34
Figure 8.20. Far-field Radiation Pattern at Phi=90° 35
Figure 8.21. Dimensions of designed second hexagon microstrip antenna 36
Figure 8.22. S_{11} parameter graph of second hexagon microstrip antenna 36

Figure 8.23. VSWR simulated result of second hexagon microstrip antenna 37
Figure 8.24. 3D Radiation Pattern of second hexagon microstrip antenna 37
Figure 8.25. Far-field Radiation Pattern at Phi=90° 38
Figure 8.26. Dimensions of designed patch antenna with RT5880 39
Figure 8.27. S_{11} graph of patch antenna with RT5880 39
Figure 8.28. VSWR simulated result of patch antenna with RT5880 40
Figure 8.29. 3D Radiation Pattern of patch antenna with RT5880 40
Figure 8.30. Far-field Radiation Pattern at Phi=0° and Phi=90° 41
Figure 8.31. Dimensions of the designed two-element array antenna with RT5880 42
Figure 8.32. S_{11} graph of two-element array antenna with RT5880 42
Figure 8.33. VSWR simulated result of two-element array antenna with RT5880 43
Figure 8.34. 3D Radiation Pattern of two-element array antenna with RT5880 43
Figure 8.35. Far-field Radiation Pattern at Phi=0° and Phi=90° 44
Figure 8.36. Dimensions of the designed dipole antenna with RT5880 45
Figure 8.37. S_{11} graph of the designed dipole antenna with RT5880 45
Figure 8.38. VSWR simulated result of the designed dipole antenna with RT5880 46
Figure 8.39. 3D Radiation Pattern of the designed dipole antenna with RT5880 46
Figure 8.40. Far-field Radiation Pattern at Phi=0° and Phi=90° 47
Figure 8.41. Dimensions of the hexagon microstrip antenna 48
Figure 8.42. S_{11} parameter graph of hexagon microstrip antenna 48
Figure 8.43. VSWR simulated result of hexagon microstrip antenna 49
Figure 8.44. 3D Radiation Pattern of hexagon microstrip antenna 49
Figure 8.45. Parameter sweep sample 50
Figure 8.46. LPKF Protomat S104, LPKF Contac S4 and LPKF ProtoLaser U4 51
Figure 8.47. Stages of hole plating 51
Figure 8.48. Stages of production 52
Figure 8.49. Front and back sides of the hexagonal microstrip patch antenna 53
Figure 8.50. Front and back sides of the dipole microstrip patch antenna 54
Figure 8.51. Antenna dimensions 55
Figure 8.52. Antenna feeds 56
Figure 8.53. Vector Network Analyzer 57
Figure 8.54. S-parameter measurement set-up 57
Figure 8.55. S_{11} comparison for hexagon microstrip antenna 58

Figure 8.56. S_{11} comparison for dipole antenna 58
Figure 8.57. Antenna positions on the car 60
Figure 8.58. Measured car 61
Figure 8.59. Handheld Vector Network Analyzer and calibration kit 61
Figure 8.60. Hexagon microstrip antenna on front position 62
Figure 8.61. Hexagon microstrip antenna on back position 62
Figure 8.62. Dipole antenna on back position 63
Figure 8.63. S_{11} comparison for hexagon microstrip antenna 63
Figure 8.64. S_{11} comparison for dipole antenna 64
Figure 8.65. Box plot of dipole antenna S_{11} 66
Figure 8.66. Box plot of hexagon microstrip antenna S_{11} 68
Figure 8.67. S_{11} Means±Standart Deviations for hexagon microstrip antenna 68
Figure 8.68. S_{11} Means±Standart Deviations for dipole antenna 69
Figure 8.69. Test setup in the anechoic chamber 70
Figure 8.70. Radiation Pattern at Phi=90° 71
Figure 8.71. Radiation Pattern at Phi=90° 71

LIST OF TABLES

Table 8.1. Dimensions of designed patch antenna 24
Table 8.2. Dimensions of designed antenna-2 28
Table 8.3. Antenna Simulation Performance Comparison 50
Table 8.4. Comparison of the simulated and measured parameter results for hexagon microstrip antenna 64
Table 8.5. Comparison of the simulated and measured parameter results for dipole antenna 64
Table 8.6. Descriptive statistics and comparison of application groups for Dipole S_{11} values66
Table 8.7. Descriptive statistics and comparison of application groups for Hex S_{11} values ... 67
Table 8.8. Comparison with existing designs 72

LIST OF ABBREVIATIONS

AM	: Amplitude Modulation
BW	: Bandwidth
CPW	: Coplanar Waveguide
CST	: Computer Simulation Technology
DMAA	: Directional Microstrip Array Antenna
DSRC	: Dedicated Short Range Communications
ETSI	: European Telecommunications Standards Institute
FCC	: Federal Communications Commission
GHz	: Gigahertz
FM	: Frequency Modulation
GPS	: Global Positioning System
HPBW	: Half Power Beam Width
IEEE	: Institute of Electrical and Electronics Engineers
IoT	: Internet of Things
ITS	: Intelligent Transportation System
IOQ	: Interquartile Range
LPKF	: Laser Welding Technology
LTE	: Long-Term Evolution
MHz	: Megahertz
NHTSA	: National Highway Traffic Safety Administration
PIFA	: Planar Inverted-F Antennas
RMSPA	: Rectangular Microstrip Patch Array Antenna
R&S	: Rohde & Schwarz
SDARS	: Satellite Digital Audio Radio Service
VNA	: Vector Network Analyzer
VSWR	: Voltage Standing Wave Ratio
V2X	: Vehicle 2 Everything
V2V	: Vehicle 2 Vehicle
V2I	: Vehicle 2 Infrastructure
V2N	: Vehicle 2 Network

V2P : Vehicle 2 Pedestrian

WAVE : Wireless Access in Vehicular Environments

WHO : World Health Organization

LIST OF SYMBOLS

c	: Speed of Light
ε_r	: Dielectric Constant of the Substrate
dB	: Decibel
dBi	: Decibel isotropic
ε_{eff}	: Effective Dielectric Constant
f_r	: Resonant Frequency
f_h	: Highest Frequency in the Band
f_l	: Lowest Frequency in the Band
f_c	: Center Frequency
h	: Thickness of Substrate
L	: Length of the Patch
RL	: Return Loss
R_{in}	: Input Resistance
r	: Reflection Coefficient
Z_{in}	: Input Impedance
tan δ	: Electrical Loss Tangent
V	: Voltage
Z_o	: Transmission Line
X_{in}	: Input Reactance
W	: Width of the Patch

1. INTRODUCTION

1.1. The Evolution of V2X

According to a report published by the World Health Organization (WHO) on June 20, 2022, approximately 1.3 million people die each year due to motor vehicle crashes, and according to a statement dated December 13, 2023, this number is around 1.19 million annually. National Highway Traffic Safety Administration (NHTSA) estimates that V2X (Vehicle 2 Everything) technologies could reduce the number of crashes by up to 80%. V2X is the next generation technology that provides safety alerts to drivers. The V2X communication system can be implemented to enhance road communication and safety more efficiently, where data from vehicles collected by various sensors would be transmitted to a database via IoT. [1]. This concept is fundamental to the intelligent transportation system (ITS). The V2X includes four types: V2V (it means vehicle2vehicle), V2I (vehicle2infrastructure), V2N (vehicle 2 network) and V2P (vehicle 2 pedestrian)[2]. Wireless communication systems are widely used in vehicles for functions like emergency services, navigation, in-car entertainment, toll payment, obstacle detection, and crash prevention. V2X communication systems, which include two communication systems together, from V2V and from vehicle to roadside base station (V2I), are nowadays causing traffic-related problems that negatively affect daily life in many aspects, especially in big metropolises. The solutions it has proposed have attracted increasing attention from official institutions, standard-setting organizations, especially companies in the automotive and information technology sectors, and researchers conducting theoretical studies at universities.

So far, two primary communication standards for V2X systems are dedicated short range communications (DSRC) and cellular-V2X (C-V2X). The frequency range for DSRC is 5.85–5.925 GHz. [3]. The main purpose of DSRC is to enable vehicles to communicate with each other directly. On the other hand, C-V2X allows vehicles to communicate with each other via base stations (such as LTE, 5G). Figure 1.1 shows the scenarios of V2X in the future IoT systems.

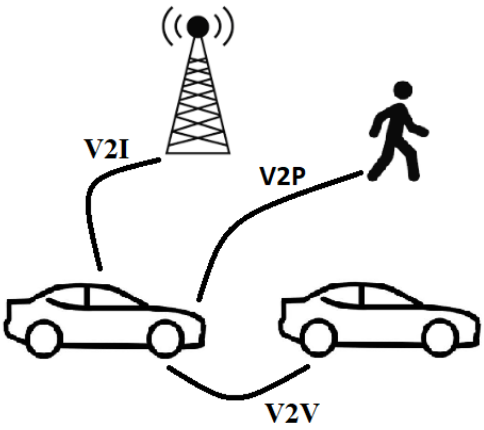

Figure 1.1. The scenarios of V2X

Many countries around the world have allocated the 5.9 GHz band for V2X communications. The Federal Communications Commission (FCC) in the U.S., Canada, and Mexico have allocated 75 MHz, while Australia and Korea have allocated 70 MHz, and Singapore has allocated 50 MHz [1], [4].

After the FCC outlined the equipment requirements for intelligent transportation systems in 2003, standardization efforts for V2X systems began in 2004 under the title Dedicated Short Range Communication. In 2010, the IEEE 802.11p standard was introduced as an approved amendment to the IEEE 802.11 standard to incorporate wireless access in vehicular environments (WAVE), a system for vehicle communication. Currently, numerous research groups in academia are focused on topics related to vehicular communications. Additionally, significant EU projects have been initiated by the industry, including the CAR2CAR Communication Consortium, Secure Vehicular Communication (SeVeCom), and NEARCTIS. As a promising technology, V2X communications have also attracted the attention of the automotive industry, prompting leading automotive manufacturers worldwide to collaborate under the initiative known as the "Crash Avoidance Metrics Partnership".

In Europe, ETSI released a standard for V2X communication called ITS-G5. It is based on Wireless LAN and working in the upper 5 GHz band (5.855 to 5.925 GHz) with partially similar maximum transmission powers as in cellular mobile radio (33 dBm, 23 dBm, 0 dBm depending on the allocated channel) but without any centrally coordinated power control. Due to the higher frequencies, as compared to cellular mobile radio, the propagation is expected to be worse especially in urban environments, where it is dominated by diffractions and reflections.

An urban environment poses several challenges for V2V communications, including multiple propagation paths, buildings, and other barriers. A significant issue is integrating multiple frequency bands into a compact model. At this stage, it's crucial to minimize coupling between antennas and enhance radiation efficiency. Antennas used in vehicular communication must exhibit an effective radiation pattern to ensure broad coverage for improved communication from all directions [5]. Extensive research has been conducted on antenna designs for cellular networks.

It is inevitable that there will be an increase in the number of antennas due to the increasing needs and requirements in the vehicle industry. There are difficulties in having more than one antenna in the vehicle;

1- Coupling and scattering effects,
2- Sufficient spacing between antennas is necessary to reduce mutual coupling,
3- The total expense of the antenna system, including additional cable costs, connector costs, and assembly labor expenses,
4- It is challenging to position and solder a large number of antenna elements in a compact area.

In V2V wireless communication systems, due to the mobility of the end points in the communication network, the communication environment can change very quickly in the environment, and especially when considering the traffic in the residential areas, there will be no direct view between the two communicating ends (transmitting and receiving antenna) most of the time. This means that wide antenna coverage is a critical parameter in terms of continuity and reliability of communication.

Additionally, the positioning of the antenna is highly constrained due to aesthetic considerations set by the automotive industry and the placement of other electronic components. Until today automotive manufacturers have mostly chosen the vehicle roof as the location for all-direction reception of GPS, FM/AM signals, and cellular signals (with the exception of convertibles). The reason is that the roof is the highest point of the vehicle [6]. However, this may change depending on the vehicle exterior design. Most contemporary vehicles feature a curved roof or a bonded plate at an angled position. The angle of tilt, curvature, and design of the ground plane will influence the patterns of the antenna.

Most automotive antennas are designed for low frequency applications such as FM/AM radio and GPS. However, in order to meet today's demand, vehicle antennas need development and change. A limited number of studies are available for automotive antennas operating at high frequencies (3-6 GHz). In line with end-user demands, V2V technology has become popular for manufacturers and researchers. The number of antenna structures for the V2V communication has started to increase recently [3].

2. LITERATURE REVIEW

Klemp et al. designed an antenna array comprising four elements, each featuring shorting pins positioned at the center of the circular patches. A configuration of multiple antennas compatible with various standards, including two antennas specifically for 5.9 GHz V2V communication, along with antennas designed for GPS and reception of signals across multiple cellular bands, was examined. Metrics assessing antenna performance, such as average antenna gain and power correlation, were assessed using a simplified model focusing on the Angle of Arrival within the complex multipath channels present in vehicular environments [7].

Varum et al. [8] designed two square printed monopole antennas for vehicle installation, using Ansoft HFSS electromagnetic simulation software due to the properties of the substrate material, Arlon CuClad 217, which has a relative dielectric constant (ε_r) of 2.17, a thickness of 0.787 mm, and a loss tangent (tanδ) of 0.0009.

Westrick et al. [9] designed wire antenna solution that is both low-profile and cost-effective, boasting enhanced gain. To achieve this, a specialized feed network incorporating a metallic base is developed. The antenna design features a monopole wire surrounded by eight parasitic elements, enabling the generation of an omnidirectional radiation pattern. Additionally, the antenna array is seamlessly integrated with both a feed network board and a supportive metal enclosure. Through comprehensive evaluation, it is demonstrated that the proposed integrated antenna meets the necessary reflection coefficient (S_{11}) requirements across the entire DSRC frequency spectrum. Furthermore, the antenna demonstrates a crucial omnidirectional H-plane pattern, ideal for facilitating DSRC communications between vehicles and infrastructure.

Aloi et al. [10] explored the utilization of directors to enhance the gain of a quarter-wave monopole antenna, specifically for DSRC applications requiring omnidirectional coverage. Four variations of the antenna are fabricated using Rogers RO3003 laminate, each differing in the number of passive directors. The laminate boasted a thickness of 0.13 mm and a relative dielectric constant of 3.0. Results showed that the inclusion of three directors on each side led to an approximate 4 dB increase in gain towards both the front and rear of the vehicle.

Figure 2.1 illustrates a shark fin antenna system housed within a 23.5 cubic inch area and 3.5 inches in height, consisting of a planar inverted-F antenna (PIFA) for LTE 800, a monopole antenna for WLAN, another monopole for V2X, and a patch antenna for GPS [11].

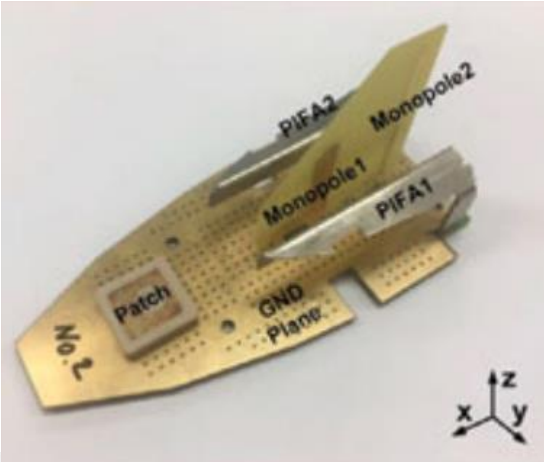

Figure 2.1. Shark fin antenna

Luo et al.[12] designed a monopole antenna operating in LTE, 5G and DSRC frequency bands. Researchers tried to determine the most efficient location by placing the antenna they designed at different points on the vehicle roof. The antenna achieves a favorable omnidirectional radiation pattern and impedance matching without the need for an additional matching network, enhanced by incorporating a toothed capacitor and an impedance matching disk. Simulations of the electric field distribution and transmission coefficient for the antenna mounted on the vehicle roof indicate high gain with minimal loss [12].

Guan ve et al. [13] presented a roof-mounted automobile antenna module (Figure 2.2) that includes two LTE antennas designed for MIMO operation: one is a monopole antenna printed on a shark-fin-shaped substrate oriented perpendicular to the vehicle's roof, while the other is a planar inverted-F antenna (PIFA) located on a lower plane parallel to the roof, and both antennas, fed from separate ground planes and positioned at different heights, effectively cover the LTE bands and provide omni-directional radiation in the horizontal plane with high radiation gain.

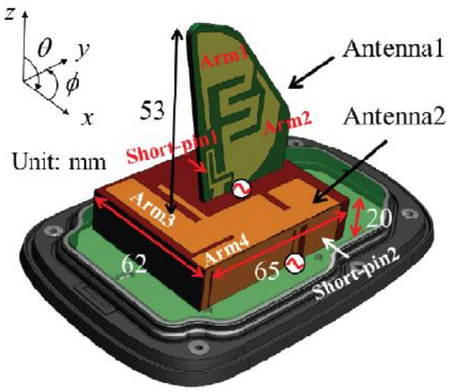

Figure 2.2. Roof automobile antenna

Huang et al. [14] developed a switchable, 4-port directional antenna designed to enhance gain and suppress interference for V2X communication. By incorporating a cylindrical element at the center of the antenna, they were able to focus the energy in one direction, with the cylinder acting as a barrier. This barrier improves the antenna's gain in that specific direction while also creating space and flexibility for other antennas. Both simulation and experimental results demonstrate that the antenna performs effectively within the DSRC frequency band.

Ramya et al.[5] designed a dual-band, circularly polarized, omnidirectional patch antenna for vehicular wireless communication systems, operating at 2.45 GHz and 5.5 GHz, with respective gains of 2.24 dB and 4.97 dB. The antenna offers an impedance bandwidth of 320 MHz in the 2.4 GHz band and 450 MHz in the 5 GHz band.

Guan et al. [15] proposed a flat antenna module for car roofs designed for LTE, GPS, and Satellite Digital Audio Radio Service (SDARS) applications. This module includes a PIFA for LTE, along with a square loop antenna for GPS and a circular loop antenna for SDARS. All three antennas are situated in the same plane, parallel to the vehicle's roof, and are positioned close together, resulting in a compact module measuring only 70 x 70 mm^2. This low-profile design makes the module nearly imperceptible once installed on the car roof.

Kaul et al. [16] investigated the impact of antenna placement in vehicular networks operating within the 5 GHz band. They assessed the relative performance of various vehicle-mounted antennas connected to 802.11a radios, focusing on packet error rate (PER) and received signal strength indicator. Their findings revealed that different antenna positions resulted in a 25-30%

variation in cumulative link PER performance. Additionally, they noted that the gain patterns of omnidirectional antennas became asymmetric in many mounting configurations, leading to distortions of up to 15 dB across different angles of arrival for an 802.11a radio at 5.18 GHz.

Leelaratne et al. [17] developed two types of PIFA antennas. One is a compact variation of a traditional antenna, while the other is a novel planar design tailored for specific applications. Both antennas were created to cover the mobile telephone frequency range from 890 to 2100 MHz. They were mounted and tested in various locations on vehicles, including the front and rear windscreens, bumpers, and roof panels. The results demonstrated that a PIFA offers a satisfactory level of horizontal polarization sensitivity and provided typical three-dimensional coverage for both primary polarizations when mounted discreetly on the windscreen.

In the study titled "Compatible CP Antenna for V2X Applications Below 6 GHz Band" by Virothu et al. [18], a consistent, circularly polarized antenna is presented for wireless and traffic safety applications below 6 GHz. The square slotted antenna equipped with a single-plane waveguide achieves a wide impedance bandwidth. A feeding structure with four nitrogen lines is included to create a sharp transverse electric field. Three strip conductors are connected to the ground in an L shape to enhance circular polarization (CP) characteristics. Gain in the CP bandwidth is achieved by altering the ground surface. The antenna is fabricated on a flexible substrate with a dielectric constant of ε_r = 3.5 and a height of h = 0.1 mm. Operating in the 3.23 – 6.26 GHz band, the antenna has CP bandwidths of 3.02 – 4.25 GHz and 5.30 – 6.07 GHz.

In the study by Rajesh Kumar et al. [19] a compact Coplanar Waveguide (CPW)-supported antenna resonating at 3.5 GHz and 5.9 GHz for next-generation vehicle communication is presented. The antenna has a single-cell structure measuring 35 mm × 20 mm and is designed with a 1.6 mm thick FR-4 substrate. The antenna's gain ranges from 2.8 dBi to 2.9 dBi at 3.5 GHz and from 3.6 dBi to 3.7 dBi at 5.89 GHz, with overall efficiency between 60% and 80%, and the measured results confirm its suitability for V2V and V2I applications.

Singhal et al. [2] developed a hexagonal patch antenna featuring six elliptical slots for V2V communication, constructed on an FR-4 substrate and utilizing a coaxial probe for feeding; the inclusion of elliptical slots was intended to improve directivity and gain, with simulation results indicating a gain of 6.021 dB and a directivity of 9.443 dB across the frequency range of 5.8 GHz to 6 GHz.

Wnuk et al. [20] proposed a GPS antenna utilizing microstrip technology, with the windscreen chosen as the installation location. The design incorporated a 1.5 mm thick FR-4 laminate, metal-plated on both sides and featuring a dielectric permittivity of ε_r= 4.6. Its compact size makes this antenna model ideal for use in the automotive sector.

Mondal et al. [21] proposed a tri-band microstrip patch antenna featuring a multi-layered design that employs a hexagonal Sierpinski fractal pattern for the patch. This antenna operates at 1.575 GHz for GPS L1, 3.71 GHz for WiMAX, and 5.9 GHz for DSRC bands. Researchers conducted an analysis of the proposed patch antenna and compared it to a hexagonal patch without a fractal design. Their approach allowed them to achieve a reduction in antenna size by approximately 75% compared to other well-known fractal designs.

3. ANTENNA TYPES

An antenna is a transducer capable of radiating and receiving electromagnetic waves. For an antenna to be able to receive the desired electromagnetic wave, the transmitter system and the receiver system must operate at the same frequency [22].

3.1. Monopoles

Monopole antennas are among the most widely used types due to their affordability, ease of production, and straightforward assembly. A monopole antenna typically consists of an antenna base and a rod of specific length. While the roof of the vehicle is the most common installation site, there are instances where they are mounted on the vehicle's side rails or trunk lid. This type of antenna necessitates a direct connection to the ground. However, since they cannot visually adapt to modern vehicle designs, automobile manufacturers avoid the use of monopole antennas [23]. In addition, rod antennas particularly suffer from theft and breakage.

3.2. On-glass antenna

This type of antenna gained popularity in the premium automobile sector during the 1980s as design considerations became more important, allowing for the integration of multiple antennas out of the user's sight by utilizing on-glass antennas, where the vehicle's metallic body serves as part of the antenna and the glass (such as the windshield, side windows, or rear window) acts as the slot within this metallic structure, with a thin conductor coupled to the slot to enable resonance and function as an antenna [24].

3.3. Glued foil antenna

Like slot antennas and patch antennas, these structures can be mounted on metallic foil that is adhered to a plastic component. Therefore, it can be easily mounted on rear view mirrors, bumpers and fenders, which are generally made of plastic parts. However the biggest disadvantages are narrow usable bandwidth and diffuculty to connect coaxial cables to the flat foil antenna [20].

3.4. Fractal antenna

Basically, fractal technology allows the design of miniature antennas and can accommodate multiple frequencies in a single device. Koch, Minkowski and Hilbert fractal geometries are generally used in fractal antenna design. Fractals are fragmented geometric shapes that can be subdivided in parts, they display self-similarity on all scales [21], [25].

3.5. Patch antenna

Basically microstrip antennas are a panel of dielectric substrate sandwiched between two conductors. The conductor in the lower part is called the ground and the conductor in the upper part is called the patch (Figure 3.1). The operating frequencies of microstrip antennas are generally between 1 GHz to 100 GHz. Patch pieces are usually made of metals such as gold or copper. These conductive metals are used because of their low resistivity and resistance to oxidation. The patch can be designed in various forms according to the need. Generally, circular, rectangular and square forms are used. The performance of a microstrip antenna depends on the shape of the patch and the characteristics of the substrate material. The size of a microstrip antenna is inversely proportional to its frequency [26], [27]. Microstrip patch antennas have several advantages such as low profile, light weight, easy fabrication and assembly [23], [28]. Due to its geometrically flat structure, it is increasingly used in the automotive industry nowadays.

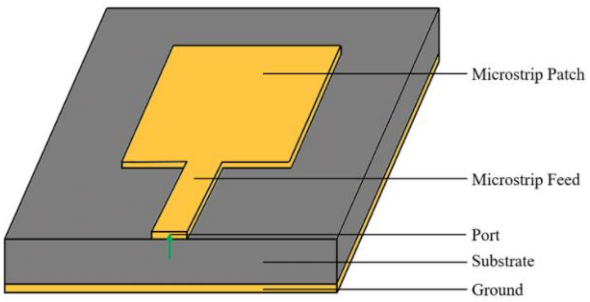

Figure 3.1. Structure of patch antenna[29]

4. ANTENNA PARAMETERS

There are some parameters that affect the microstrip antenna performance directly or indirectly. The radiation pattern of antennas shows the distribution of the power they emit. Directionality in antennas is the comparison of the radiation in a particular direction with the isotropic antenna radiation in that direction. Antenna gain is the portion of the antenna's radiation to the radiation that an ideal, i.e. isotropic antenna, gives off when the same amount of energy is applied. Antenna efficiency is defined as the ratio of the energy supplied to the antenna and the energy consumed, that is, converted into a signal. Since the materials used in antennas cause temperature loss, antenna efficiency is never 100% in practice [30], [31].

4.1. Antenna Efficiency

The mathematical expression of total efficiency shown below:

$$e_0 = e_r e_c e_d \tag{4.1}$$

where e_0 represents total efficiency, e_r represents reflection efficiency, e_c represents conduction efficiency, and e_d represents dielectric efficiency (they are all dimensionless). Multiplying these three efficiencies together gives the overall efficiency of the antenna system, which represents how effectively the antenna converts input power into useful radiated energy while considering losses associated with impedance matching and dielectric materials [32].

4.2. Gain

Antenna gain is one of the most important parameters when evaluating antenna performance. It reflects the antenna's capacity to direct or concentrate radio frequency energy in a specific direction compared to an isotropic radiator. An isotropic radiator is a hypothetical antenna that emits energy uniformly in all directions, serving as a benchmark for assessing the directional characteristics of actual antennas. Antenna gain is usually represented in decibels (dB) with reference to an isotropic radiator, commonly abbreviated as dBi [33], [34].

4.3. Directivity

Directivity is a fundamental concept in antenna engineering, defining an antenna's ability to concentrate its radiation in a particular direction compared to an isotropic radiator (a theoretical antenna that radiates equally in all directions). The formula for directivity (D) is:

$$D = \frac{U}{U_0} = \frac{4\pi U}{P_{rad}} \quad (4.2)$$

where:

U = radiation-intensity (W/unit solid angle) it calculated by multiplying radiation-density (W_{rad}) with square of distance (r^2).

$$U = r^2 W_{rad} \quad (4.3)$$

U_0= the radiation-intensity of isotropic-source (W/unit solid angle) [35].

4.4. Antenna Polarization

The polarization of a wave determines the shape traced by the electric field over time as the wave propagates. Polarization types are divided into three categories: linear polarization, circular polarization, and elliptical polarization. If the change in an electric field vector over time occurs along only one axis at a point in space, the wave polarization is referred to as linear polarization. Circular polarization occurs when the electric field vector traces a circular path as it progresses. If the electric field vector traces an elliptical path, the polarization is termed elliptical polarization [36].

4.5. Bandwidth

Bandwidth (BW) is a fundamental characteristic of antennas and plays a vital role in antenna performance. It determines the frequency range in which the antenna can effectively emit or capture energy. Additionally, the bandwidth can also be described in terms of percentage of the center frequency of the band.

$$BW = 100 * \frac{F_h - F_l}{F_c} \quad (4.4)$$

In this equation, F_h is denotes the highest frequency in the band, F_l is the lowest frequency and F_c is the center frequency [37].

4.6. Input Impedance

Input impedance, expressed as "Z_{in}" in a microstrip antenna, represents the impedance of the antenna at the feed point. It is a complex number value and changes depending on the frequency. Input impedance relation (real and imaginary) is given in Equation 4.5. "R_{in}" represents the input resistance and "X_{in}" represents the reactance part [28].

$$Z_{in} = R_{in} + jX_{in} \quad (4.5)$$

4.7. Reflection Coefficient, Return Loss and Voltage Standing Wave Ratio (VSWR)

The input impedance of the antenna and the characteristic impedance of the feed line should not be different. A cable with an actual value of 50 Ω is generally used for the supply line. In order to prevent losses, the imaginary part of the impedance is required to be close to zero. In equation 4.6, the reflection coefficient, gives the back reflection rate of the waves coming out of the antenna. "Z_{in}" represents the input impedance and "Z_o" represents the transmission line [38].

$$r = \frac{Z_{in} - Z_0}{Z_{in} + Z_0} \quad (4.6)$$

The measurement of the light intensity reflected back toward the source is referred to as Return Loss (RL). It is desirable that the return loss be in small values. In well-designed antennas, this loss should be -10 dB and below. The return loss formula is given in equation 4.7.

$$RL = -20 \log |r| \quad (4.7)$$

The VSWR is determined by the ratio of the maximum voltage to the minimum voltage on the transmission line. It reflects the degree of matching between the input impedance and the transmission line’s characteristic impedance. The VSWR formula is given in equation 4.8 [39].

$$VSWR = \frac{|V_{max}|}{|V_{min}|} = \frac{1 + |r|}{1 - |r|} \quad (4.8)$$

4.8. Radiation Pattern

The radiation pattern model for antennas is defined as a mathematical representation of spatial coordinates. This model is established in the far-field region and is expressed as a function of directional coordinates. By utilizing either the "electric current model" (E) or the "magnetic current model" (H), the radiation pattern of a microstrip antenna can be visualized in two or three dimensions. The radiation pattern indicates the power radiated or received as a function of angular position and radial distance, illustrating how the antenna directs the energy it emits. The main lobe signifies the maximum value and direction of the antenna's radiation. Essentially, all lobes outside the main lobe are referred to as minor lobes (side and back lobes). These lobes are usually unwanted, and the intensity of minor lobes is typically measured as the ratio of the power density in these lobes to the power density in the main lobe. When analyzed more closely, side lobes are the most significant among the minor lobes and can substantially affect the antenna's overall radiation. In contrast, back lobes are minor lobes positioned opposite the main lobe. The radiation pattern may change depending on factors such as the design of the antenna, the operating frequency, and other influencing variables [40].

4.9. Beamwidth

Beamwidth is defined as the angular width between points on either side of the main lobe of any pattern of an antenna having the same maximum value. Although there are several types of beamwidth, the most commonly used one is Half Power Beamwidth (HPBW). Beamwidth is defined as the angle between two directions in the plane containing the maximum direction of radiation in which the radiation intensity drops to half its maximum value." The situation where the maximum value of the pattern drops to half is referred to as the point where the field pattern decreases to 0.707 times in linear scale representation, 0.5 times in power pattern linear scale representation, and -3dB in power pattern dB representation [34], [41].

5. FEEDING TECHNIQUES

Microstrip patch antennas employ various feeding methods, which can be categorized into two types (contacting and non-contacting) based on the primary mechanism of power transfer from the feed line to the patch. [42]. In the contacting feed technique, RF power is directly supplied to the patch via a contact element. In contrast, the non-contacting techniques do not provide direct RF power to the patch. Instead, power is transferred to the patch from the feed line through electromagnetic coupling. There are various feeding methods available. The two most commonly used techniques in contacting feeding are microstrip line feed and coaxial probe feed. In non-contacting feeding techniques, the two most widely used methods are aperture coupling and proximity coupling [41], [43], [44].

5.1. Microstrip line feed

Microstrip line feed is the simplest and most straightforward feeding technique for manufacturing, involving a conducting strip directly connected to the microstrip patch; however, a significant drawback of this method is that increasing the substrate thickness leads to higher surface waves and unwanted feed radiation, which can limit the bandwidth [43], [45], [46].

5.2. Coaxial line feed

In the coaxial probe feed method, the inner conductor is attached to the antenna's radiation patch, while the outer conductor is linked to the ground plane. The structure of coaxial line feed is illustrated in Figure 5.1. The advantage of this feeder arrangement is that the feeder can be placed anywhere on the patch to match the cable impedance with the antenna input impedance, and it is easy to fabricate. The disadvantage is that it has narrow bandwidth [44],[47], [48],[49].

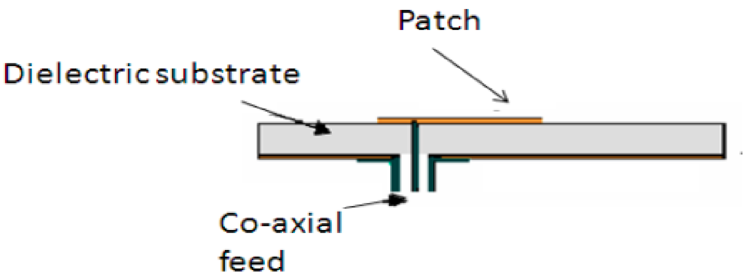

Figure 5.1. Structure of coaxial line feed [48]

5.3. Proximity coupling

This excitation approach is commonly known as the electromagnetic coupling configuration. In the proximity feeding method, two dielectric materials are employed, with the feed line positioned between these layers. The radiating patch is placed on the upper dielectric layer. [41], [48], [50]. The structure of proximity coupling method is shown in Figure 5.2.

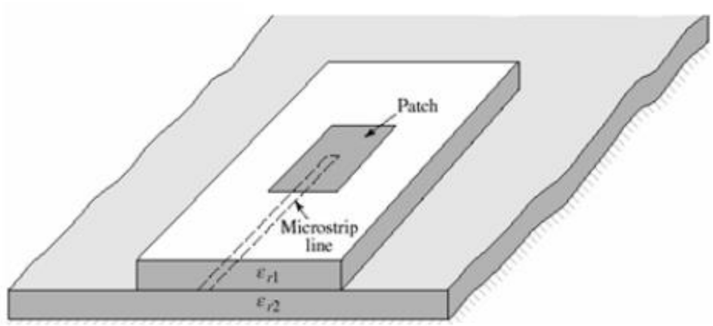

Figure 5.2. Structure of proximity coupling [51]

5.4. Aperture coupling

Aperture coupling is a method of feeding an antenna in which the radiating patch is electrically separated from the microstrip feed line by the ground plane. Instead of directly connecting the feed line to the patch, energy is transferred through a slot or opening in the ground plane. This configuration helps to improve isolation between the feed line and the patch, minimizing interference. The structure of aperture coupling method is shown the illustrated in Figure 5.3 [50].

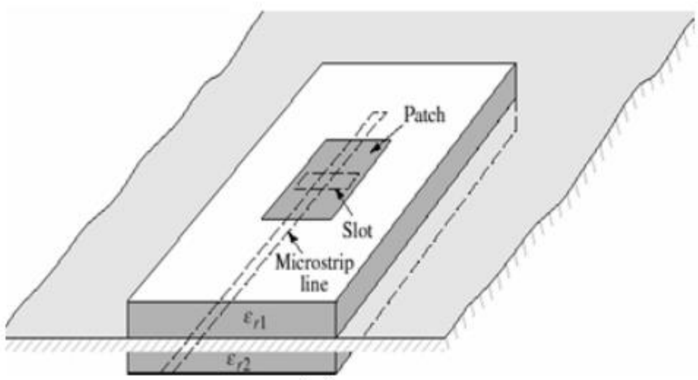

Figure 5.3. Structure of aperture coupling [51]

6. DESIGN OF PATCH ANTENNA

Although the idea of using microstrip structures as antennas was first proposed by Deschamps in 1953, it wasn't until approximately 20 years later that a practical antenna could be produced, despite Gutton and Baissinot being awarded the first patent in this area in 1955. It wasn't until the early 1970s, with the development of low-loss, mechanically, and thermally suitable dielectric substrate materials, that the first microstrip antennas were realized by Munson (1974) and Howell (1975) [52]. In our study, the main reasons for using microstrip antennas include ease of production, occupying small volumes, and low costs.

The dielectric constant of the substrate, the substrate thickness, and the operating frequency are three crucial parameters vital for antenna design. The electrical permeability (dielectric coefficient) of each substrate is different. This study investigates the effects of the dielectric coefficient on factors such as bandwidth, gain, and return loss. There are many substrates available for use in microstrip antenna design.

All printed antennas are made with substrate materials that offer mechanical support and influence radiation characteristics. Therefore, choosing the right substrate material is a critical factor in antenna design [23]. There are many substrates that can be used in microstrip patch antenna design. Each substrate type has different electrical conductivity, namely dielectric coefficient. Therefore, the dielectric coefficient has a direct effect on factors such as bandwidth, gain and return loss [25]. The substrates can be classified as:

a) Ceramic substrates (Alumina),
b) Semiconductor substrates (Si or GaAs),
c) Ferrimagnetic substrates (Ferrite and YIG),
d) Synthetic substrates (PTFE (Teflon), polystyrene, polyolefin and polyphenylene),
e) Composite Material substrates (By adding fiberglass (woven or random), quartz, or ceramic in suitable proportion to the synthetic materials),
f) Low Cost Low Loss substrates (FR-4 substrate) [53].

The use of a thick dielectric substrate will significantly enhance the performance of a microstrip antenna electrically. The thickness of the dielectric substrate is proportional to the antenna bandwidth. The primary function of the substrate material for a microstrip antenna is to mechanically support the radiating patch and create the necessary separation between the patch and the ground plane. With substrates having a high dielectric constant, it is possible to reduce the size of the patch due to the loading effect. However, along with the reduced antenna volume, a high dielectric constant will also decrease the antenna bandwidth. When selecting the substrate material for a microstrip antenna, factors such as the desired patch size, bandwidth, additional losses, thermal stability, cost, etc., should be taken into consideration [49].

In this study, FR-4 and Rogers 5880 substrate types are used and the most suitable dielectric coefficient is determined for the microstrip antenna. During the antenna design process, designs are created with attention to ensuring they can be applied to the vehicle's side mirrors and roof in appropriate sizes. For a microstrip antenna, it is preferred that the gain and bandwidth are high, while the return loss and electrical tangent loss are low. While designing a microstrip patch antenna with a bandwidth at the desired resonance frequency and showing band-pass or band-stop characteristics, having a new antenna produced for each change that needs to be made in the microstrip patch antenna according to the measurement results, and making reflection/transmission measurements is time consuming and costly.

Step 1: A parameter width of the radiating patch antenna is compute from this equation:

$$W = \frac{C}{2\,f_r}\sqrt{\frac{2}{\varepsilon_r+1}} \tag{6.1}$$

c: velocity of light, 3*10^8 m/s,

ε_r :dielectric constant of the substrate,

f_r: resonant frequency,

W: width of the patch,

L: length of the Patch,

h: thickness of substrate,

ε_{eff}: effective dielectric constant.

Step 2: Effective dielectric constant of the patch antenna is determined as:

$$\varepsilon_{eff} = \frac{\varepsilon_r + 1}{2} + \frac{\varepsilon_r - 1}{2}\left(\frac{1}{\sqrt{1 + 12\left(\frac{h}{W}\right)}}\right) \tag{6.2}$$

Step 3: Calculation of the effective length at the resonance frequency

$$L_{eff} = \frac{C}{2\, f_r \sqrt{\varepsilon_{eff}}} \tag{6.3}$$

Step 4: Extension length of the patch antenna compute with this equation:

$$\Delta L = h * 0.412 * \frac{(\varepsilon_{eff} + 0.3)\left(\frac{W}{h} + 0.264\right)}{(\varepsilon_{eff} - 0.258)\left(\frac{W}{h} + 0.8\right)} \tag{6.4}$$

Step 5: The length of the patch antenna is as:

$$L = L_{eff} - 2\Delta L \tag{6.5}$$

The size of the rectangular patch antenna is calculated by the formulas shown step by step above [54].

7. ANTENNA PLACEMENTS

Location selection is vital for antenna performance, as aesthetic considerations limit the available mounting positions, and the chosen position significantly affects the antenna's functionality and radiation pattern; thus, antennas can be placed in various locations on the vehicle based on their intended purpose [6], [55], [56], [57]. To determine the ideal position, factors such as the service and frequency band must be taken into account, along with the chosen antenna technology. Figure 7.1 shows alternative positions for antenna placements.

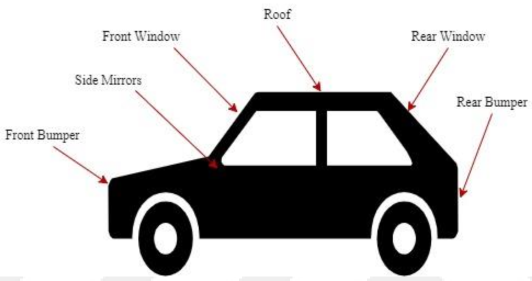

Figure 7.1. Alternative positions for antenna placements

7.1. Roof

Most car manufacturers place antennas on the roof because it is a suitable position for antennas with an omnidirectional pattern, given that the vehicle roof is elevated from the ground.

7.2. Screens and windows

Integrating antenna structures into windshields, rear and side windows has been a popular practice in the automobile industry since 1980. Although the design and testing phase is long, it is a cheap and effective method. Additionally, the glass itself provides ample space to accommodate various antennas.

7.3. Fender and bumper

Fenders and bumpers are usually made of plastic and provide ample space for antenna placement since they do not contain any electronics. However, a drawback of positioning antennas on fenders and bumpers is that these areas are the first to be damaged in a collision. On the other hand, this placement is advantageous for vehicles equipped with an integrated emergency warning system.

7.4. Trunk cover

It is a good solution for the trunk cover, as the antennas cannot be placed on the roof on convertibles. It is only suitable for omnidirectional antennas due to its parallel orientation to the ground.

7.5. Side-Mirrors

Side mirrors are standard equipment on all vehicles, varying in size: smaller for motorcycles and much larger for trucks and buses. Due to their size, there is sufficient space to position the antenna in the rear section of the mirror. The shells of these mirrors are usually made of plastic.

8. MATERIAL AND METHOD

In this study, the aim is to design antennas that can operate in the DSRC frequency band for road applications using the CST program and LPKF device. The study involves simulating these antennas and realizing the most suitable design. To achieve this goal, microstrip antenna designs found in the literature for DSRC applications are examined, leading to the development of a new antenna based on this information. The reason for conducting design and optimization studies using computer-aided simulations is that the actual product manufacturing process, prototype production, testing, and making improvements are costly and time-consuming. Computer-aided simulations allow for the rapid evaluation of different design parameters and facilitate an iterative process to determine the most suitable design.

CST Studio Suite is a high-performance 3D electromagnetic (EM) analysis software designed for the design, analysis, and optimization of electromagnetic components and systems. This advanced simulation software can analyze and design electronic circuit components, including complex microwave, RF printed circuit boards, and antennas. Versatile, user-friendly, efficient, and accurate, CST Studio Suite serves as a comprehensive tool for electromagnetic simulation. It enables users to obtain near and far-field analysis, S-parameters, three-dimensional surface current distributions, and both two- and three-dimensional radiation patterns, along with efficiency, gain, and directivity graphs.

8.1. Simulation Design and Results with FR-4

In the first antenna designed, the length of the feed line of the conventional antenna, the dimensions of the rectangular patch and other parameters are determined by mathematical calculations with the transmission line model. To keep the design cost-effective, FR-4 with relative dielectric constant $\varepsilon_r = 4.3$, loss tangent tanδ = 0.025 is chosen as the suitable substrate material, and the dielectric material thickness is determined as h = 1 mm as is shown in Figure 8.1. The dimensions of the designed antenna are listed in Table 8.1.

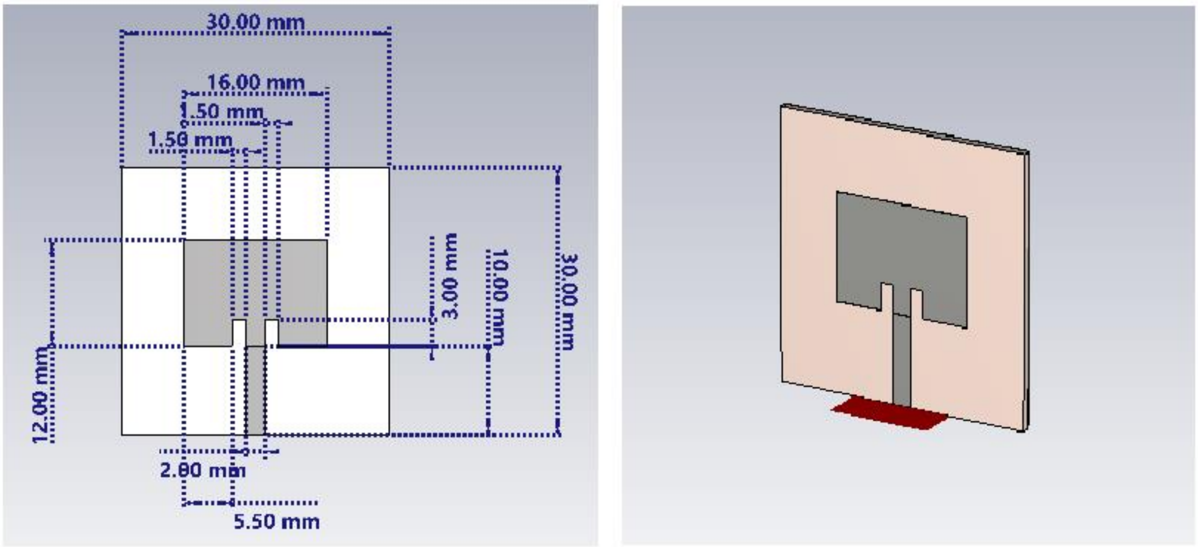

Figure 8.1. Dimensions of designed patch antenna, a) Front view b) Perspective view

Table 8.1. Dimensions of designed patch antenna

Components	Dimensions (mm)
Substrate width	30
Substrate length	30
Substrate thickness	1
Patch width	16
Patch length	12
Feed length	10
Feed width	2
Slot width	1
Slot length	3

An antenna's efficiency in the desired frequency bands can be determined by the return loss value, which represents the ratio of reflected waves to transmitted waves and should be less than -10 dB within that frequency band. The 10 dB bandwidth of the antenna is found to be 203 MHz, ranging from 5.8032 to 6.0066 GHz. The return loss simulation results for the schematic model of the rectangular antenna are shown in Figure 8.2.

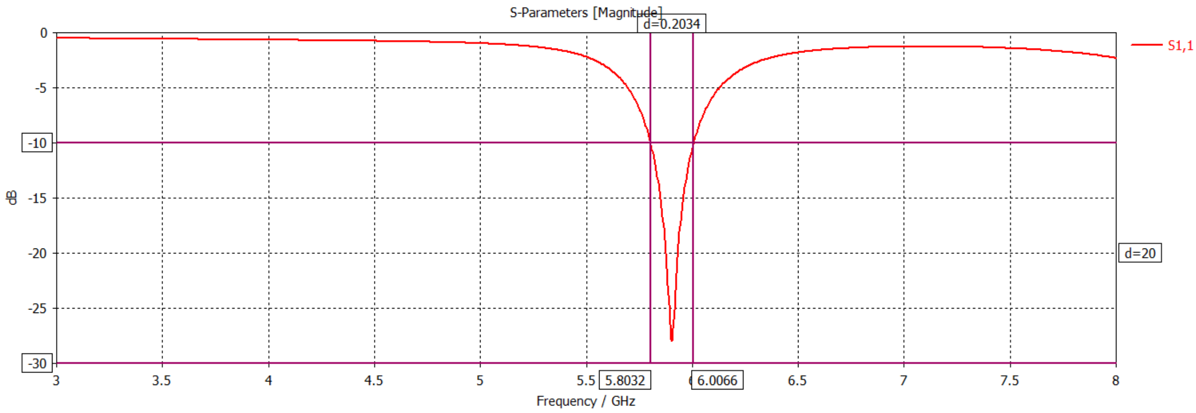

Figure 8.2. S_{11} parameter graph of patch antenna

The VSWR graph shows the reflection ratio of the antenna as a function of frequency. The optimal operating frequency of the antenna is typically at the point where the lowest VSWR value is found. The trends in the graph reveal how efficiently the antenna operates across the frequency range. This graph is a critical tool for evaluating the effectiveness of antenna design and tuning. The theoretical VSWR value ranges from 1 to 2. In this work, the VSWR value at 5.9 GHz is 1.0828551, as shown in Figure 8.3.

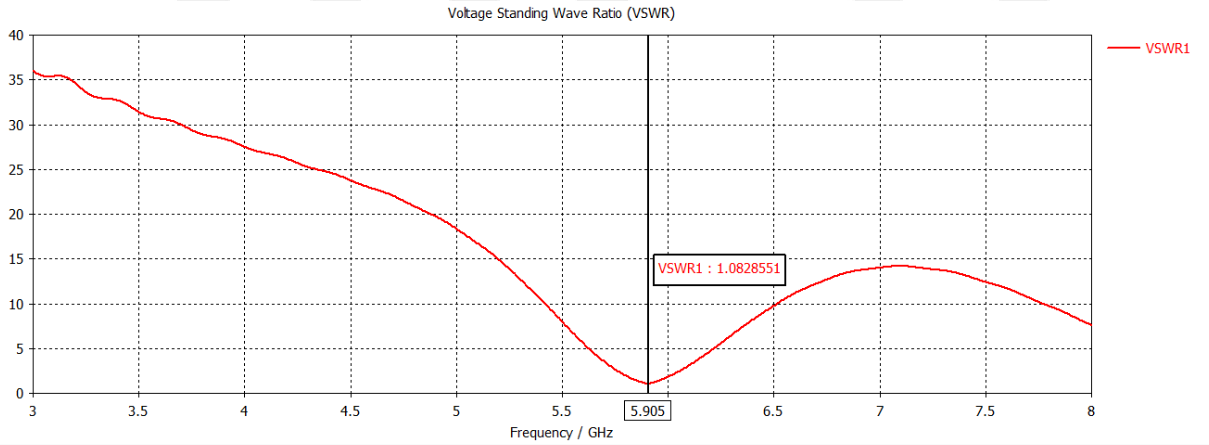

Figure 8.3. VSWR simulated result of patch antenna

Figure 8.4 shows a radiation diagram of the angular variation of the power (electromagnetic field strength) emitted by the antenna at a fixed distance, which is created in a certain distant area of the antenna.

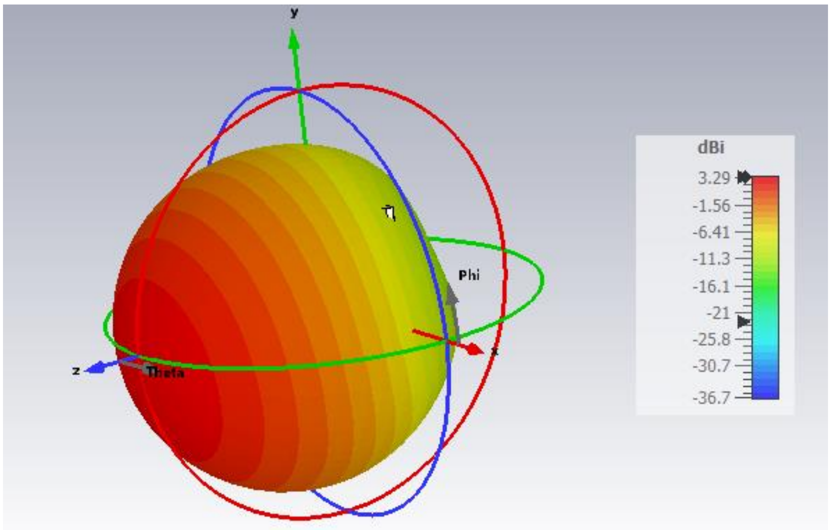

Figure 8.4. 3D Radiation Pattern of patch antenna

Figure 8.5 shows radiation patterns of the designed antenna. For phi=0° at 5.9 GHz, the amplitude (maximum gain) of the main lobe is 3.22 dB and the 3dB angular bandwidth (HPBW) is 84.1°. For phi=90° at 5.9 GHz, the amplitude of the main lobe is 3.29 dB and the 3dB angular bandwidth (HPBW) is 87.7°.

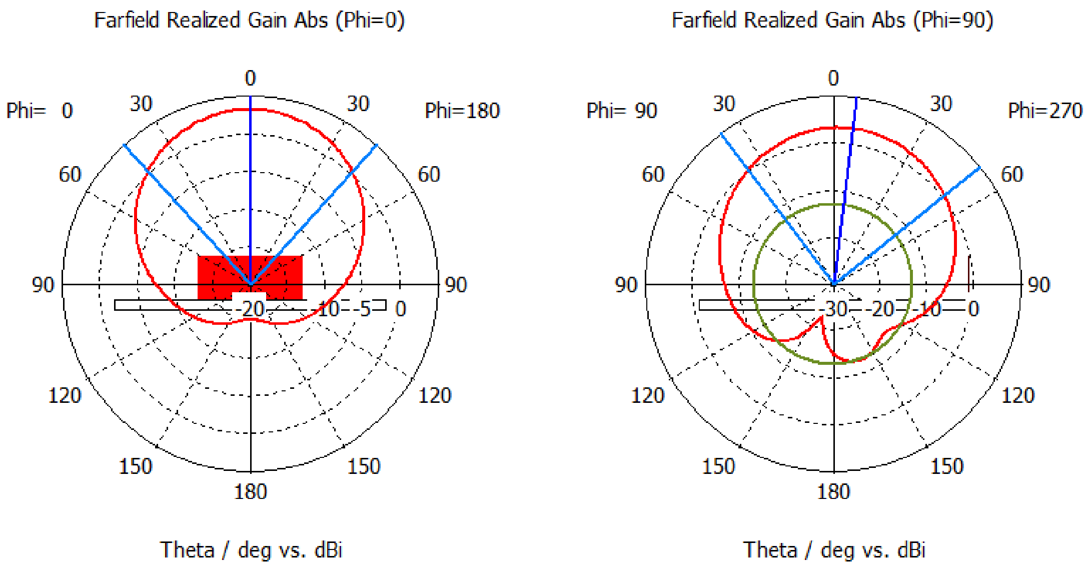

Figure 8.5. Far-field Radiation Pattern at Phi=0° and Phi=90°

Once a single patch element is designed to meet the desired antenna performance, the next step involved combining these patch elements to create a two-element antenna. It is common to use microstrip antennas not only as single elements but also in arrays. In this part, a new directional microstrip array antenna (DMAA) is proposed for V2V applications.

Arrays can be employed to create essential patterns that cannot be achieved with a single element. The array antenna system enhances directivity and gain, while also serving various other functions that would be complicated with just one element.

The elements of a microstrip array are fed using various feeding methods to enhance the performance of antenna systems. When a single feed line is used, all elements receive the same signal through this line, providing a simple and low-cost solution. However, the elements of a microstrip array can also be fed using multiple lines. On the other hand, when multiple feed lines are employed, independent feeding for each element can be achieved. Feeding networks are generally classified into three main categories:

1. Series Feed: The elements are connected in sequence along the feed line.
2. Corporate Feed: Each element is connected to a central feed point.
3. Series-Corporate Feed: This structure is created by combining both methods.

In the second phase of the study, a 2×1 Rectangular Microstrip Patch Array Antenna (RMSPAA) with a corporate feeding network has been designed, and this antenna consists of a two-element array with a spacing of 51.68 mm between the patch centers, as shown in Figure 8.6.

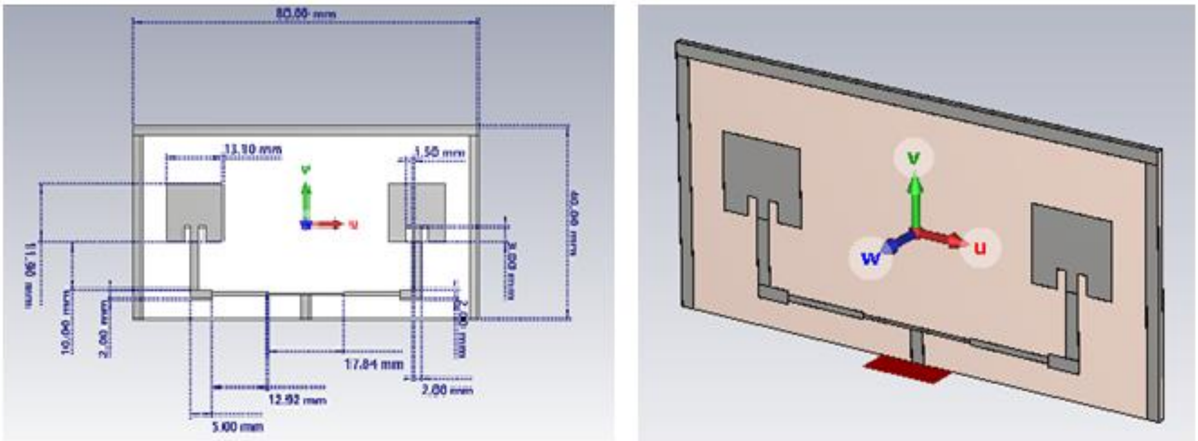

Figure 8.6. Dimensions of the designed two-element array antenna

Table 8.2. Dimensions of designed antenna-2

Components	Dimensions (mm)
Substrate width	80
Substrate length	40
Substrate thickness	1
Patch width	13.1
Patch length	11.9
Feed length	10
Feed width	2
Slot width	1.5
Slot length	3
50 ohm transmission line width	2
50 ohm transmission line length	5
70 ohm transmission line width	1
70 ohm transmission line length	12.92
100 ohm transmission line width	0,5
100 ohm transmission line length	17.84

The graph of the antenna's S_{11} parameter is shown in Figure 8.7. As shown in the graph, the antenna's return loss is around -55 dB and operates at a center frequency of 5.9 GHz, with a bandwidth of 180 MHz (5.8131 – 5.9934 GHz).

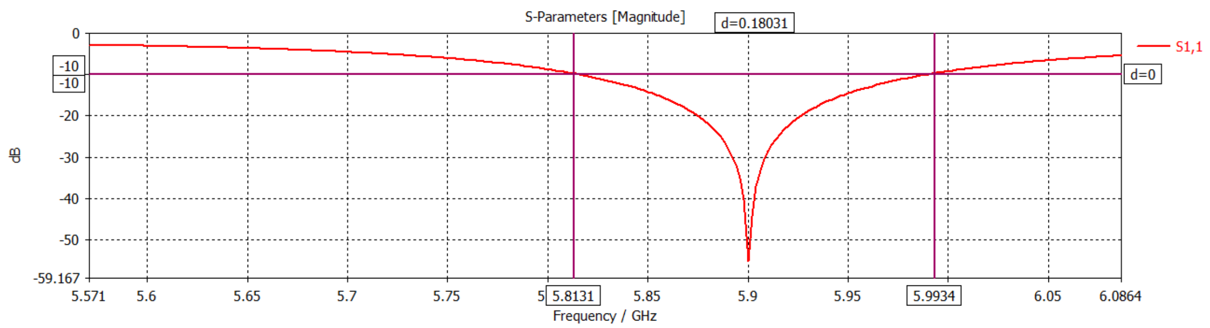

Figure 8.7. S_{11} parameter graph of two-element array antenna

The two-element array antenna has a VSWR value of 1.0034696 at 5.9 GHz, as shown in the simulated plot in Figure 8.8.

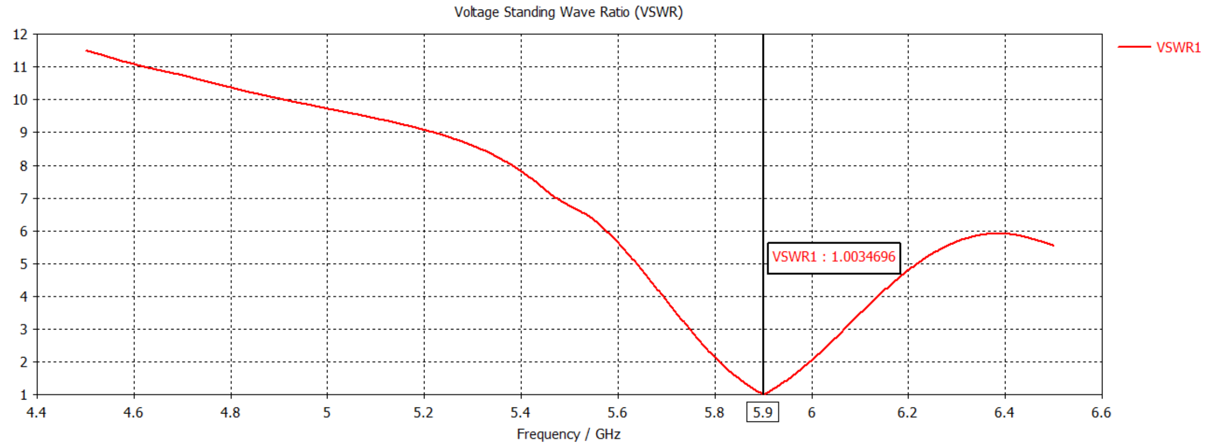

Figure 8.8. VSWR simulated result of two-element array antenna

The far field gain of 3D radiation pattern is shown in Figure 8.9. According to the figure, the 3D far field gain value is 5.704 dBi and total efficiency value is -5.372 dB at 5.9 GHz.

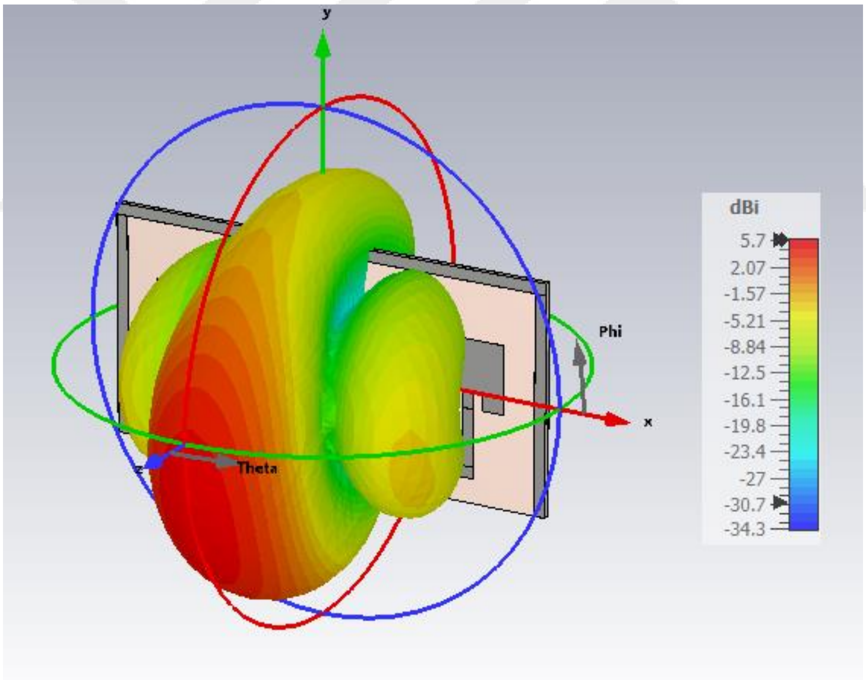

Figure 8.9. 3D Radiation Pattern of two-element array antenna

Figure 8.10 shows radiation patterns of the designed array antenna. For phi=0° at 5.9 GHz, the amplitude of the main lobe is 4.77 dB and the 3 dB angular bandwidth (HPBW) is 28.4°. For phi=90° at 5.9 GHz, the amplitude of the main lobe is 5.88 dB and the 3 dB angular bandwidth (HPBW) is 72°.

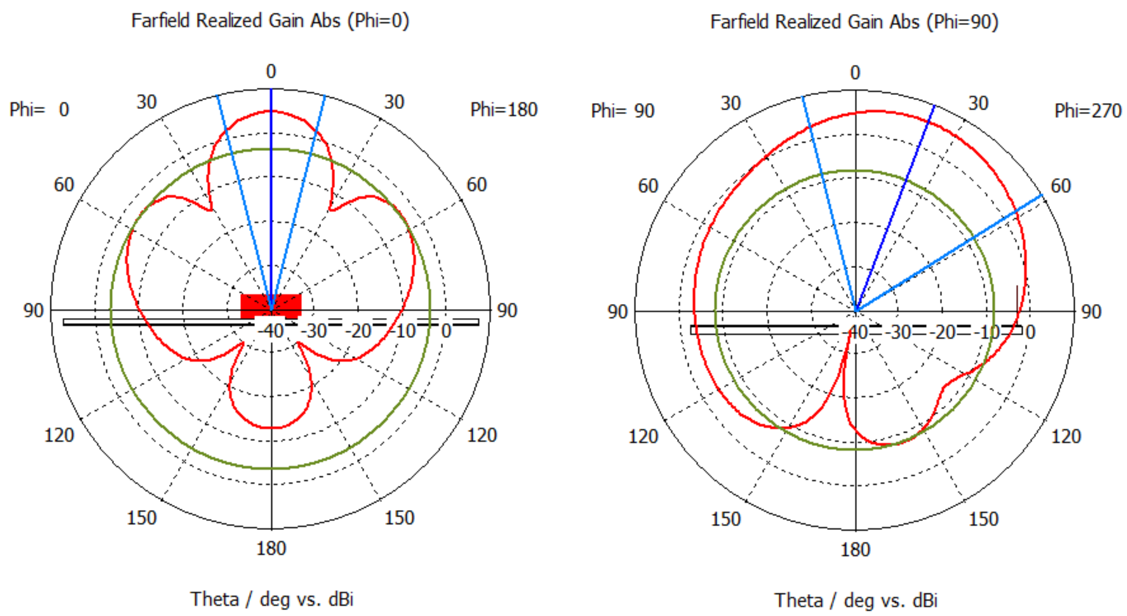

Figure 8.10. Far-field Radiation Pattern at Phi=0° and Phi=90°

In this part, a new dipole microstrip antenna is proposed for V2V application. The designed antenna, along with its dimensions, is shown from different angles in Figure 8.11. VSWR, radiation pattern and gain of the antenna are analyzed numerically using the software of CST. In order for the designed antenna to be low cost, FR-4 with relative dielectric constant $\varepsilon_r = 4.3$, loss tangent tanδ = 0.035 is preferred as the suitable substrate material, and the dielectric material thickness is determined as h = 1 mm.

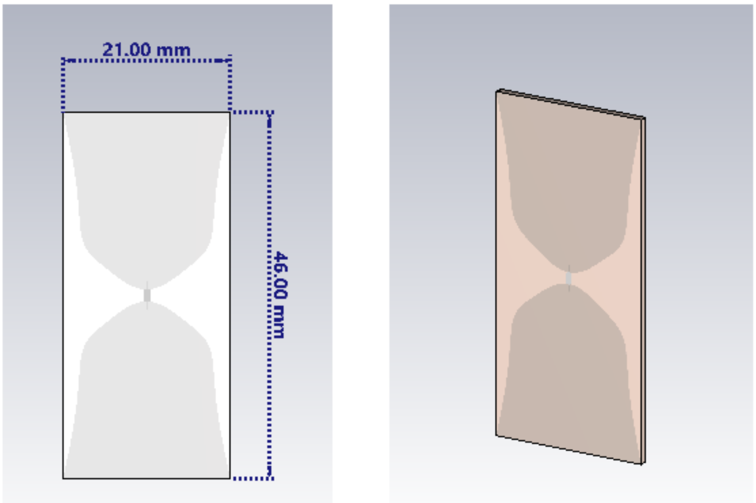

Figure 8.11. Dimensions of the designed antenna

The return loss of the designed third antenna is approximately -21 dB, as shown in Figure 8.12, which indicates that the antenna has a bandwidth of 2201 MHz, spanning from 4.3031 GHz to 6.5047 GHz.

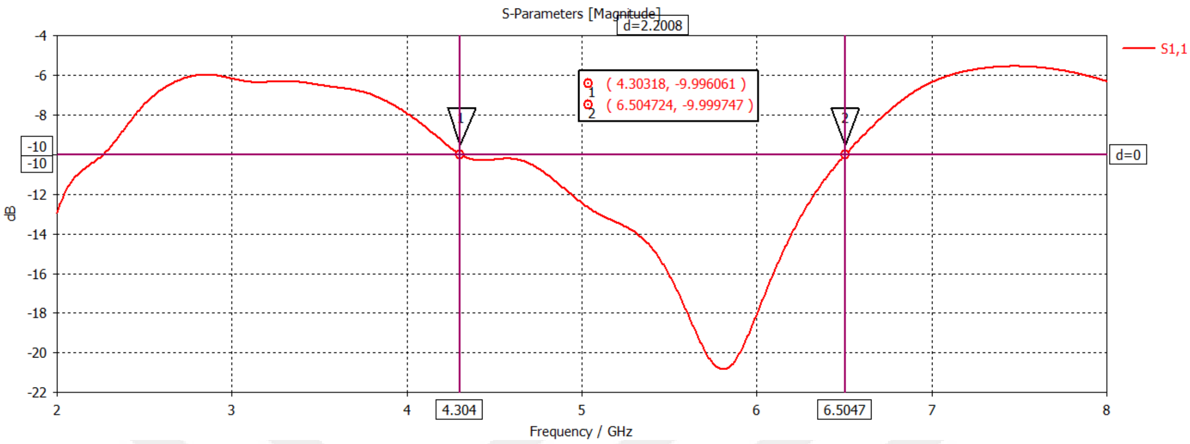

Figure 8.12. S_{11} graph of dipole antenna

The dipole microstrip antenna has a VSWR value of 1.1996785 at 5.9 GHz, as shown in the simulated plot in Figure 8.13.

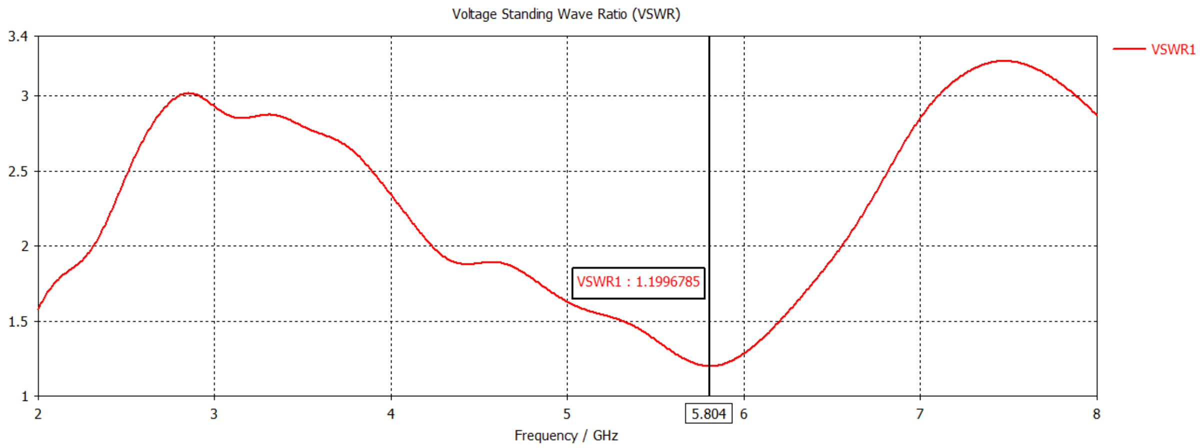

Figure 8.13. VSWR simulated result of dipole antenna

The far-field gain of the 3D radiation pattern, shown in Figure 8.14, indicates a value of 6.037 dBi at 5.9 GHz.

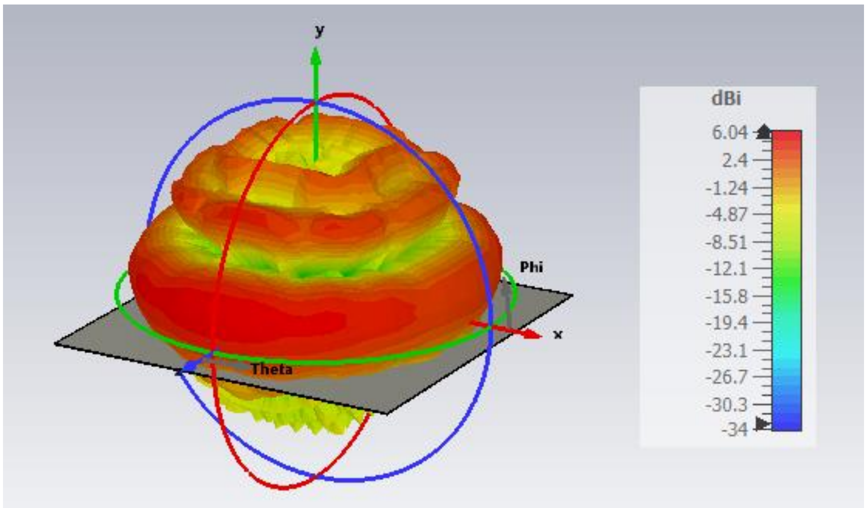

Figure 8.14. 3D Radiation Pattern of dipole antenna

Figure 8.15 shows radiation patterns for phi=0° at 5.9 GHz, the amplitude of the main lobe is 3.97 dBi, for phi=90° at 5.9 GHz, the amplitude of the main lobe is 6.07 dB and the 3dB angular bandwidth (HPBW) is 24°.

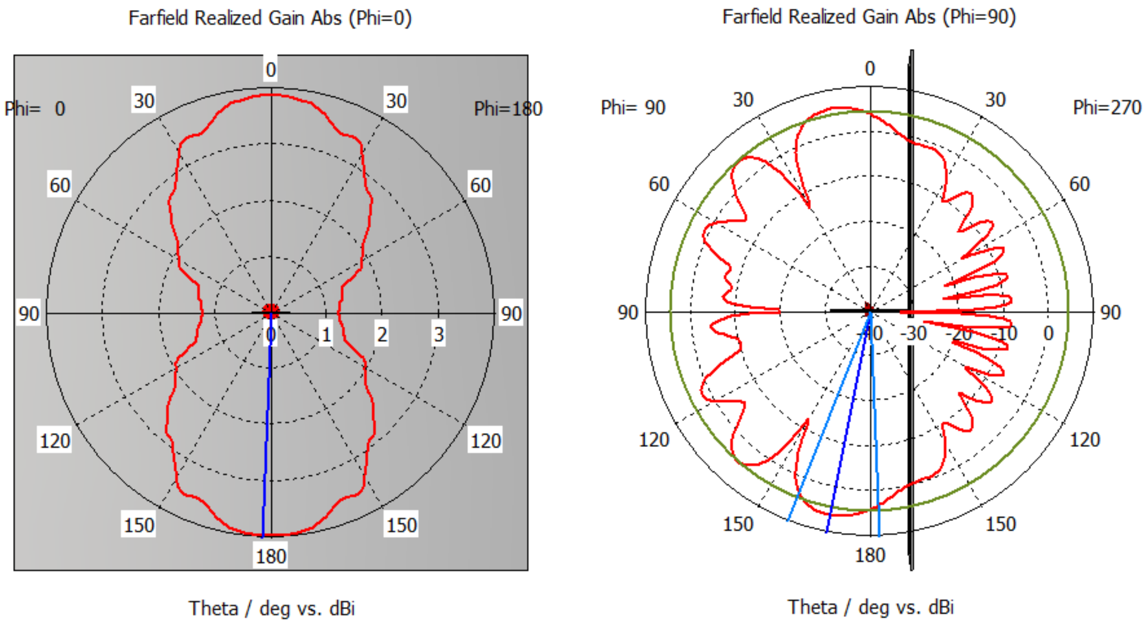

Figure 8.15. Far-field Radiation Pattern at Phi=0° and Phi=90°

A regular hexagonal microstrip antenna featuring shorting pins and V-shaped slots has been designed for V2V applications. The Return Loss, VSWR, radiation pattern, and gain of the antenna have been analyzed numerically using CST software. For the substrate material, FR4 is selected due to its favorable properties, characterized by a relative dielectric constant ε_r = 4.3, loss tangent tanδ = 0.035. The thickness of the dielectric material is set at h = 3 mm, as illustrated in Figure 8.16.

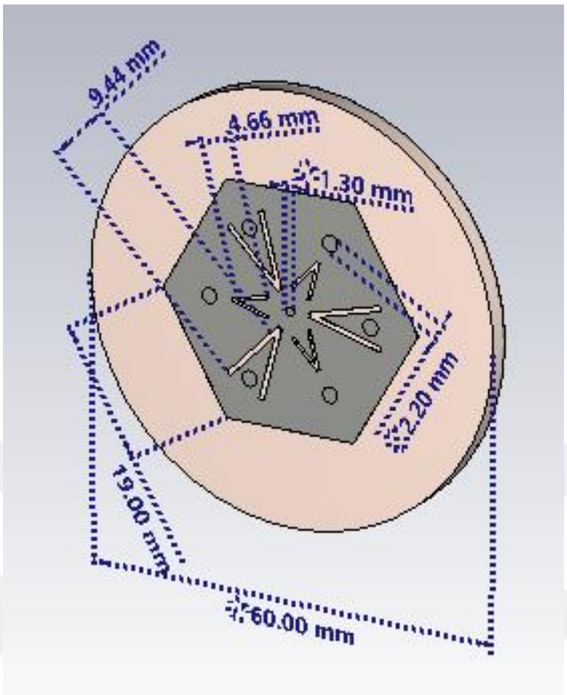

Figure 8.16. Dimensions of designed hexagon microstrip antenna

The bandwidth of the antenna is determined to be 102 MHz, ranging from 5.847 to 5.9492 GHz, while the return loss simulation results for the schematic model of the rectangular antenna are approximately -15 dB and are presented in Figure 8.17.

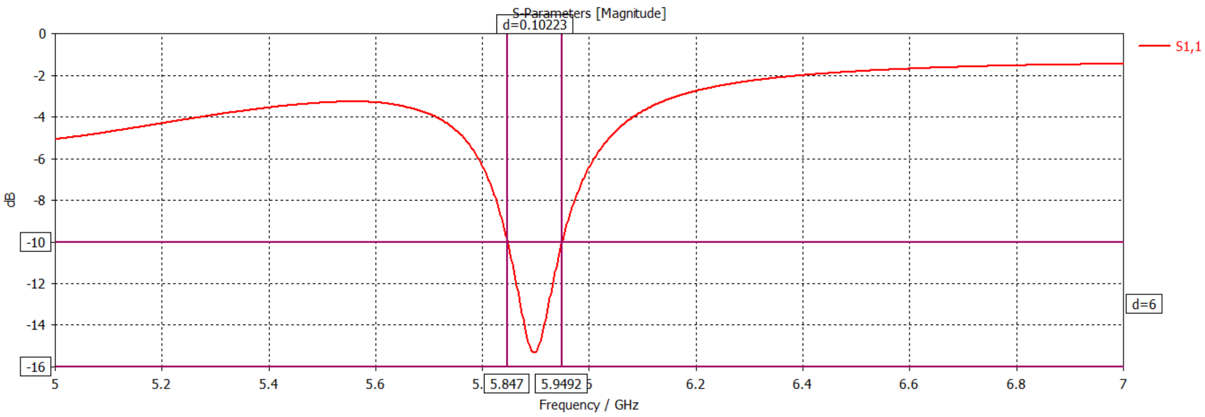

Figure 8.17. S_{11} graph of hexagon microstrip antenna

The hexagon microstrip antenna has a VSWR value of 1.4129257 at 5.9 GHz, as shown in the simulated plot in Figure 8.18.

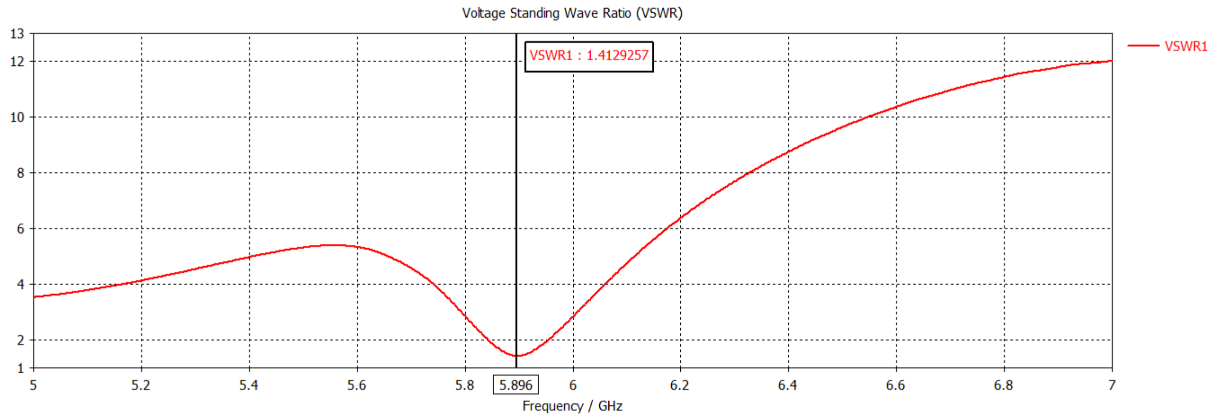

Figure 8.18. VSWR simulated result of hexagon microstrip antenna

The far-field gain of the 3D radiation pattern, illustrated in Figure 8.19, has the value of 4.88 dBi at 5.9 GHz.

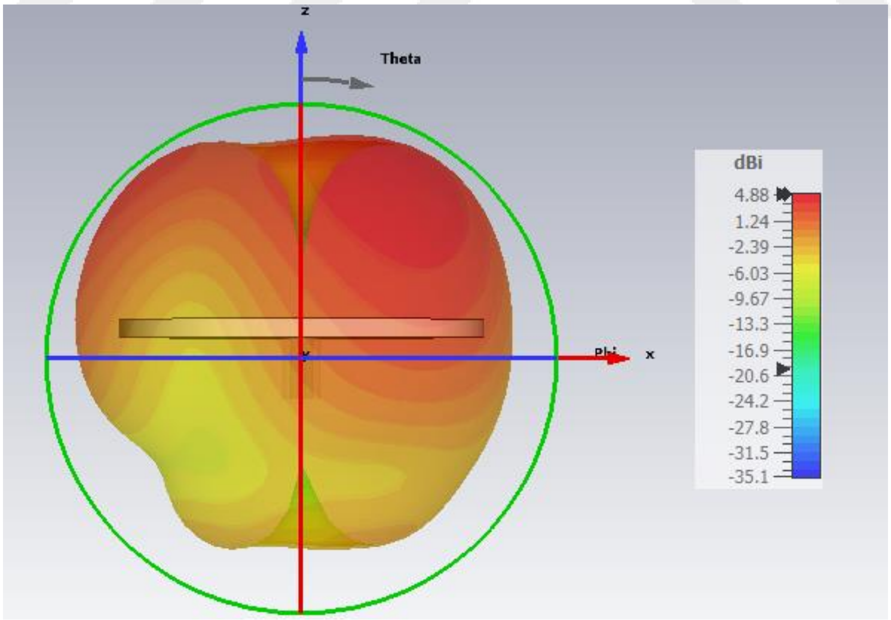

Figure 8.19. 3D Radiation Pattern of hexagon microstrip antenna

Figure 8.20 shows radiation patterns for phi=90° at 5.9 GHz, the amplitude of the main lobe is 3.64 dBi and the 3dB angular bandwidth (HPBW) is 59.5°.

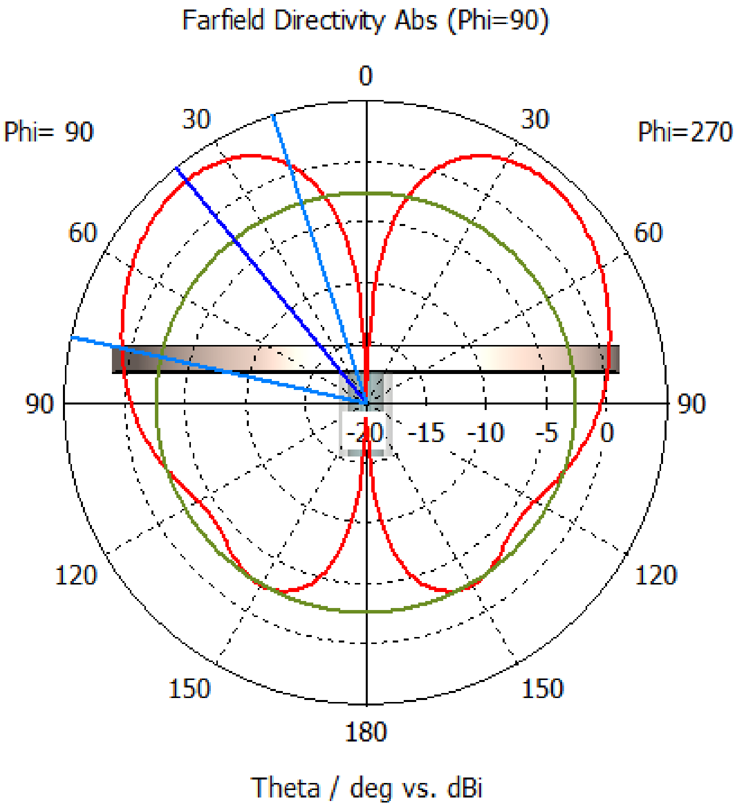

Figure 8.20. Far-field Radiation Pattern at Phi=90°

Due to ease of manufacturing, the regular hexagonal microstrip antenna has been optimized with a substrate thickness of 1 mm. Center frequency alignment optimization has been achieved by adjusting the patch size while keeping the shorting pins and V-shaped slots design unchanged. The new antenna dimensions resulting from the change in substrate thickness are shown in Figure 8.21.

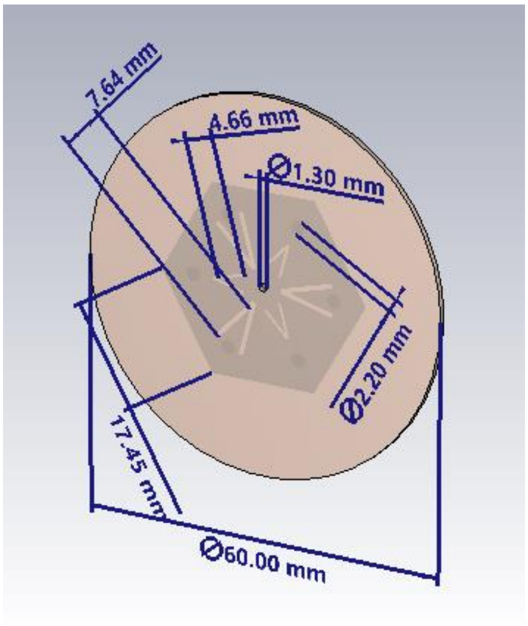

Figure 8.21. Dimensions of designed second hexagon microstrip antenna

The bandwidth of the antenna is determined to be 232 MHz, ranging from 5.794 to 6.026 GHz, while the return loss simulation results for the schematic model of the rectangular antenna are approximately -17 dB and are presented in Figure 8.22.

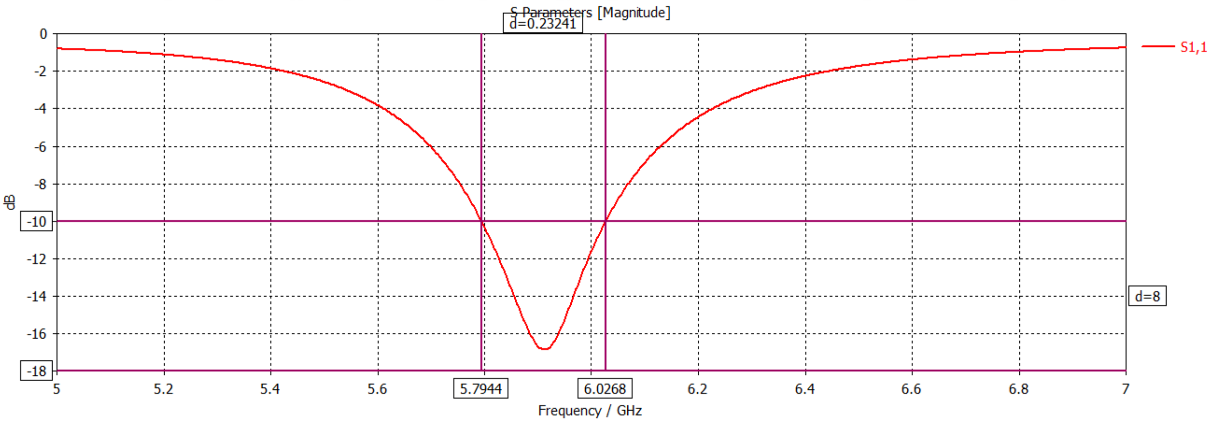

Figure 8.22. S_{11} parameter graph of second hexagon microstrip antenna

The optimized substrate thickness of the hexagon microstrip antenna has a VSWR value of 1.3348526 at 5.9 GHz, as shown in the simulated plot in Figure 8.23.

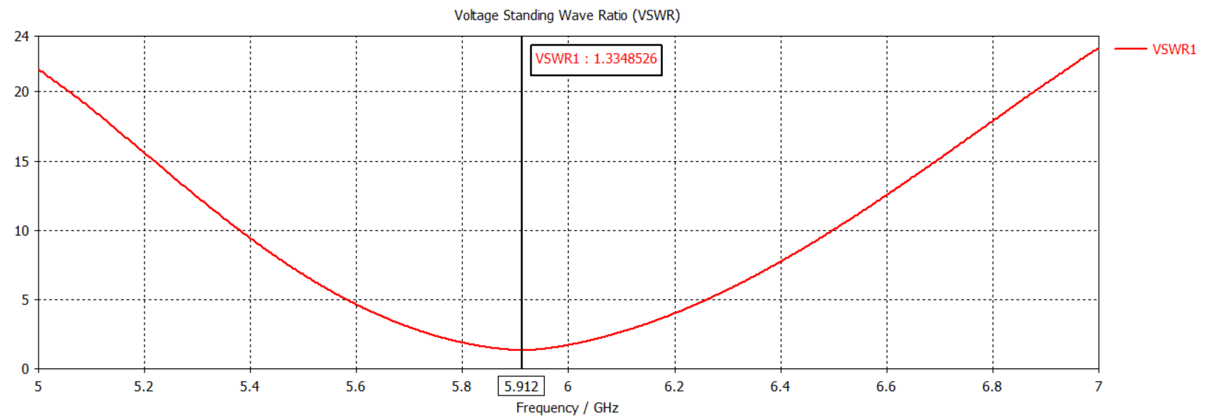

Figure 8.23. VSWR simulated result of second hexagon microstrip antenna

The far field gain of 3D radiation pattern is shown in Figure 8.24. According to the figure, the 3D far field gain value is 4.43 dBi at 5.9 GHz.

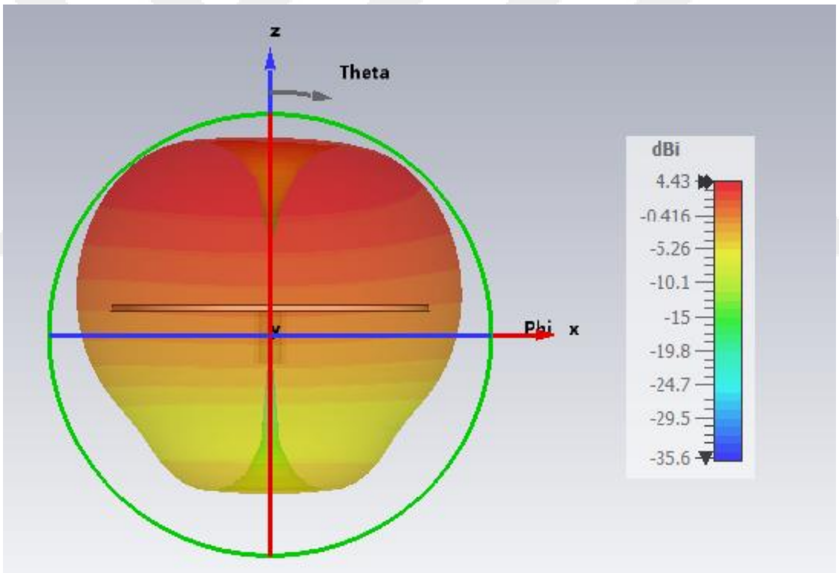

Figure 8.24. 3D Radiation Pattern of second hexagon microstrip antenna

Figure 8.25 shows radiation patterns for phi=90° at 5.9 GHz, the amplitude of the main lobe is 4.43 dBi and the 3dB angular bandwidth (HPBW) is 53.8°.

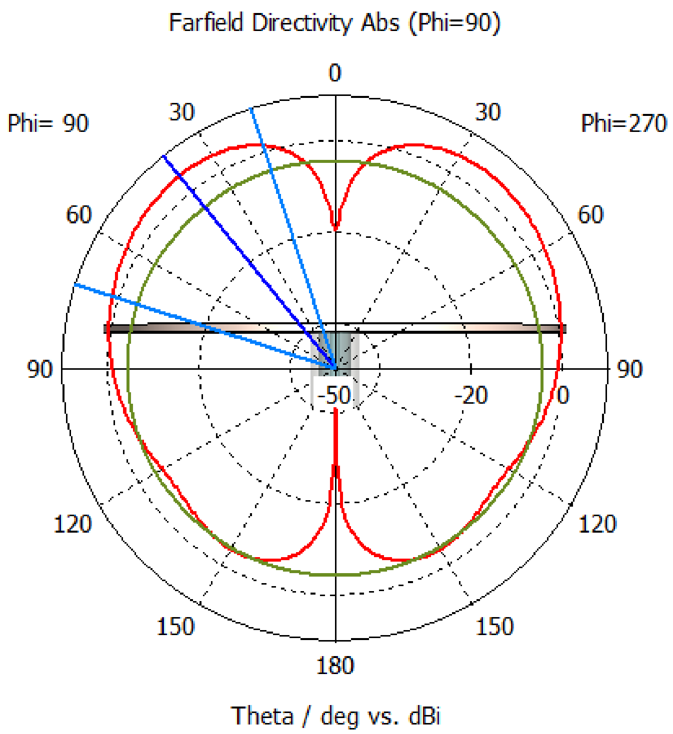

Figure 8.25. Far-field Radiation Pattern at Phi=90°

8.2. Simulation Design and Results with ROGERS RT5880

In the previous sections, issues such as adjusting the size of the substrate used in the microstrip patch antenna and the effect of its electrical permittivity on antenna performance are discussed, leading to optimal selections. In this section, parameters such as patch size, substrate dimensions (width and length), and feeding inlet dimensions of the microstrip antenna will be minimally altered, and simulation studies will be conducted using the RT5880 substrate. The dielectric constant of the Rogers RT5880 substrate is 2.2, and the changes in the physical dimensions required for the operating frequency of 5.9 GHz are shown in the table below (as illustrated in Figure 8.26).

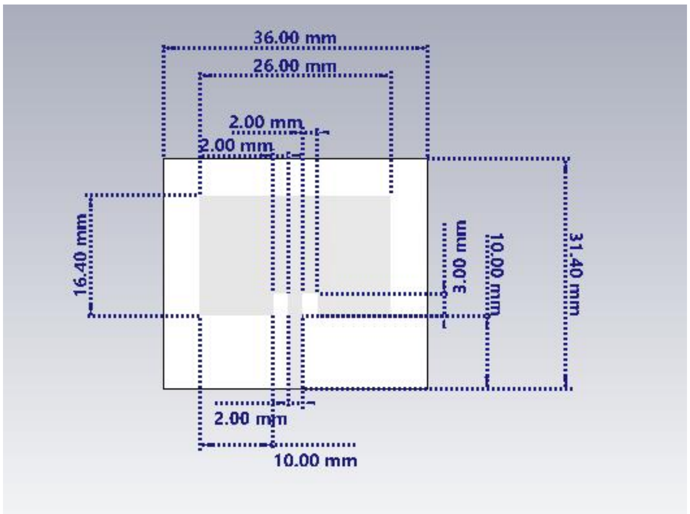

Figure 8.26. Dimensions of designed patch antenna with RT5880

In Figure 8.27, the graph of the antenna's S_{11} parameter is presented. As shown in the graph, the antenna operates at a center frequency of 5.9 GHz, with a return loss of -38.8 dB and a bandwidth of 145 MHz (5.8266 – 5.9725 GHz).

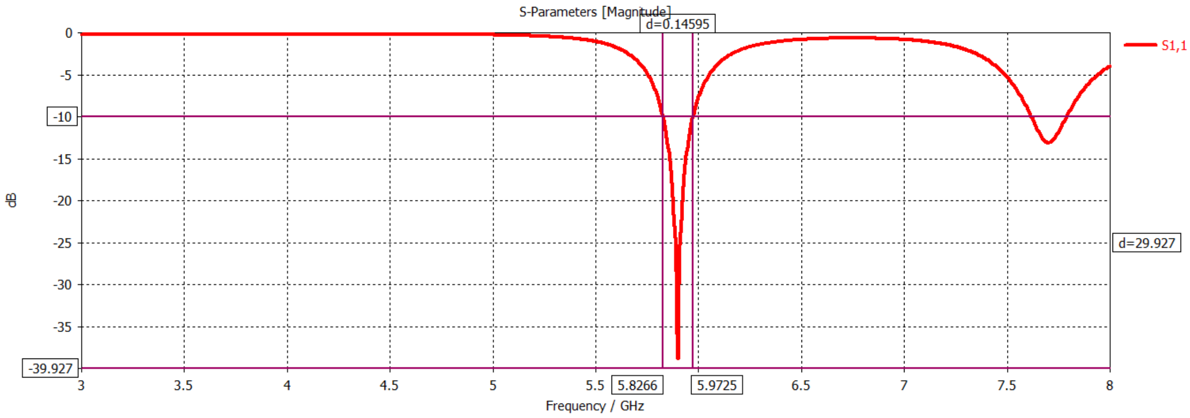

Figure 8.27. S_{11} graph of patch antenna with RT5880

The designed patch antenna with RT5880 has a VSWR value of 1.0231604 at 5.9 GHz, as shown in the simulated plot in Figure 8.28.

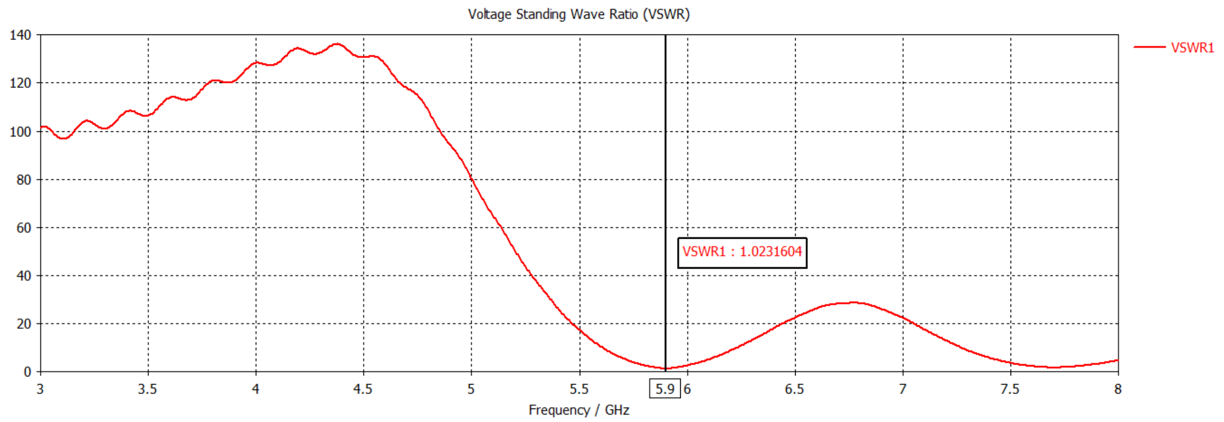

Figure 8.28. VSWR simulated result of patch antenna with RT5880

As seen in the Figure 8.29, the gain is obtained as 7.81 dBi at the 5.9 GHz center frequency. It is observed that the antenna gain increased by 137% when Rogers substrate is preferred compared to the FR-4 substrate.

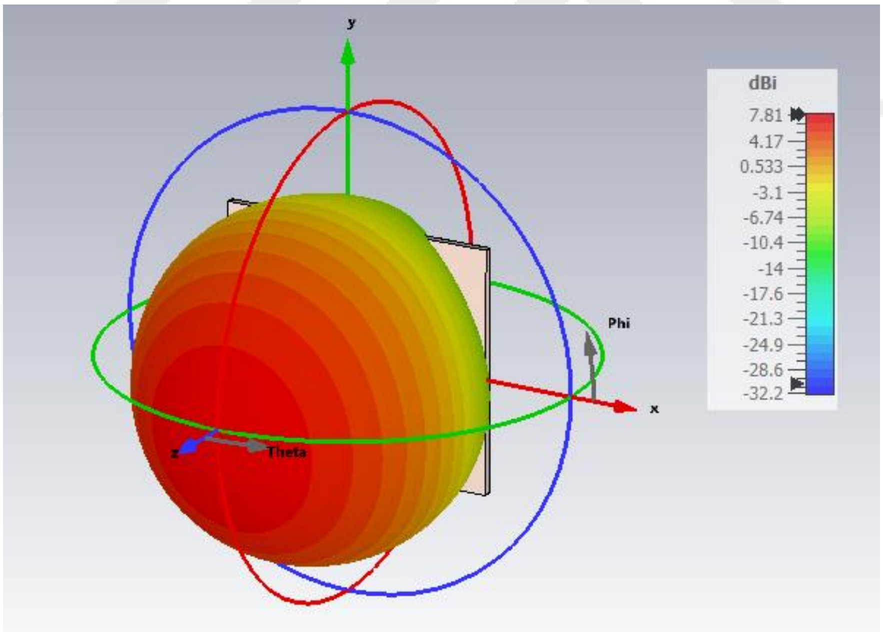

Figure 8.29. 3D Radiation Pattern of patch antenna with RT5880

Figure 8.30 shows radiation patterns for phi=0° at 5.9 GHz, the amplitude (maximum gain) of the main lobe is 7.76 dB and the 3dB angular bandwidth (HPBW) is 69.6°, for phi=90° at 5.9

GHz, the amplitude of the main lobe is 7.81 dB and the 3dB angular bandwidth (HPBW) is 76.8°.

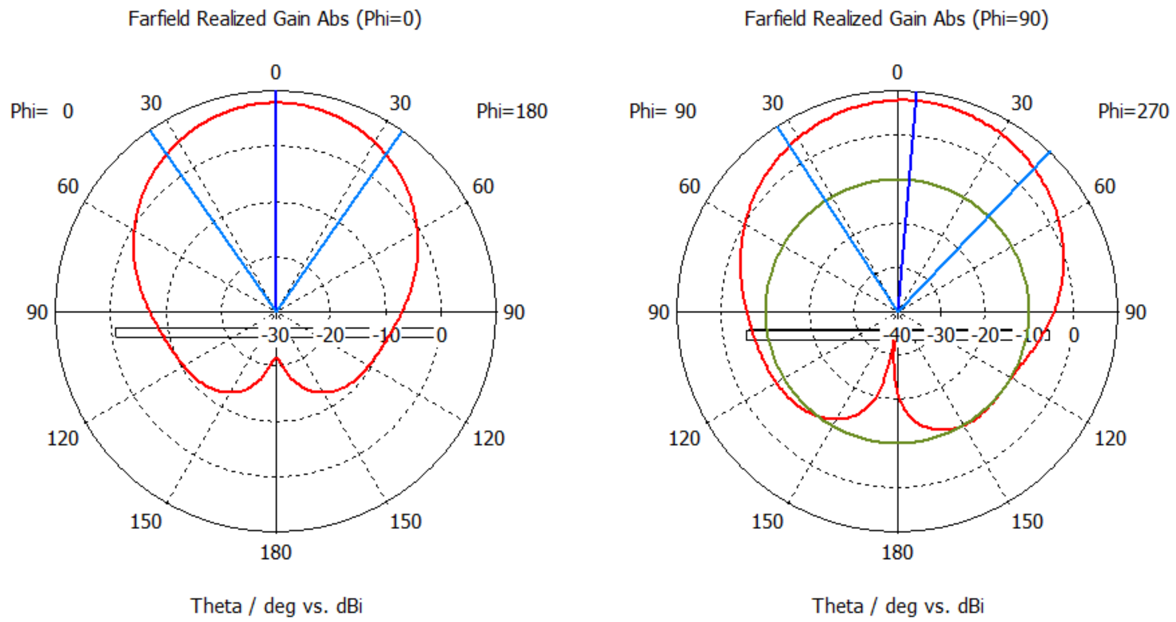

Figure 8.30. Far-field Radiation Pattern at Phi=0° and Phi=90°

The proposed RMSPAA modified with RT5880 substrate for working frequency of 5.9 GHz as is shown in Figure 8.31. With these simulation results, the total area of the antenna has increased by 14%.

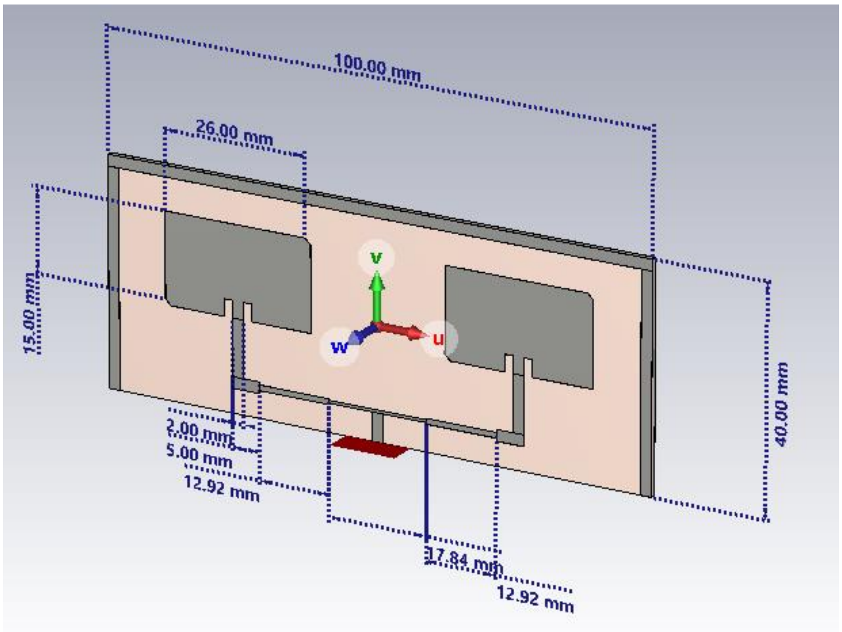

Figure 8.31. Dimensions of the designed two-element array antenna with RT5880

The return loss of the proposed RMSPAA is approximately -13 dB, as illustrated in Figure 8.32, with the antenna's bandwidth measured at 74 MHz, ranging from 5.9045 to 5.9786 GHz, indicating a 58% decrease compared to the FR-4 substrate.

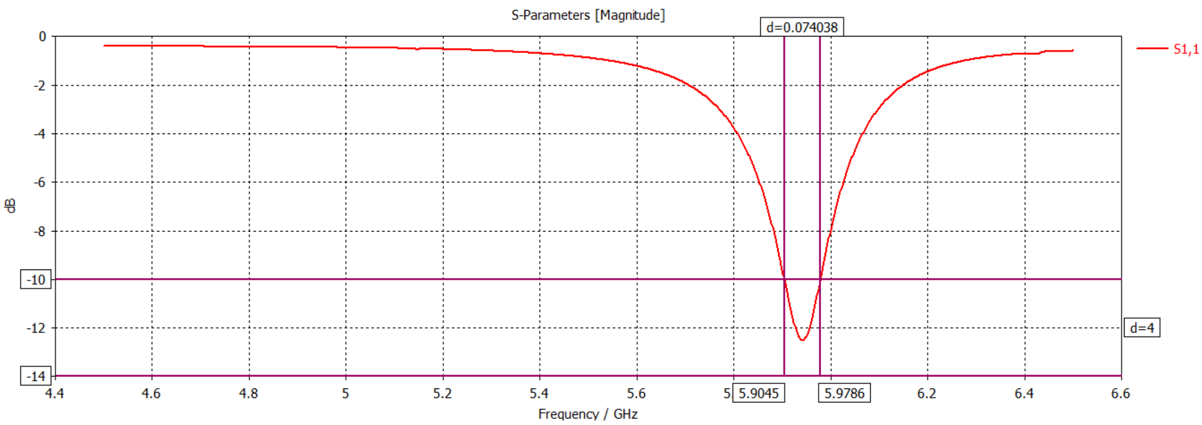

Figure 8.32. S_{11} graph of two-element array antenna with RT5880

In this work VSWR value is 1.6211939 at 5.9 GHz and figure 8.33 illustrates the simulated result of VSWR against frequency (GHz).

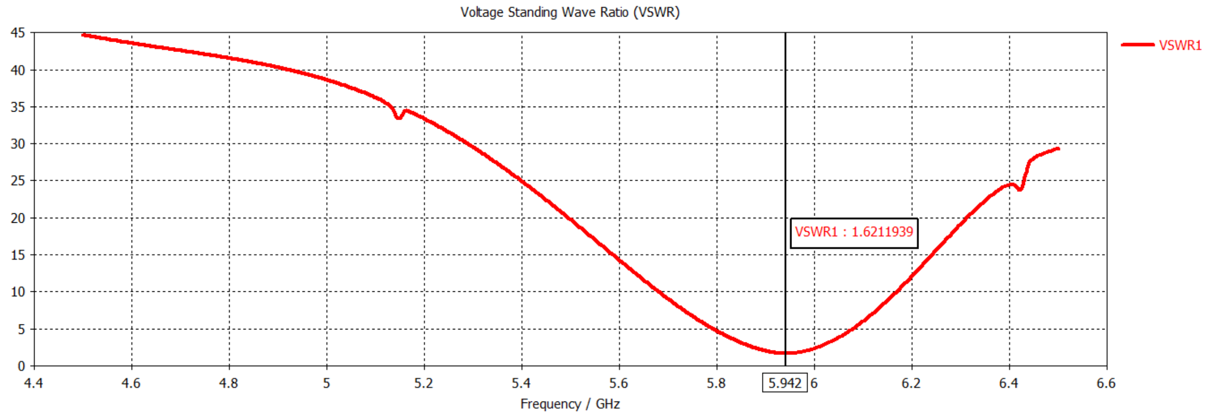

Figure 8.33. VSWR simulated result of two-element array antenna with RT5880

As seen in Figure 8.34, the gain is determined as 10.8 dBi at the 5.9 GHz center frequency. It is observed that the antenna gain increases by 83% when the Rogers substrate is used compared to the FR-4 substrate.

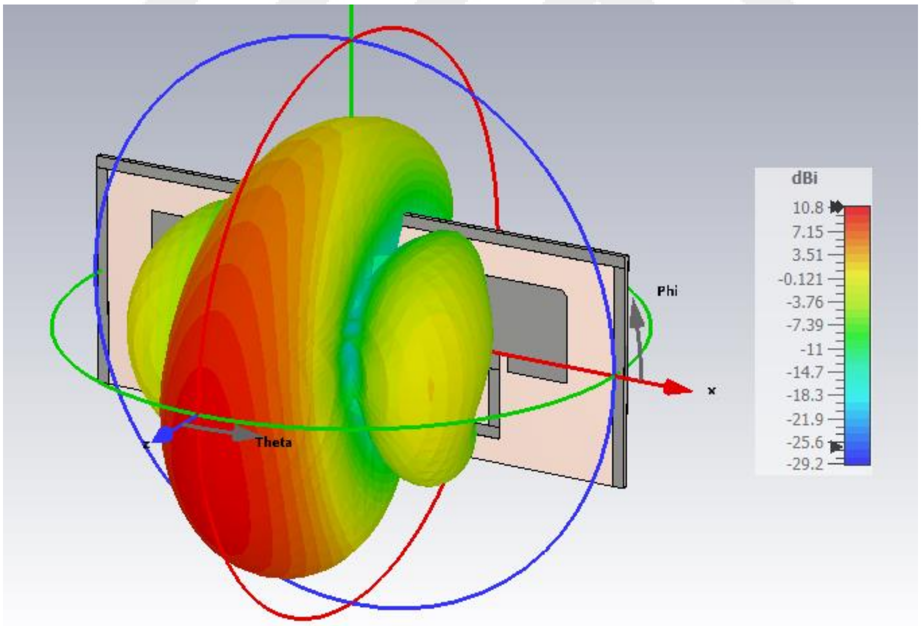

Figure 8.34. 3D Radiation Pattern of two-element array antenna with RT5880

Figure 8.35 shows radiation patterns for phi=0° at 5.9 GHz, the amplitude (maximum gain) of the main lobe is 10.3 dB and the 3dB angular bandwidth (HPBW) is 26°, for phi=90° at 5.9

GHz, the amplitude of the main lobe is 10.8 dB and the 3 dB angular bandwidth (HPBW) is 73.6°.

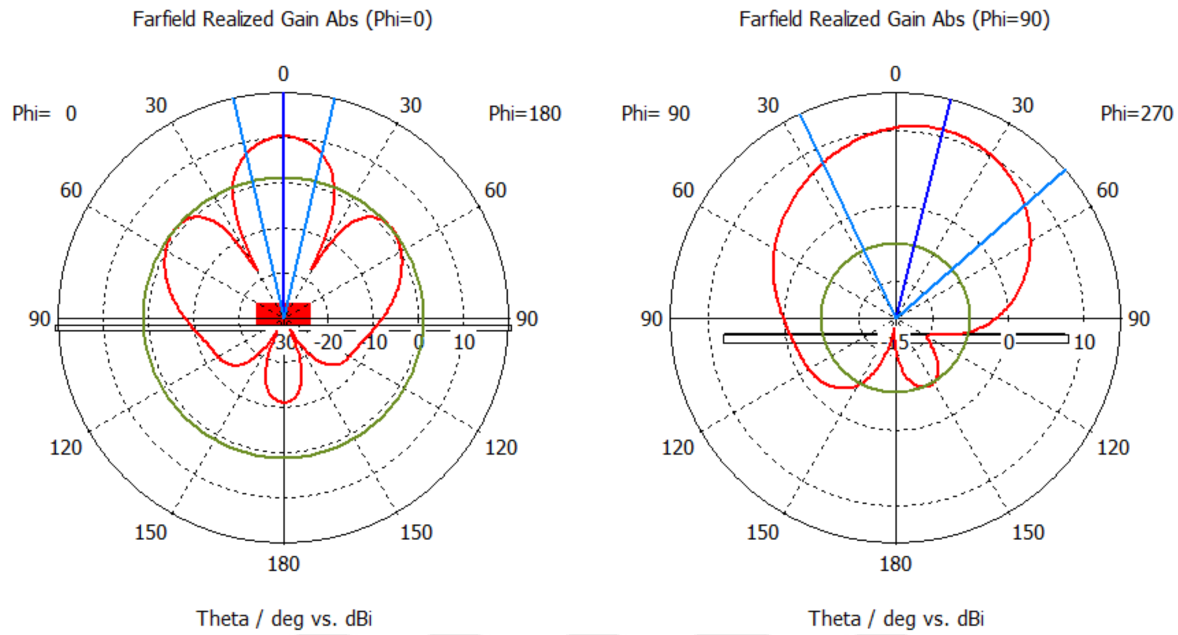

Figure 8.35. Far-field Radiation Pattern at Phi=0° and Phi=90°

The proposed dipole microstrip antenna modified with RT5880 substrate for working frequency of 5.9 GHz is shown in Figure 8.36. With these simulation results, the total area of the antenna has increased by 11%.

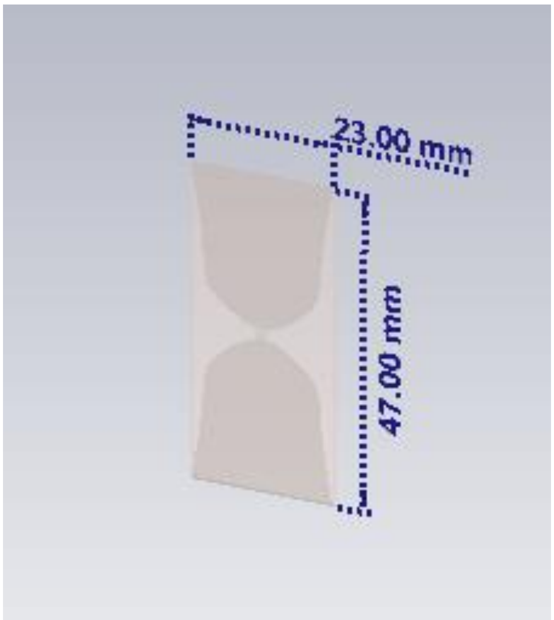

Figure 8.36. Dimensions of the designed dipole antenna with RT5880

In Figure 8.37, the graph of the antenna's S_{11} parameter is presented. As shown in the graph, the antenna operates at a center frequency of 5.88 GHz, with a return loss of -15.6 dB and a bandwidth of 1667 MHz (4.882 – 6.549 GHz).

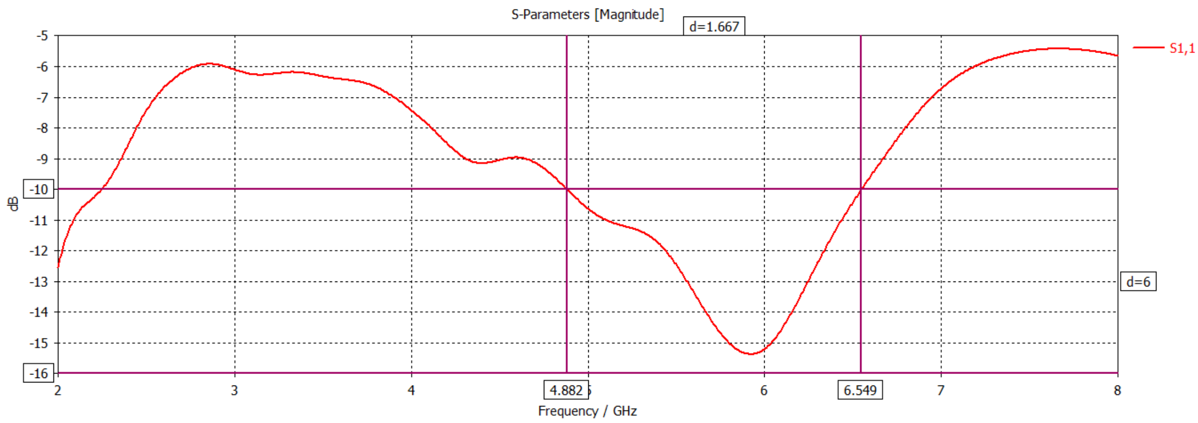

Figure 8.37. S_{11} graph of the designed dipole antenna with RT5880

In this work VSWR value is 1.4391463 at 5.9 GHz. Figure 8.38 shows the simulated result of VSWR against frequency (GHz).

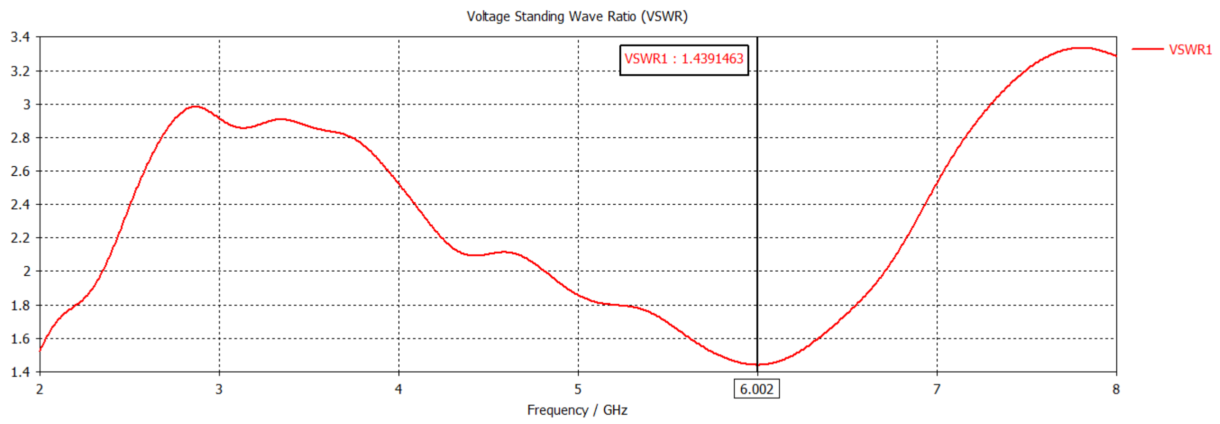

Figure 8.38. VSWR simulated result of the designed dipole antenna with RT5880

The far field gain of 3D radiation pattern is shown in Figure 8.39. According to the figure, the 3D far field gain value is 6.1 dBi at 5.9 GHz. It is observed that the antenna gain is increased by 1% when Rogers substrate is preferred compared to the FR-4 substrate.

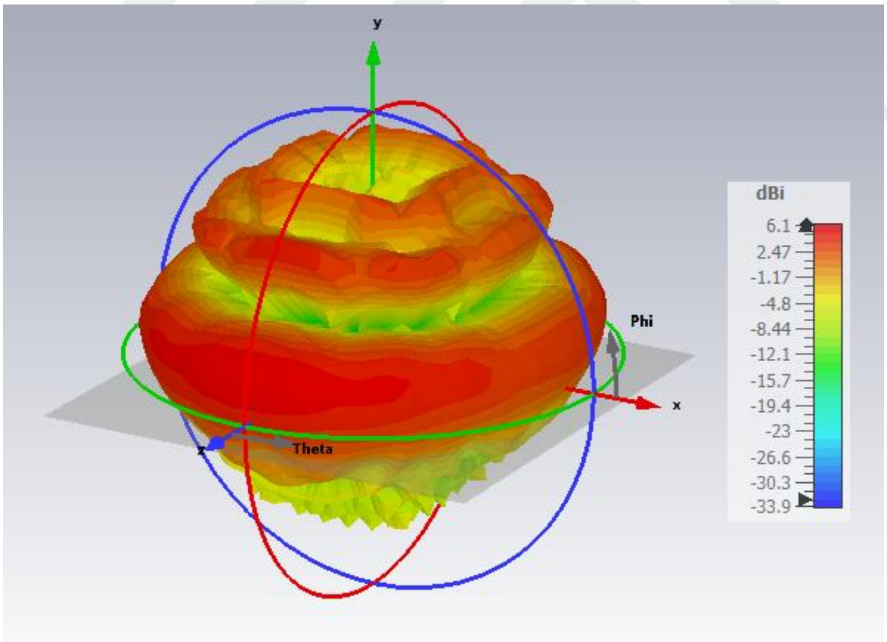

Figure 8.39. 3D Radiation Pattern of the designed dipole antenna with RT5880

Figure 8.40 shows radiation patterns for the designed antenna. For phi=0° at 5.9 GHz, the amplitude (maximum gain) of the main lobe is 4.04 dB and the 3dB angular bandwidth (HPBW) is 157.5°. For phi=90° at 5.9 GHz, the amplitude of the main lobe is 6.14 dB and the 3dB angular bandwidth (HPBW) is 24°.

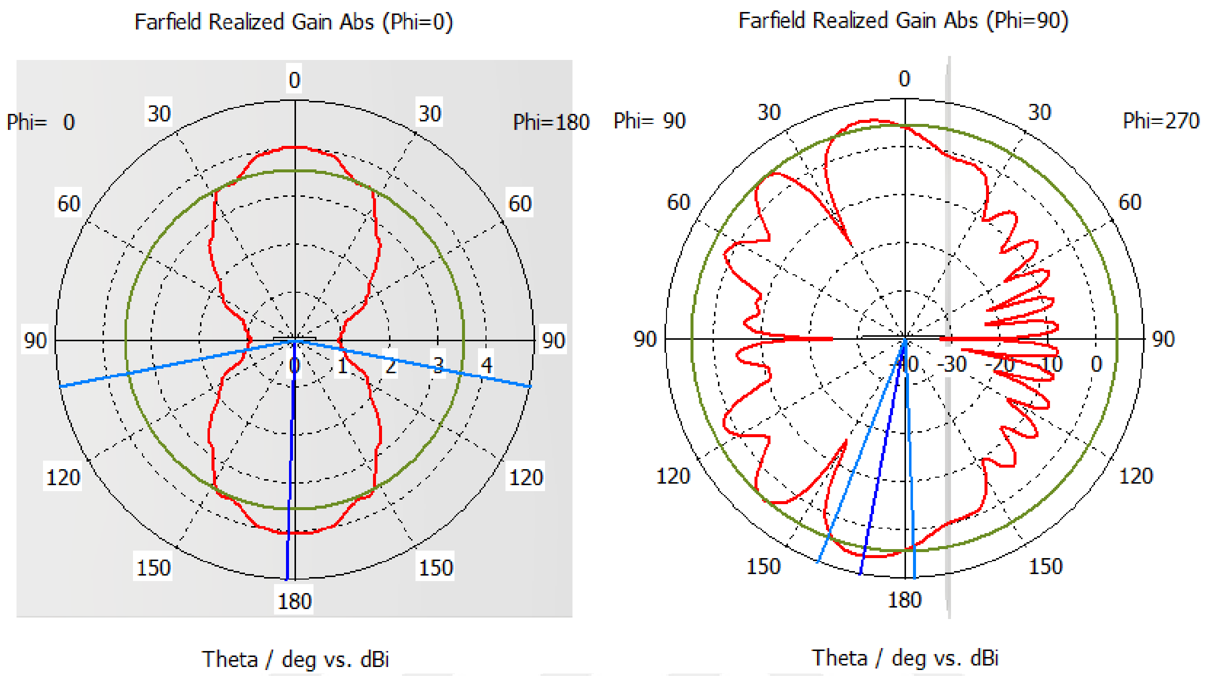

Figure 8.40. Far-field Radiation Pattern at Phi=0° and Phi=90°

The proposed hexagon microstrip antenna modified with RT5880 substrate for working frequency of 5.9 GHz is shown in Figure 8.41. With these simulation results, the total area of the antenna has increased by 15%.

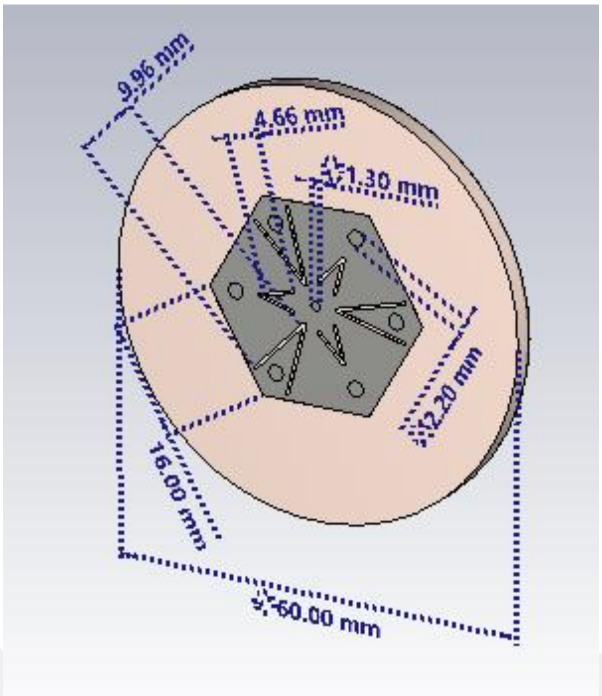

Figure 8.41. Dimensions of the hexagon microstrip antenna

The return loss of the hexagonal microstrip antenna is approximately -18 dB, as illustrated in Figure 8.42, with the antenna's bandwidth measured at 654 MHz, ranging from 5.5124 to 6.1669 GHz.

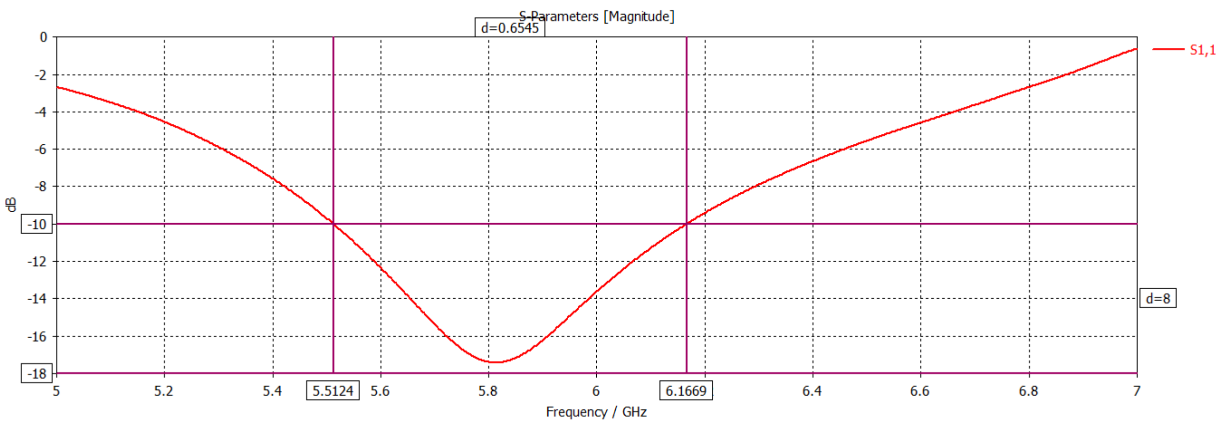

Figure 8.42. S_{11} parameter graph of hexagon microstrip antenna

In the hexagon microstrip antenna VSWR value is 1.3105723 at 5.9 GHz. Figure 8.43 shows the simulated result of VSWR as a function of frequency (GHz).

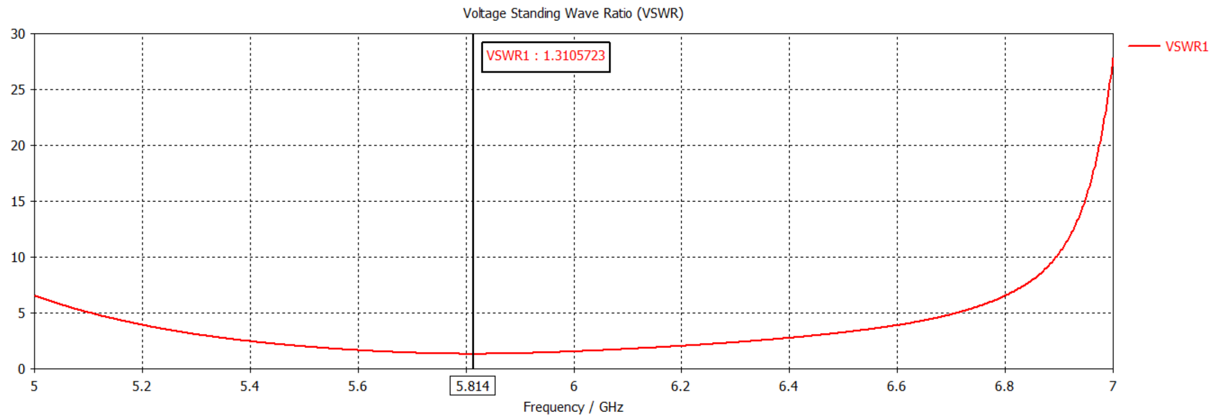

Figure 8.43. VSWR simulated result of hexagon microstrip antenna

As seen in Figure 8.44, the gain is determined as 4 dBi at the 5.9 GHz center frequency. It is observed that the antenna gain decreases by 18% when the Rogers substrate is used compared to the FR-4 substrate.

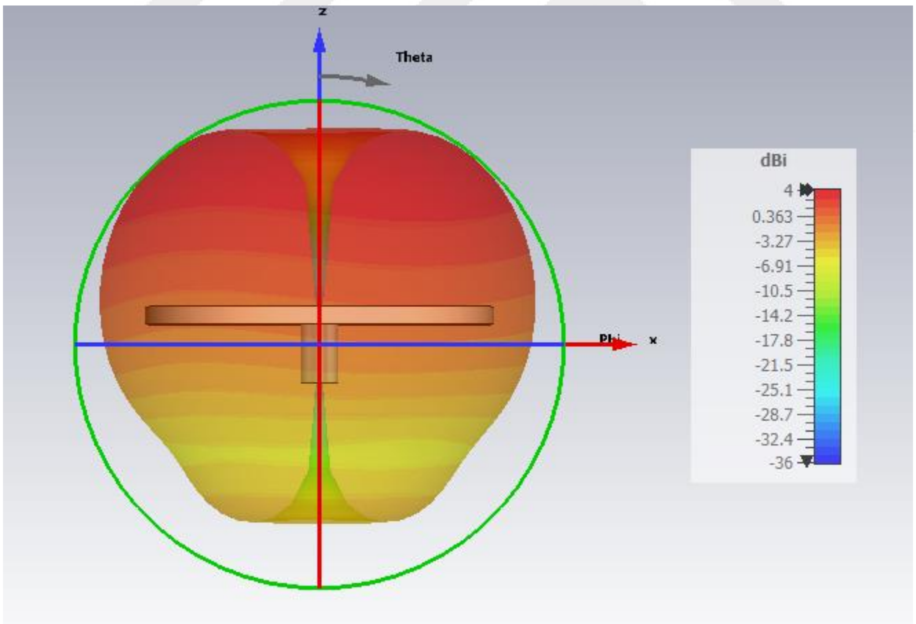

Figure 8.44. 3D Radiation Pattern of hexagon microstrip antenna

In summary, simulation studies are conducted using four different antenna designs with various substrate models and different substrate thicknesses for the designs and analyses. The detailed dimensions of proposed antennas and the details of the gain, BW, VSWR and S_{11} are shown in Table 8.3.

Table 8.3. Antenna Simulation Performance Comparison

	Patch Antenna		RMSPA Antenna		Dipole antenna		Hexagon Microstrip antenna		
	FR-4	RT5880	FR-4	RT5880	FR-4	RT5880	FR-4	FR-4	RT5880
Substrate width (mm)	30	36	80	100	21	23	60	60	60
Substrate length (mm)	30	31.4	40	40	46	47	60	60	60
Substrate thickness (mm)	1	1	1	1	1	1	1	3	3
Patch width (mm)	16	26	13.1	26	10	10	17.4	19	16
Patch length (mm)	12	16.4	11.9	15	46	46	17.4	19	16
Bandwidth (MHz)	203	145	180	74	2201	1667	232	102	654
Working Frequency (GHz)	5.8032-6.006	5.8266-5.9725	5.8131-5.9934	5.9045-5.9786	4.3031-6.5047	4.882-6.549	5.794–6.026	5.847-5.949	5.5124-6.1669
VSWR	1.082	1.023	1.003	1.621	1.199	1.439	1.334	1.412	1.310
Gain (dBi)	3.29	7.81	5.7	10.8	6.03	6.1	4,43	4.88	4

8.3. Fabrication Stage

A parameter sweep is an iterative procedure where simulations are executed multiple times with varying values of the chosen parameter(s). In our study, optimization is conducted using the parameter sweep feature of CST to achieve desired performance characteristics based on parametric variations in the radiating patch and ground plane. Sample images of the experimental trials conducted using the parameter sweep feature are shown in Figure 8.45.

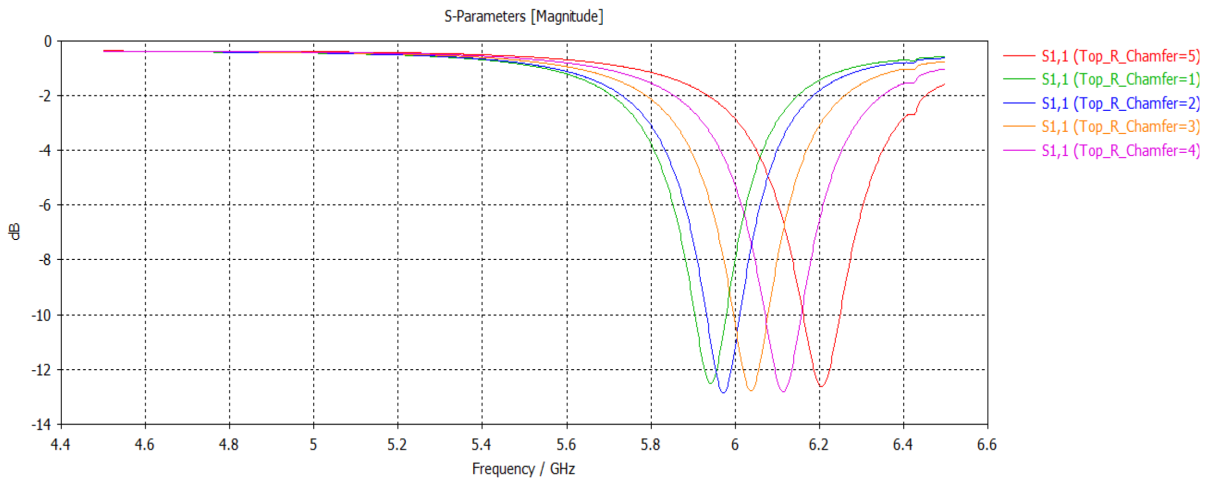

Figure 8.45. Parameter sweep sample

To verify the simulation analysis, prototypes of antennas with completed design models and optimal performance parameters (dipole microstrip and second hexagon microstrip) are fabricated and analyzed. The prototypes of microstrip patch antennas are manufactured and measurements of bandwidth, return loss values at a center frequency of 5.9 GHz are conducted at the KTO Karatay University Smart Technologies Center.

The prototypes of the microstrip patch antennas are produced using LPKF devices. The LPKF Contac S4, LPKF Protomat S104, and LPKF ProtoLaser U4 printed circuit board milling machines (Figure 8.46) are used in the production stage, as shown below.

Figure 8.46. LPKF Protomat S104, LPKF Contac S4 and LPKF ProtoLaser U4

The LPKF ProtoMat S104 utilizes laser welding technology and is employed for the precise joining or processing of materials. This technology allows for the materials to be heated and melted together by a high-density laser beam, enabling their fusion. It is a preferred method, particularly for applications requiring high precision. The LPKF Contac S4 produces dependable copper layers on the surfaces of all existing vias and employs advanced methods to enhance copper layer buildup. An optimized anode plate combined with pulse reverse plating guarantees uniform deposition, while carbon activation using black hole technology, integrated air blow-in, and an extra step for via cleaning ensure reliable connections to the copper surface, preventing layer detachment issues. This process results in consistent layer thickness both in the holes and on the flat metal surface of the substrate (Figure 8.47).

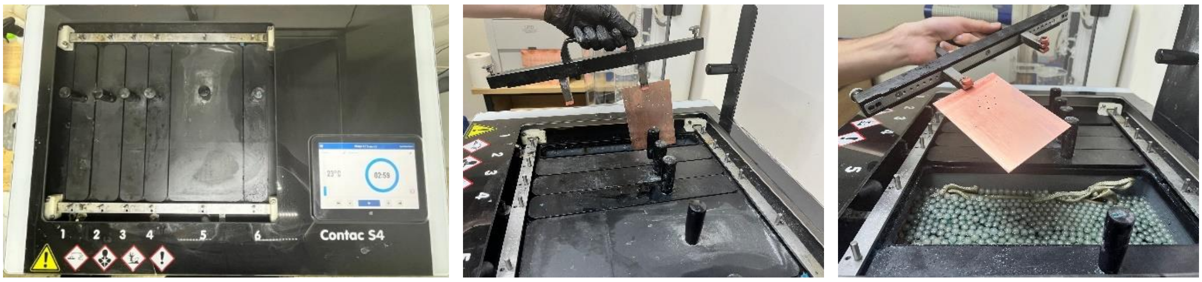

Figure 8.47. Stages of hole plating

The LPKF ProtoLaser U4 is capable of structuring, engraving, and cutting materials all in one process. A UV laser beam can accurately cut individual boards from large panels without causing stress, drill holes and microvias, and create openings in solder masks. The specific wavelength employed makes the UV laser a highly versatile tool.

FR4 is chosen as the dielectric substrate material, and copper conductors measuring 150×100 mm with a thickness of 0.0035 mm are used for the patch and ground planes. The selection of FR4 is based on the inadequate performance values of other dielectric materials tested during the design phase (compared to Rogers RT5880).

Drill operations are performed on a 1 mm FR-4 substrate using the LPKF Protomat S104 device, with three reference coordinates established. Subsequently, the substrate is transferred to the device for hole plating. It is then moved to the LPKF ProtoLaser U4 device for etching operations on both the front and back sides. To separate the antenna structures from the FR-4 substrate, the Protomat S104 device is used again. The visuals depicting the production process step by step are shown in Figure 8.48.

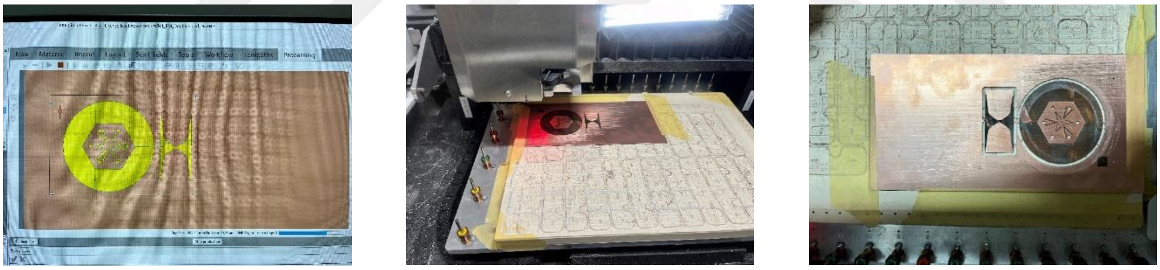

Figure 8.48. Stages of production

The images showing the front and rear views of the hexagonal microstrip patch antenna after manufacturing, captured with a magnifying glass and from various angles, are presented in Figure 8.49.

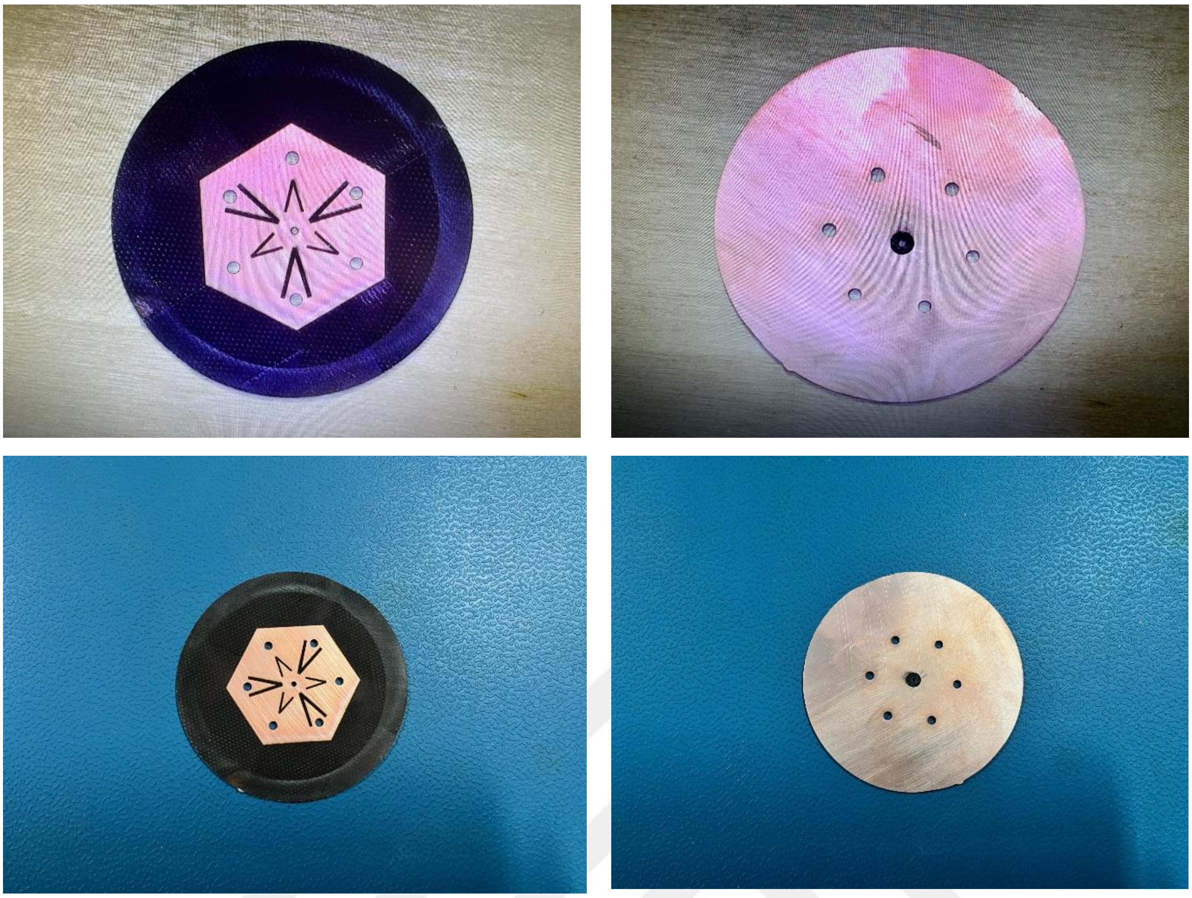

Figure 8.49. Front and back sides of the hexagonal microstrip patch antenna

The images depicting the front and rear views of the dipole microstrip patch antenna post-production, captured under a magnifying glass and from various angles, are illustrated in Figure 8.50.

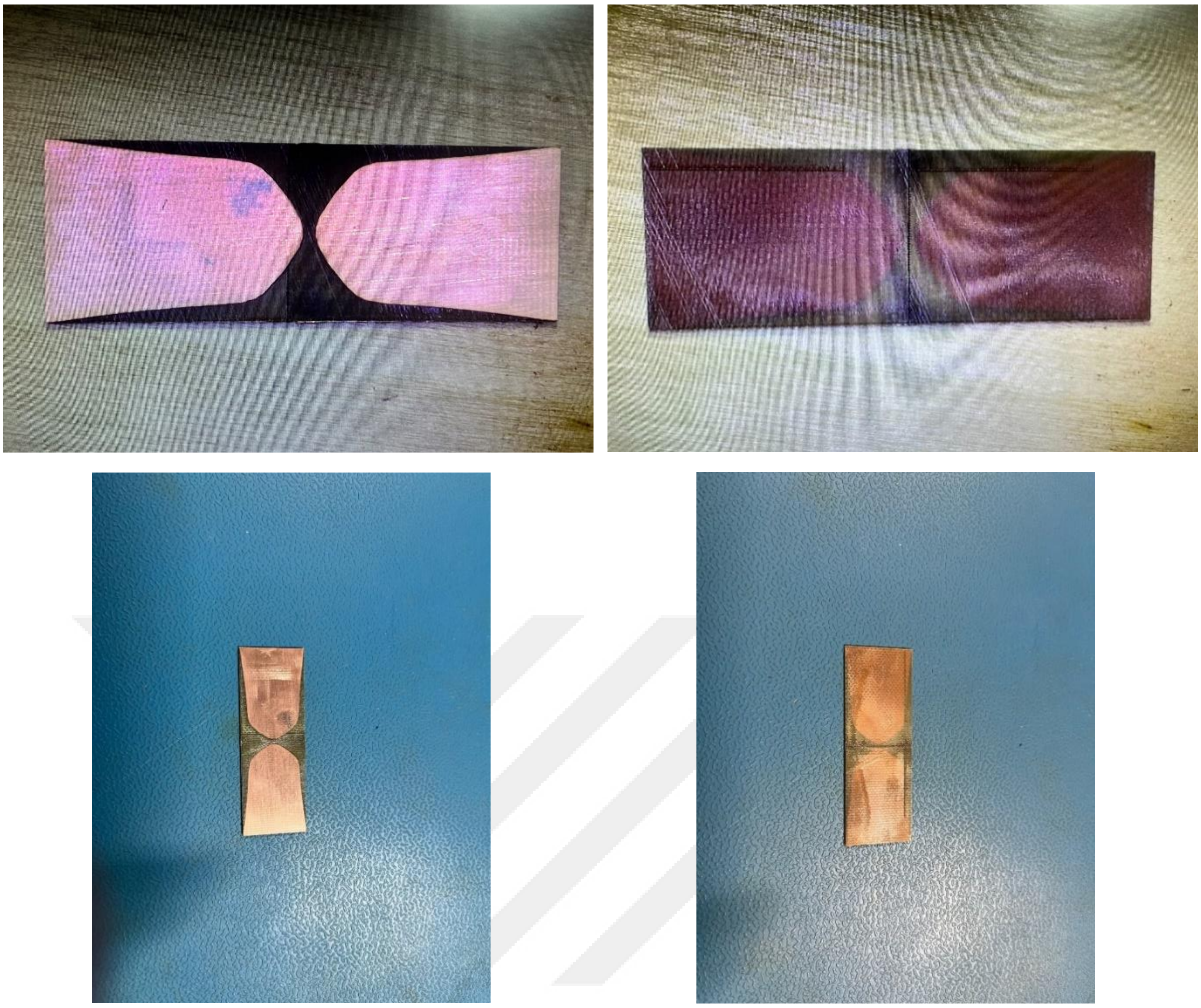

Figure 8.50. Front and back sides of the dipole microstrip patch antenna

It has been observed that the dimensions of the antennas produced with the specified dimensions in the simulation are consistent. A Holex Digital Caliper ABS device is used for measurements. The measurement results are shown in Figure 8.51.

Figure 8.51. Antenna dimensions

As shown in Figure 8.52, RG316 cable is used for the dipole microstrip antenna feeding, while an SMA connector is used for the hexagonal microstrip antenna. RG316 is a high-frequency coaxial cable known for its flexibility and excellent performance in various demanding environments. It features a stranded silver-covered copper-clad steel conductor made with seven strands of 0.0067-inch diameter wire and a PTFE dielectric insulator, making it highly resistant to heat, moisture, and chemicals. This cable is ideal for applications in telecommunications, radio transmission, military, aerospace, and other industries requiring robust and reliable signal transmission. RG316 is especially suited for high-frequency interconnects and microwave applications due to its low signal loss and high-temperature tolerance. SMA connectors are semi-precision coaxial RF connectors developed in the 1960s as a compact connector interface for coaxial cables, featuring a screw-type coupling mechanism. These connectors have a 50 Ω impedance and were initially designed for frequencies ranging from DC (0 Hz) to 12 GHz. Over time, their capabilities have been enhanced, with variants now available for use up to 18 GHz and 26.5 GHz. They are most commonly utilized in microwave systems, handheld radios, mobile phone antennas, and, more recently, in WiFi antenna systems and USB software-defined radio dongles.

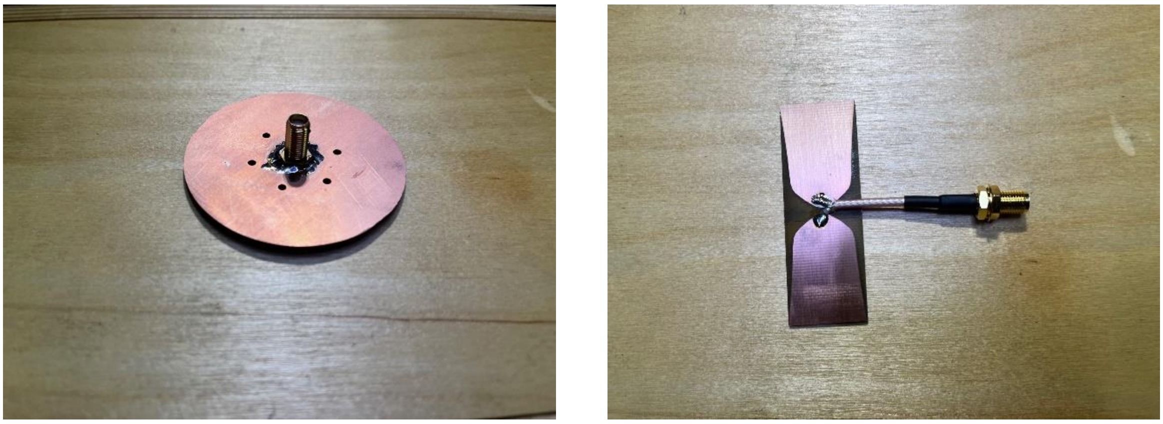

Figure 8.52. Antenna feeds

Initially, general test conditions are established during the measurement procedures. The experiments are conducted at temperatures of 15-35°C and humidity levels of 30-60%. Additionally, the calibration of the testing equipment is performed as part of the quality management system of Konya Smart Technologies Center, ensuring that measurements conform to the standards of Konya Karatay University.

The Rohde & Schwarz ZVA50 (Figure 8.53) Vector Network Analyzer (VNA), capable of measuring scattering parameters up to 50 GHz, is used to measure the input values of the generated models under real-world conditions and to validate the simulation results. VNAs are measurement devices designed primarily for analyzing and measuring various aspects of electrical and RF signals passing through devices or components, and they are commonly used in high-power systems and radio frequency (RF) applications.

Figure 8.53. Vector Network Analyzer

The prototype antennas are subjected to testing for return loss (S_{11}) measurements. Tests are conducted for the dipole antenna in the 4-7 GHz range. The measurements of the antennas produced with the VNA device are shown in Figure 8.54.

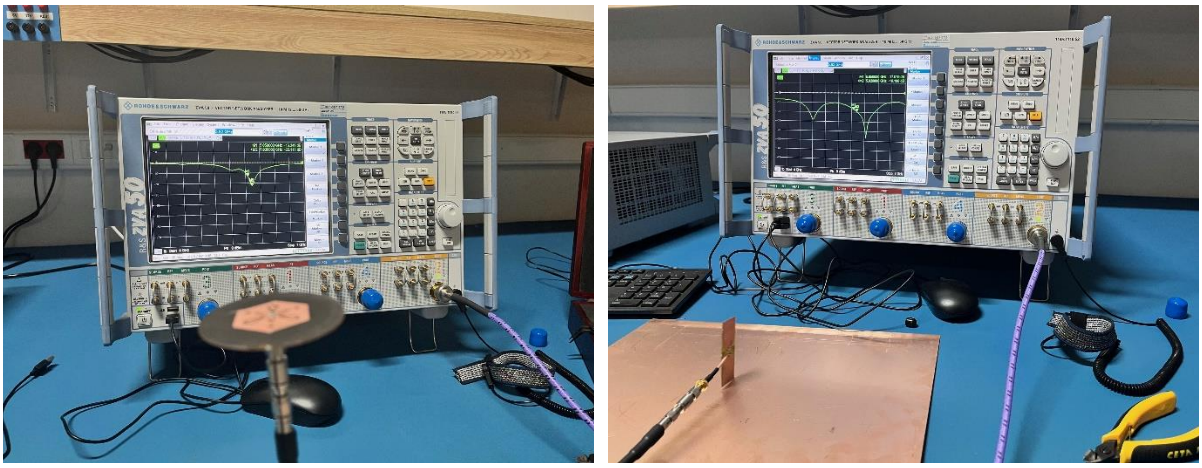

Figure 8.54. S-parameter measurement set-up

Figures 8.55 and Figure 8.56 illustrate the return loss (S_{11}) of the proposed antenna structures. The results of the obtained S_{11} measurements are redrawn to display both simulation and measurement results on the same graph. According to the measurement results, it is observed that S_{11} is below -10 dB at 5.9 GHz. The measurement and simulation results show consistent alignment at the target frequency values.

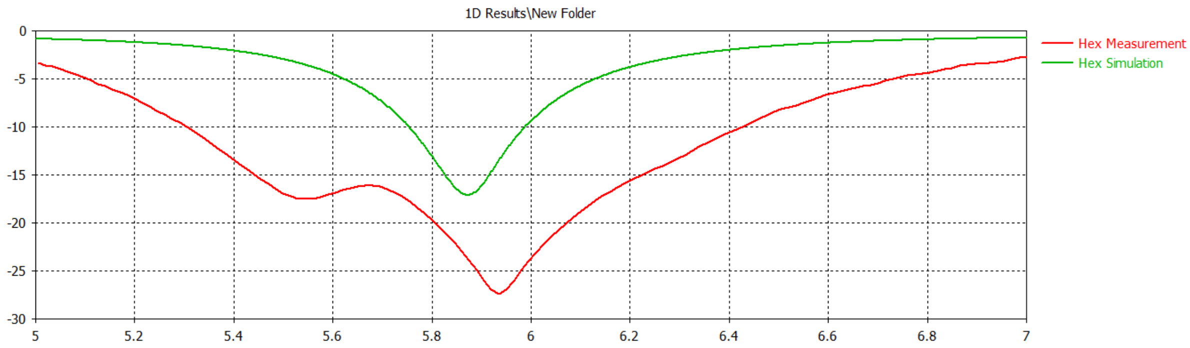

Figure 8.55. S_{11} comparison for hexagon microstrip antenna

The proposed structure radiates operating frequency bands, including a resonance frequency of 5.9 GHz.

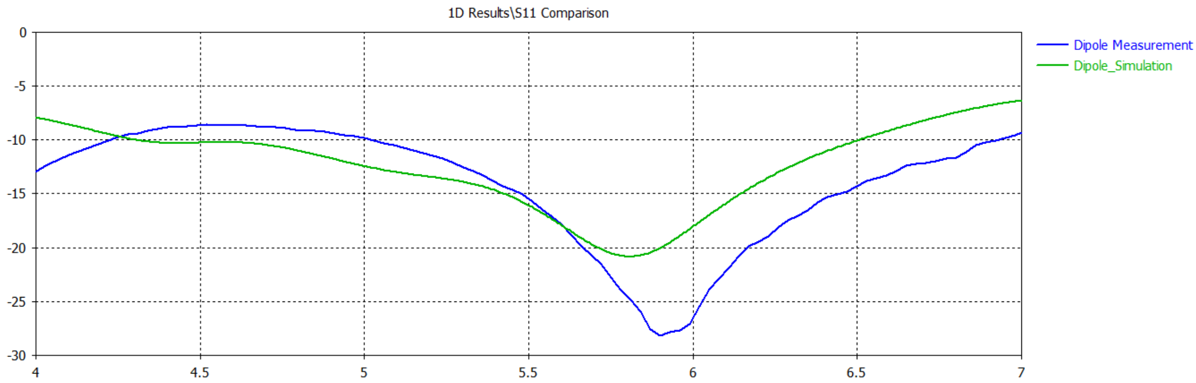

Figure 8.56. S_{11} comparison for dipole antenna

To validate and compare the simulation and measurement results, it is planned to mount the produced antennas on the vehicle and repeat the measurements. Effective V2V and V2I communication necessitates strong signal reception from every direction. As a result, there is often an effort to determine the best placement for antennas on the vehicle. While the roof of the car is a frequently used site for antenna installation, there are no standardized or specific guidelines for determining the exact placement of antennas on the vehicle's roof.

In a study conducted by Asghar and colleagues [57] in Germany in 2021, the impact of antenna mounting positions on the radiation pattern across a wide frequency range was investigated. By selecting several mounting positions on the roof of a vehicle for measurements, it was demonstrated that the optimal mounting position of the antenna varies with the operating frequency. Analyzing the cumulative distribution function of the measured gain patterns reveals that for high-frequency applications, antennas positioned on the sides and center of the vehicle perform better than those mounted at the front or rear.

In 2013 research, Abbas and associates proposed that using a pair of antennas with complementary characteristics, like combining a roof-mounted antenna with a bumper antenna, offers an effective solution for attaining optimal reception performance in various propagation conditions [58].

In 2014 study, Imai and colleagues explored how the car body affects the radiation pattern of a car antenna mounted on the side mirror for inter-vehicle communication. The findings suggest that the radiation patterns exhibit similar trends in both detailed and simplified models for the antenna positioned on the right side mirror [59].

In 2009 study, Reichardt and colleagues utilized a channel model that relies on three-dimensional ray-optical wave propagation simulations within two realistic motorway scenarios. They computed key radio channel parameters from simulations involving six different antenna positions for both the transmitter and receiver. The roof-mounted antenna exhibited the highest level of long-term fading amplitude [60].

In 2015 study, Diez and colleagues introduced a novel approach for analyzing both near and far-field propagation of C2C antennas. This method, demonstrated through various examples, allows for the examination of the entire car chassis using asymptotic techniques, thereby significantly reducing computational requirements compared to full-wave analysis. The study also explores how the radiation pattern is influenced by antennas mounted on the roof, side mirrors, and bumpers [6].

In 2010 study, Kornek and colleagues equipped a vehicle with appropriate antenna solutions placed in three distinct locations: a monopole antenna mounted at the center of the roof, and patch antennas on both the left and right side mirrors. Researchers analyzed the effects of various antenna combinations based on the impulse response for a specified V2V channel scenario. The scenario was explored using ray-optical simulations across all potential antenna configurations, leading to a comprehensive matrix characterization of the multiple-input multiple-output (MIMO) channel. From this characterization, they calculated and discussed the spectral efficiency [55].

Whalen and colleagues conducted a study in 2018 to investigate the effects of antenna placement on a vehicle's performance on the communication system. They performed their work on an HB vehicle, testing at four different locations both with and without a sunroof [61]. In the literature review conducted, it is observed that the optimization of the installation of various proposed antenna models is carried out at many points based on design type, vehicle type (car/truck/lorry, etc.), roof structure of the vehicle, the presence of a sunroof, and the proximity of the antenna to the front or rear window. In light of this information, we decided to analyze the hexagonal model of our designed antennas at two different points (shown as positions A and B) and our dipole antenna at a single point (position B). In selecting positions A and B, the structures of the proposed antennas and their suitability for mounting on the roof structure are considered. Position A will be referred to as the "front position," and position B as the "back position". The positions of the antennas are shown in Figure 8.57.

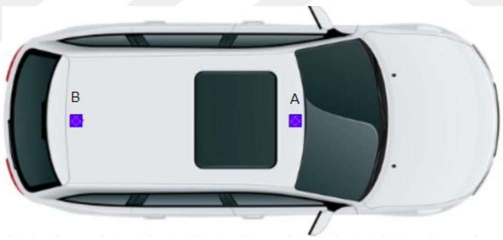

Figure 8.57. Antenna positions on the car

In our study, a Rover 25 hatchback (dimensions: width/lenght/height 1.690*3.990*1.420 mm) with sunroof is used. The roof top dimensions of Rover 25 hatckback are approximately 0.90 m x 1.25 m. The measured car is shown from three different angles in Figure 8.58.

Figure 8.58. Measured car

In the work conducted on the vehicle, the Handheld Vector Network Analyzer (Figure 8.59(a)) product from Rohde & Schwarz (R&S®) is used. The basic version of the R&S®ZNH is capable of conducting one-port cable and antenna measurements, as well as four S-parameter measurements up to 26.5 GHz. The VNA is calibrated using a R&S®ZV-Z135 calibration kit (Figure 8.59(b-c)) before the measurement.

Figure 8.59. Handheld Vector Network Analyzer and calibration kit

In case 1, the hexagonal microstrip antenna is mounted in the front position, and measurements are taken as shown in Figure 8.60.

Figure 8.60. Hexagon microstrip antenna on front position

In case 2, the hexagonal microstrip antenna is mounted in the back position, and measurements are repeated as shown in Figure 8.61.

Figure 8.61. Hexagon microstrip antenna on back position

In case 3; dipole antenna is mounted in the back position and measurements are taken as shown on Figure 8.62.

Figure 8.62. Dipole antenna on back position

According to the measurement results obtained under different conditions, the reflection coefficients of the designed hexagonal microstrip antenna varied, as shown in Figure 8.63. Comparing the simulation results with the tests conducted, it is observed that the bandwidth increased according to the laboratory results. However, it decreased in the two measurements taken from the front and back positions of the vehicle.

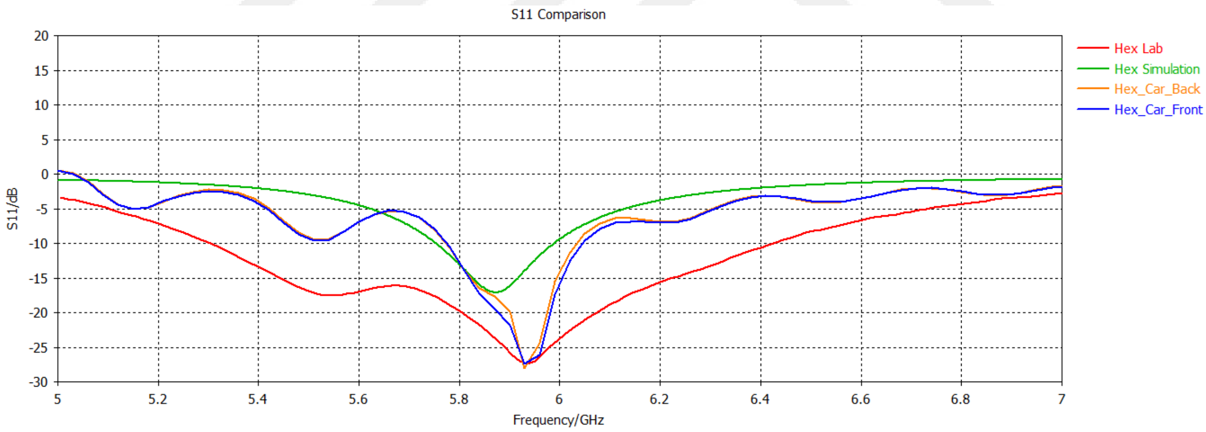

Figure 8.63. S_{11} comparison for hexagon microstrip antenna

However, the bandwidth results for the dipole antenna showed opposite behavior compared to the hexagon microstrip antenna. While the simulation and laboratory results for the dipole antenna exhibited similar behavior, it is observed that the bandwidth decreased in the tests conducted on the vehicle, as shown in Figure 8.64.

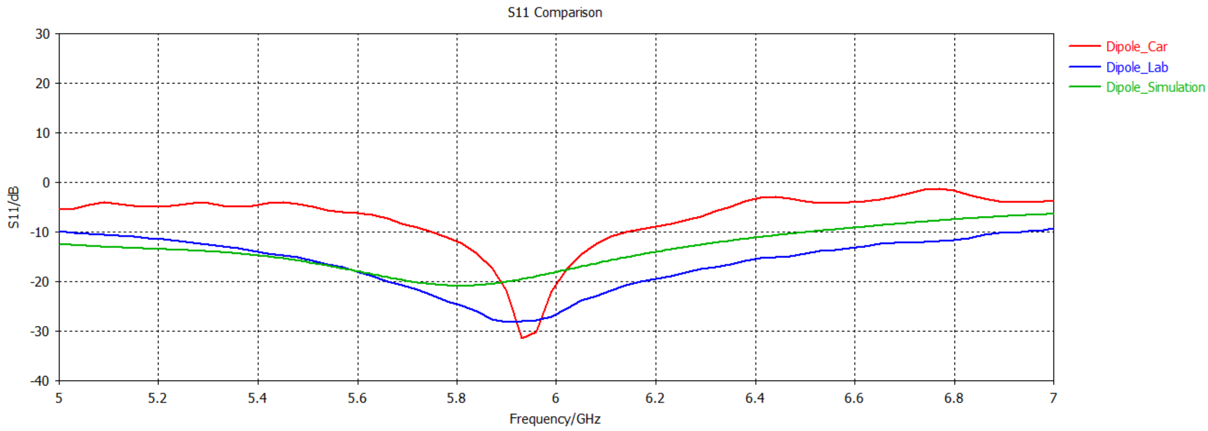

Figure 8.64. S_{11} comparison for dipole antenna

A return loss of less than -10 dB suggests that the antenna will demonstrate strong performance. Measurement results indicate that at a frequency of 5.9 GHz, the return loss falls below -10 dB. The measurement and simulation results align well with the intended frequency values. Tables 8.4 and 8.5 present a comparison of the simulated and measured parameters for the proposed antennas.

Table 8.4. Comparison of the simulated and measured parameter results for hexagon microstrip antenna

Proposed Hexagon Microstrip Positions	Frequency (GHz)	Bandwidth (MHz)	Return Loss	VSWR
Simulation	5.872	5.75-5.98 (230)	-17.1	1.324
Laboratory	5.935	5.30-6.42 (1120)	-27.3	1.278
Front Position	5.930	5.77-6.04 (270)	-27.3	1.101
Back Position	5.930	5.77-6.03 (260)	-27.9	1.089

Table 8.5. Comparison of the simulated and measured parameter results for dipole antenna

Proposed Dipole Positions	Frequency (GHz)	Bandwidth (MHz)	Return Loss	VSWR
Simulation	5.804	4.30-6.50 (2200)	-20.8	1.199
Laboratory	5.900	5.02-6.93 (1910)	-28.1	1.343
Back Position	5.900	5.75-6.14 (390)	-31.3	1.627

The test results show that the operating frequency bandwidth is from 5.77 GHz to 6.04 GHz for hexagon microstrip antenna and 5.75 GHz to 6.14 GHz for dipole antenna. The results show a good return loss, with a maximum value of -27.9 dB for the hexagonal microstrip antenna and

-31.3 dB for the dipole antenna. The simulated VSWR of the antenna correlated with acceptable values for VSWR, and it is noted that the measured VSWR remained below 2 across the V2X operational bands.

Since it is observed that the dataset did not conform to a normal distribution and that all groups had a right-skewed distribution, the Kruskal-Wallis H Test is preferred to compare the groups in terms of S_{11}. This test is used to determine whether there is a difference in median values among three or more independent groups. In the case of a significant difference among the antenna groups, post-hoc (all-pairwise) analysis is conducted to identify which pairs of groups differed. In the post-hoc tests, significant differences are detected by comparing the means of the groups. Additionally, box-plot graphs are used to illustrate the variation of the data. For each antenna group, the mean, standard deviation, median, minimum, maximum, and interquartile range (IQR) values are calculated. The statistical significance level in group comparisons is accepted as $p < 0.05$. All statistical analyses are performed using SPSS 25 software.

In Table 8.6, summary statistics for dipole S_{11} values are provided for three different applications (CST, Car, Lab). Descriptive statistics include mean, standard deviation, median, IQR, minimum, and maximum values. Additionally, the Kruskal-Wallis test is applied to compare the applications and examine whether there is a significant difference among the groups. The highest mean value is observed in the CST antenna group (-13.67 dB), while the lowest mean is in the Car group (-17.24 dB). The CST group shows a statistically significantly higher mean than the other two groups, with this difference being found statistically significant by the Kruskal-Wallis test ($p < 0.001$). Similarly, the median of the CST group (-12.76 dB) is higher than that of the other two groups. The Car and Lab groups have similar median values (-15.30 and -14.84 dB, respectively), but the differences between them are still significant. The IQR value of the Car group (9.17) is wider compared to the other groups, indicating greater variation in the data for this group. The Car group also has the highest standard deviation (6.33), suggesting that its distribution is broader compared to the other groups. The results of the Kruskal-Wallis test indicate that there is a significant difference among the antenna groups ($p < 0.001$). In the pairwise comparisons of the groups, a statistically significant difference is particularly noted between the CST group and the other two groups.

Table 8.6. Descriptive statistics and comparison of application groups for Dipole S_{11} values

Groups	n	Mean	Std. Deviation	Median	IQR	Min.	Max.	Kruskal-Wallis p value
Cst	412	-13.67	3.36	-12.76	5.16	-20.84	-9.99	
Car	68	-17.24	6.33	-15.30	9.17	-39.63	-10.20	<0.001
Lab	145	-15.88	4.68	-14.84	7.13	-28.17	-10.03	
Total	625	-14.57	4.30	-13.30	6.18	-39.63	-9.99	

Figure 8.65 shows box plots for the three antenna groups. The graph provides a visual overview of the distribution of the data. The box plot for the CST group is narrower compared to the other groups, indicating less variation. The box plot for the Car group has both lower and upper whiskers that extend over a wide range, exhibiting greater variation. Additionally, several outliers are observed in this group. The Lab group shows moderate variation and presents a more balanced distribution compared to the Car group. The crosses in the graph represent the means, while the lines inside the boxes represent the medians. The CST group has a higher mean and a narrower distribution compared to the other groups.

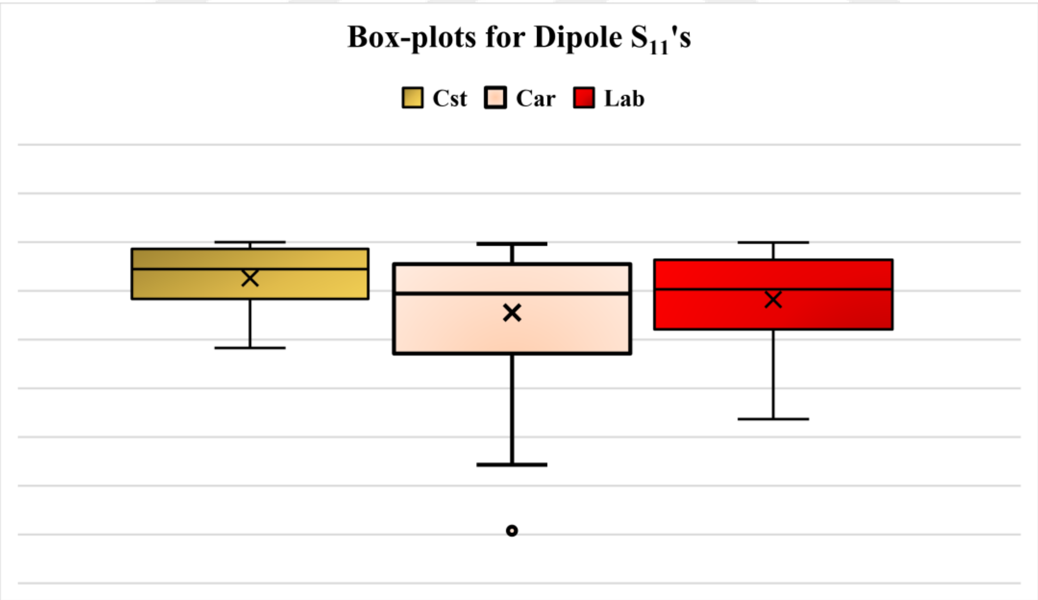

Figure 8.65. Box plot of dipole antenna S_{11}

In Table 8.7, descriptive statistics for Hex S_{11} values are presented for four different groups. The differences among the groups are statistically evaluated using the Kruskal-Wallis test. The highest mean value is observed in the CST group (-13.76 dB), while the lowest mean is in the

Car Front group (-18.47 dB). The CST group has a higher mean than the other three groups, and this difference is statistically significant ($p < 0.001$). The median of the CST group (-13.81 dB) is higher than that of the other groups, while the median of the Car Front group (-17.35 dB) shows the lowest value. The IQR values for the Car Back and Car Front groups are wider (9.60 and 10.78, respectively), indicating greater data spread in these groups. The highest standard deviation is observed in the Car Front group (5.83), while the lowest standard deviation is found in the CST group (2.20). The results of the Kruskal-Wallis test indicate a significant difference among the groups ($p < 0.001$). According to the post-hoc analysis results, significant differences are particularly noted between the CST group and the other groups.

Table 8.7. Descriptive statistics and comparison of application groups for Hex S_{11} values

Groups	n	Mean	Std. Deviation	Median	IQR	Min.	Max.	Kruskal-Wallis p value
Cst	116	-13.76	2.20	-13.81	4.13	-16.87	-10.04	p < 0.001
Car Back	9	-17.50	5.79	-16.41	9.60	-27.96	-10.67	
Car Front	9	-18.47	5.83	-17.35	10.78	-27.30	-10.51	
Lab	75	-17.22	4.43	-16.73	5.64	-27.37	-10.00	
Total	209	-15.36	3.95	-15.07	4.44	-27.96	-10.00	

Figure 8.66 shows box plots for the four groups, visually presenting the Hex S_{11} distribution for each group. The CST group exhibits a narrower distribution compared to the other groups, with the data clustered within a closer range. The Car Front and Car Back groups show greater variation, particularly with the Car Front group having a significantly low lower boundary. The Lab group has a distribution of moderate width. The graph clearly highlights the differences among the groups, indicating that the CST group has a higher mean with lower variation.

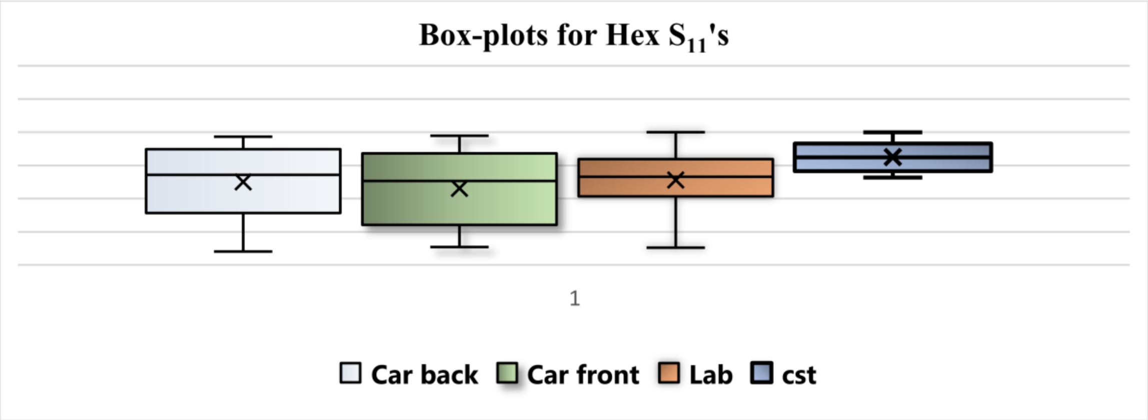

Figure 8.66. Box plot of hexagon microstrip antenna S_{11}

Figure 8.67 and 8.68 shows the comparison of mean and standard deviation for S_{11}.

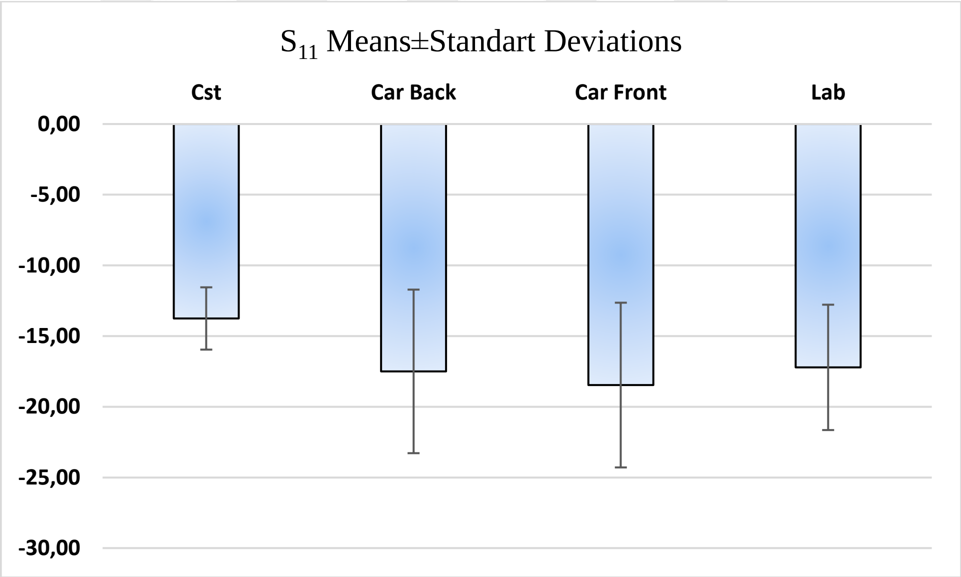

Figure 8.67. S_{11} Means±Standart Deviations for hexagon microstrip antenna

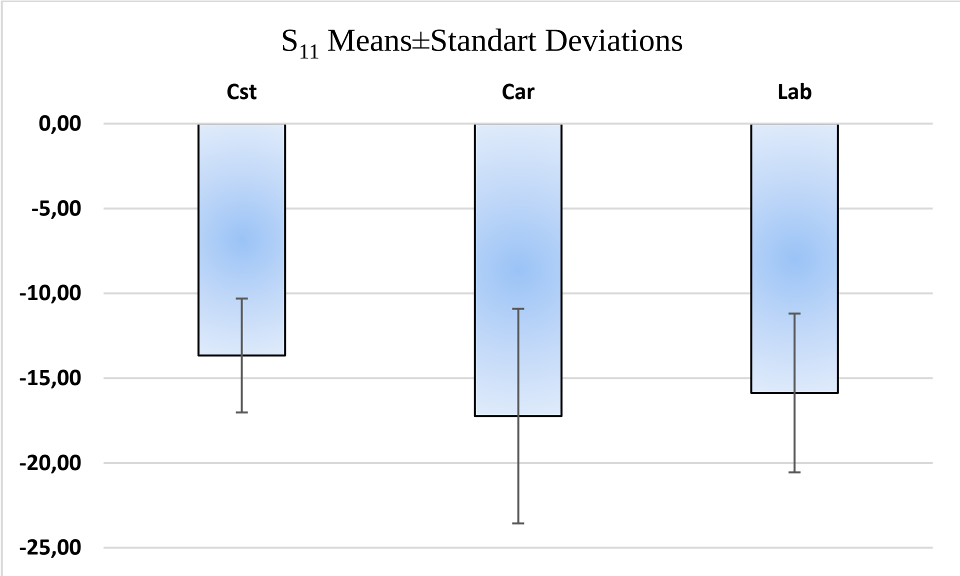

Figure 8.68. S_{11} Means±Standart Deviations for dipole antenna

Anechoic chamber tests are conducted to assess the external electromagnetic interference and to measure the true performance of the proposed and fabricated antennas. Fully and partially anechoic chambers are specialized environments designed to be isolated from external electromagnetic interference, with their interiors coated with electromagnetic shielding materials. The measurements are conducted at the Akdeniz University Microwave Application and Research Center for Industrial and Medical Applications. The fully anechoic chamber employed for the study measures 8 meters in length, 4 meters in width, and 4 meters in height. Taking into account the operating frequency range of the antenna and the characteristics of the reference antenna measurements, the antenna is positioned 1 meter away from the reference antenna on an autonomous turntable capable of 360° rotation, within an anechoic chamber, to perform the measurements. A photograph of the corresponding test setup is provided in Figure 8.69.

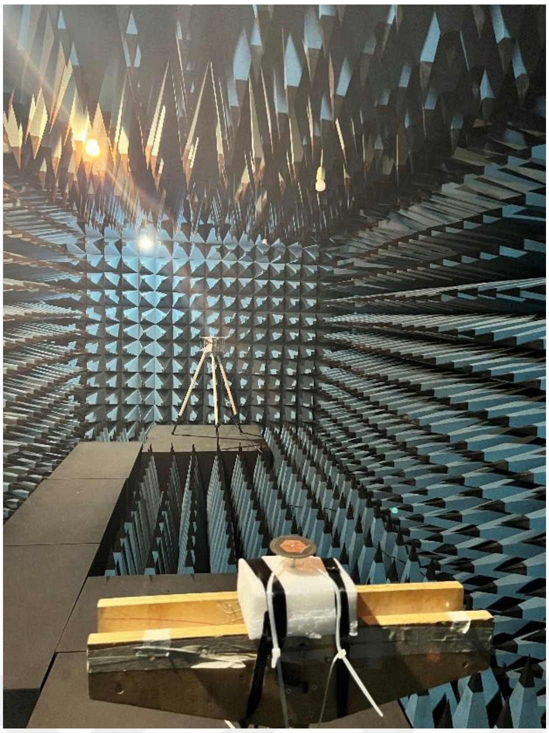

Figure 8.69. Test setup in the anechoic chamber

The CST simulation radiation patterns and the measured radiation pattern for Phi=90° of the dipole microstrip antenna at 5.9 GHz are shown as a polar plot in Figure 8.70 below. The comparison between the simulation results and the anechoic chamber measurement results showed similar antenna gains, 6.07 and 6.01, respectively. While the simulation results exhibited side lobes alongside an ideal radiation pattern, the measurement results revealed a directional antenna outcome.

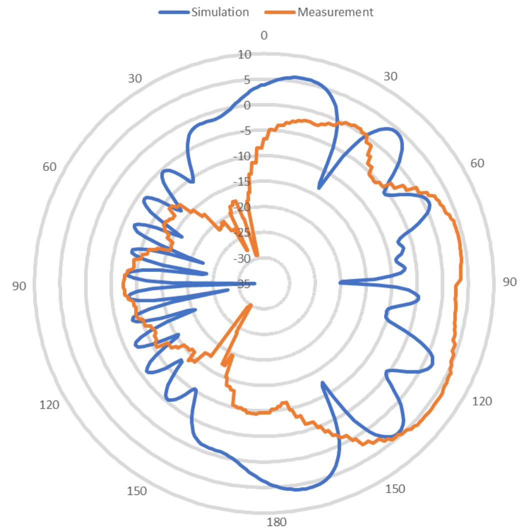

Figure 8.70. Radiation Pattern at Phi=90°

The CST simulation radiation patterns and the measured radiation pattern for Phi=90° of the hexagonal microstrip antenna at 5.9 GHz are shown as a polar plot in Figure 8.71 below. The comparison between the simulation results and the anechoic chamber measurement results showed similar antenna gains, 4.43 and 4.14, respectively. In addition, it has been observed that the radiation patterns exhibit a significant degree of similarity.

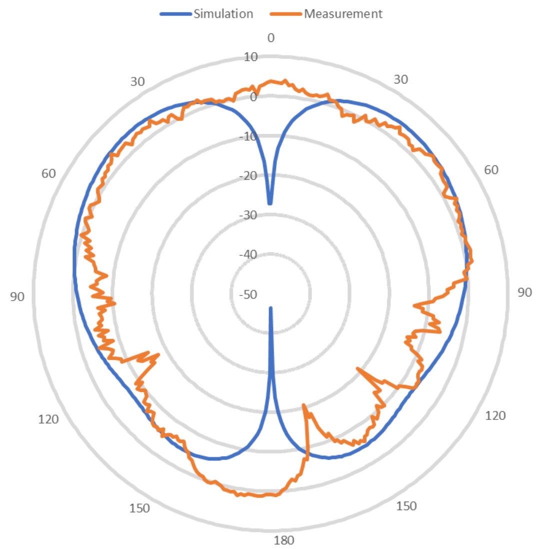

Figure 8.71. Radiation Pattern at Phi=90°

Table 8.8 depicts the comparisons of the proposed antennas structure with the other V2X antennas in the literature. When the existing studies are examined, it is observed that substrates with a thickness of 1.6 mm are generally used. Therefore, a meaningful comparison process could not be established. However, since the typical V2X application is expected to be urban areas, it is considered that an antenna gain of 4 and higher dB is at a sufficient level.

Table 8.8. Comparison with existing designs

Reference	Antenna Size (mm^3)	Substrate	Working Freq.	Gain (dB)
[2]	40 x 34,6 x 1,6	FR-4	5,8-6	6,02
[3]	30 x 25,9 x 3	FR-4	4,74-6,79	4,2
[62]	20,2 x 24,1 x 1,6	FR-4	5,85-5,92	5,6
[63]	42 x 42 x 1,6	FR-4	5,79-5.97	4,71
[64]	52 x 39 x 2	AgHT	5,48-6,23	3,97
[65]	28,5 x 77 x 1,6	FR-4	4,01-6,41	5
Dipole microstrip antenna	46 x 21 x 1	FR-4	5.75-6.14	6,01
Hexagonal microstrip antenna	34,9 x 30,2 x 1	FR-4	5,79-6,02	4,43

9. CONCLUSION

To improve traffic safety, advance autonomous driving experiences, and integrate with the IoT, vehicles have the capability to interact with each other, people, and infrastructure. For this interaction to occur, antennas are required. This study aims to design microstrip antennas for V2X band at 5.9 GHz, which can be used in next-generation data communications. To achieve the desired outcomes, a review of the antenna design process in the academic field has been conducted. Simulation studies are conducted to investigate the effects of different feeding techniques, as well as the impact of changing substrate material and thickness on antenna performance. After researching applicable methods and procuring the necessary materials, the production phase is initiated. The proposed antennas are fabricated and measured. The simulation results of the proposed antennas, along with laboratory results and the outcomes obtained after mounting them at different points on a hatchback vehicle, are compared. The overall dimensions of the proposed hexagon microstrip antenna are 60×60×1 mm^3 while the proposed dipole antenna measures 46×21×1 mm^3. Once the CST modeling program has initially predicted the antenna's performance, the S_{11} parameter and VSWR are tested. The frequency band covers the bandwidths of V2V communication. Both proposed antennas have Returl Loss values of <-10 dB within the bandwidth of interest and VSWR of less than 2. The proposed antennas designs are, in general, good fit for antenna applications in automobiles and can be easily installed on vehicle roof top shark-fin applications. Additionally, the hexagonal microstrip antenna can be placed on any vehicle, including motorcycles and bikes. Moreover, due to its thickness of 1 mm, the hexagonal microstrip antenna can be mounted without affecting the vehicle's aesthetics and aerodynamics.

REFERENCES

[1] Masmoudi, A., Mnif, K., and Zarai, F. (2019). A Survey on Radio Resource Allocation for V2X Communication. *Wirel. Commun. Mob. Comput.*, vol. 2019, 1–12.

[2] Singhal, H., Ashwin, S., Sharma, V., Prajapati, J., and Upadhayay, M.D. (2020). High Gain Hexagonal Patch Antenna for V2V Communication. *7th International Conference on Signal Processing and Integrated Networks (SPIN)*, pp. 687–691.

[3] Honggang, H., Jiayu, L., Daili, H., and Wei, L. (2016). Design of hexagon microstrip antenna for vehicle-to-vehicle communication. *J. China Univ. Posts Telecommun.*, 23(4), 69–76.

[4] Choi, J., Marojevic, V., Nealy, R., Reed, J.H., and Dietrich C.B. (2019). DSRC and IEEE 802.11ac Adjacent Channel Interference Assessment for the 5.9 GHz Band. *89th Vehicular Technology Conference (VTC2019-Spring)*, pp. 1–5.

[5] Ramya, R. and Rao, T.R. (2014). Circularly polarized dual band micro strip patch antenna for vehicular wireless network communications. *IEEE International Conference on Advanced Networks and Telecommuncations Systems (ANTS)*, pp. 1–4.

[6] Diez, M.B., Plitt, P., Pascher, W., and Lindenmeier, S. (2015). Antenna placement and wave propagation for Car-to-Car communication. *European Microwave Conference (EuMC)*, pp. 207–210.

[7] Klemp, O. (2010). Performance considerations for automotive antenna equipment in vehicle-to-vehicle communications. *URSI International Symposium on Electromagnetic Theory*, pp. 934–937.

[8] Varum, T., Matos, J.N., and Pinho, P. (2011). Printed antenna for on-board unit of a DSRC system. *IEEE International Symposium on Antennas and Propagation (APSURSI)*, pp. 457–460.

[9] Westrick, M., Almalkawi, M., Devabhaktuni, V., and Bunting, C. (2013). A low-profile, low-cost antenna system with improved gain for DSRC vehicle-to-vehicle communications. *Int. J. RF Microw. Comput. Eng.*, 23(1), 111–117.

[10] Aloi, D.N., Possa, M., Barghouti, A., Tlusty, J., and Sharawi, M.S. (2014). Printed DSRC antennas for enhanced gain coverage towards front and rear of vehicle for automotive applications. *IEEE-APS Topical Conference on Antennas and Propagation in Wireless Communications (APWC)*, pp. 349–352.

[11] Kwon, O.Y., Song, R., and Kim, B.S. (2018). A Fully Integrated Shark-Fin Antenna for MIMO-LTE, GPS, WLAN, and WAVE Applications. *IEEE Antennas Wirel. Propag. Lett.*, 17(4), pp. 600–603.

[12] Luo, W., Chen, W., Feng, Y., and Yang, Y. (2020). A novel automobile antenna for vehicles communication of IoT systems in 5G network. *J. Wirel. Commun. Netw.*, 2020(1), p. 218.

[13] Guan, N., Tayama, H., Ueyama, M., Yoshijima, Y., and Chiba, H. (2015). A roof automobile module for LTE-MIMO antennas. *IEEE-APS Topical Conference on Antennas and Propagation in Wireless Communications (APWC)*, pp. 387–391.

[14] Huang, L. and Lu, Y. (2019). A Switchable or MIMO Antenna for V2X Communication. *IEEE International Conference on Computational Electromagnetics (ICCEM)*, pp. 1–2.

[15] Guan, N., Chiba, H., Yamaguchi, Y., Niihara, Y., and Tayama, H. (2014). A flat roof automobile antenna module for LTE, GPS and SDARS applications. *IEEE-APS Topical Conference on Antennas and Propagation in Wireless Communications (APWC)*, pp. 11–14.

[16] Kaul, S., Ramachandran, K., Shankar, P., Oh, S., Gruteser, M. and Seskar, I. (2007). Effect of Antenna Placement and Diversity on Vehicular Network Communications. *4th Annual IEEE Communications Society Conference on Sensor, Mesh and Ad Hoc Communications and Networks*, pp. 112–121.

[17] Leelaratne, R. and Langley, R. (2005). Multiband PIFA Vehicle Telematics Antennas. *IEEE Trans. Veh. Technol.*, 54(2), pp. 477–485.

[18] Virothu, S. and Anuradha, S. (2022). Conformal CP antenna for sub-6GHz band V2X applications. *International Conference on Computing in Engineering & Technology*, pp. 274–279.

[19] Narayan, D. R. K. K. G., Baskaradas, J.A. (2021). Design of a CPW-Fed Compact MIMO Antenna for Next Generation Vehicle to Everything (V2X) Communication. *Wirel. Pers. Commun.*, vol. 120, pp. 2179–2200.

[20] Wnuk, M. and Nowosielski, L. (2017). Car microstrip GPS antenna. *Progress in Electromagnetics Research Symposium - Fall (PIERS - FALL)*, pp. 444–448.

[21] Mondal, T., Samanta, S., Ghatak, R., and Chaudhuri, S.R.B. (2015). A Novel Tri-Band Hexagonal Microstrip Patch Antenna Using Modified Sierpinski Fractal For Vehicular Communication. *Prog. Electromagn. Res. C*, vol. 57, pp. 25–34.

[22] Biçer M.B. (2011). WLAN/WiMAX Uygulamaları İçin Kompakt Mikroşerit Anten Tasarımı ve Gerçekleştirilmesi.

[23] Susidharan, N., Hamsagayathri, P., Poongodi, C., Shakthisandhanu, S., Sivabalan, R., and Kaviyarashu, P. (2020). Performance analysis of printed antenna on different novel substrates to enhance V2V communication in future. *IOP Conf. Ser. Mater. Sci. Eng.*, 764(1), pp. 1–9.

[24] Ahn, S., Park, S., Noh, Y., Park, D., and Choo, H. (2010). Design of an on-glass vehicle antenna using a multiloop structure. *Microw. Opt. Technol. Lett.*, 52(1), pp. 107–110.

[25] Kosem, M. (2021). 5G Haberleşme İçin Genişbant Mikroşerit Yama Anten Modellemesi, Alttaş Seçimi Ve Gerçeklemesi," Van Yüzüncü Yıl Üniversitesi / Fen Bilimleri Enstitüsü, Van.

[26] Mishra, R. (2016). An Overview of Microstrip Antenna. *HCTL Open Int. J. Technol. Innov. Res.*, 21(2), pp. 1–17.

[27] Mehta, A. (2015). Microstrip Antenna. *Int. J. Sci. Technol. Res.*, 4(3), pp. 54–57.

[28] Rathod, J.M. (2010). Comparative study of microstrip patch antenna for wireless communication application. *Int. J. Innov. Manag. Technol.*, 1(2), pp. 194–197.

[29] Hossain, S.K.J., Islam, T., Alam, S., Munna, F.S. and Mondal, T. (2023). Design and Analysis of 3.5 GHz Rectangular Patch Microstrip Antenna for S-Band Applications. *IEEE Int. Conf. Integr. Circuits Commun. Syst.*, pp. 1–5.

[30] Zorkun, A.E. (2018). Görüntüleme Dizileri İçin Süperiletken Mikroşerit Yama Anten Tasarımı Ve Testi. TOBB ETÜ, Fen Bilimleri Enstitüsü Fen Bilimleri Enstitüsü, Ankara.

[31] Emin, B. (2019). Uzak Mesafe Haberleşmesi İçin Yönlü Anten Tasarımı. Hacı Bektaş Veli Üniversitesi, Fen Bilimleri Enstitüsü, Nevşehir.

[32] Türkmen, H.A., (2021). 5G Haberleşme Sistemleri İçin Geniş Bant Milimetre Dalga Mikroşerit Antenin Tasarlanması ve Gerçekleştirilmesi.

[33] Al-Asadi, A.K.N. (2023). Design And Improvement Of Hybrid Metal-Graphene Microstrip Antenna For Indoor Applications.

[34] Khayal, B. (2022). Dual-Polarized H-Shaped Aperture-Coupled Microstrip Antenna for Sub-

6GHz 5G Communication Systems.

[35] Al-khaylani, H.H.M. (2022). "Microstrip Antenna Design And Fabrication for Self Power Modern Wireless System.

[36] Kütük, H. (2012). 3.3 GHz Mikroerit Anten Tasarımı Ve Farklı Besleme Yöntemleri için Analizi.

[37] Winchen, T. (2007). Measurements of the continuous radio background and comparison with simulated radio signals from cosmic ray air showers at the Pierre Auger Observatory.

[38] Kaka, A.O. and Toycan, M. (2016). Dual band implant antenna design with miniaturized and biocompatible characteristics for wireless health monitoring. *Signal Processing and Communication Application Conference (SIU)*, pp. 1725–1728.

[39] İbrahimli, İ. (2017). Mobil Haberleşmedeki Mikroşerit Anten Tasarımı. İstanbul Aydın Üniversitesi Fen Bilimleri Enstitüsü, İstanbul.

[40] Ataş, İ. (2019). Yüksek Kazançlı Mikroşerit Antenlerin HFSS ile Modellenmesi ve Tasarımı.

[41] Armağan, O. (2021). "Mikroşerit Antenlerde Eş Düzlemsel Yapı Parametrelerinin Anten Performansına Etkilerinin İncelenmesi.

[42] Soh, P.J., Rahim, M.K.A., Asrokin, A. and Aziz, M.Z.A.A. (2007). Design, Modeling, And Performance Comparison of Feeding Techniques for a Microstrip Patch Antenna. *Univ. Teknol. Malaysia*, vol. 47, pp. 103–120.

[43] Singh, I. and Tripathi, V.S. (2011). Micro strip Patch Antenna and its Applications: a Survey. *Int. J. Comp. Tech. Appl.*, 2(5), pp. 1595–1599.

[44] Arora, A., Khemchandani, A., Rawat, Y., Singhai, S. and Chaitanya, G. (2015). Comparative study of different Feeding Techniques for Rectangular Microstrip Patch Antenna. *Int. J. Innov. Res. Electr.*, 3(5).

[45] Bansal, A. and Gupta, R. (2020). A review on microstrip patch antenna and feeding techniques. *Int. J. Inf. Technol.*, vol. 12, pp. 149–154.

[46] Mokal, M.V., Gagare, P.S.R. and Labade, D.R.P. (2017). Analysis of Micro strip patch Antenna Using Coaxial feed and Micro strip line feed for Wireless Application. *IOSR J. Electron. Commun. Eng.*, 12(3), pp. 36–41.

[47] Chakravarthy, S.S., Sarveshwaran, N., Sriharini, S. and Shanmugapriya, M. (2016). Comparative study on different feeding techniques of rectangular patch antenna. *International Conference on Wireless and Optical Communications Networks (WOCN)*, pp. 1–6.

[48] Mandal, A., Ghosal, A., Majumdar, A., Ghosh, A., Das, A. and Das, S.K. (2012). Analysis of feeding techniques of rectangular microstrip antenna. *IEEE International Conference on Signal Processing, Communication and Computing (ICSPCC 2012)*, pp. 26–31.

[49] Yelken, E. (2021). Selçuklu Yıldızı Şekilli Mikroşerit Antenin Yapay Zeka Yöntemleri Kullanılarak Optimum Tasarımı Ve Gerçekleştirilmesi.

[50] Kumar, A., Kaur, J. and Singh, R. (2013). Performance Analysis of Different Feeding Techniques. *Int. J. Emerg. Technol. Adv. Eng.*, 3(3), pp. 884–890.

[51] Jawad, A. (2016). Cellulose Based Miniaturized Antenna for Wearable Transceiver: Antenna Designing for Dual Band Operation.

[52] Oktay, H. (2024). Dairesel Polarizasyonlu V2x Anten Tasarımı, Üretimi ve Ölçümü.

[53] Mahamine, S.D., Parbat, R.S., Bodake, S.H. and Aher, M.P. (2016). Effects of different substrates on Rectangular Microstrip patch Antenna for S-band. *International Conference on Automatic Control and Dynamic Optimization Techniques (ICACDOT)*, pp. 1142–1145.

[54] Werfelli, H., Tayari, K., Chaoui, M., Lahiani, M. and Ghariani, H. (2016). Design of rectangular microstrip patch antenna. *International Conference on Advanced Technologies for Signal and Image Processing (ATSIP)*, pp. 798–803.

[55] Kornek, D., Schack, M., Slottke, E., Klemp, O., Rolfes, I. and Kurner, T. (2010). Effects of Antenna Characteristics and Placements on a Vehicle-to-Vehicle Channel Scenario. *International Conference on Communications Workshops*, pp. 1–5.

[56] Yang, J., Li, J. and Zhou, S. (2018). Study of Antenna Position on Vehicle by Using a Characteristic Modes Theory. *Antennas Wirel. Propag. Lett.*,17(7), pp. 1132–1135.

[57] Asghar, M.E., Wollenschlager, F., Asgharzadeh, A., Singh, J. and Hein, M.A. (2018). Influence of Antenna Mounting Location on the Radiation Pattern of an Automotive Antenna. *European Conference on Antennas and Propagation (EuCAP 2018), Institution of Engineering and Technology*, pp. 641-646.

[58] Abbas, T., Karedal, J. and Tufvesson, F. (2013). Measurement-Based Analysis: The Effect of Complementary Antennas and Diversity on Vehicle-to-Vehicle Communication. *Antennas Wirel. Propag. Lett.*, vol. 12, pp. 309–312.

[59] Imai, S. Taguchi, K. Kashiwa, T. and Kawamura, T. (2014). Effects of car body on radiation pattern of car antenna mounted on side mirror for inter-vehicle communications. *Antennas and Propagation Society International Symposium (APSURSI)*, pp. 601–602.

[60] Reichardt, L., Fugen, T., Zwick, T. (2009). Influence of antennas placement on car to car communications channel. *Eur. Conf. Antennas Propag.*, pp. 630–634.

[61] Whalen, E., Elfrgani, A., Reddy, C. and Rajan, R. (2018). Antenna Placement Optimization for Vehicle-to-Vehicle Communications. *International Symposium on Antennas and Propagation & USNC/URSI National Radio Science Meeting*, pp. 1673–1674.

[62] Kanni, B., Brinda, R. (2019). Design of High Gain Microstrip Antenna for Vehicle to Vehicle Communication Using Genetic Algorithm. *Prog. Electromagn. Res.*, vol. 81, pp. 167–179.

[63] Liu, A., Lu, Y. and Huang, L. (2018). Low-profile patch antennas with enhanced horizontal omni-directional gain for DSRC applications. *IET Microwaves, Antennas Propag.*, 12(2), pp. 246–253.

[64] Rahayu, Y., Raja, D.A. and Yoga, B.P. (2019). A Compact Design of Transparent Microstrip Antenna For Wireless Car-to-Car Communication System. *Int. J. Electr. Energy Power Syst. Eng.*, 2(2), pp. 12–15.

[65] Zaw, K. K., Tun, H. M., Khin, E.E., Oo, T., Pradhan, D. (2024). Compact Design of 1x2 MIMO Microstrip Patch Antenna with Corners Trimmed for Vehicle-to-Vehicle Communication. *J. Nov. Eng. Sci. Technol.*, vol. 4, pp. 12–16, 2024.